

DYNAMIC BEHAVIORS OF LANGERHANS CELLS *IN SITU*

APPROVED BY SUPERVISORY COMMITTEE

Akira Takashima, M.D., Ph.D.

Robert Munford, M.D.

Jerry Niederkorn, Ph.D.

Iwona Stroynowski, Ph.D.

Yong-jun Liu, M.D., Ph.D.

DEDICATION

I would like to thank the members of my Graduate Committee, my mentor Akira Takashima, the friends that helped keep me sane, and most of all my family, who never stopped encouraging me.

DYNAMIC BEHAVIORS OF LANGERHANS CELLS *IN SITU*

by

BRANT RUSSELL WARD

DISSERTATION

Presented to the Faculty of the Graduate School of Biomedical Sciences

The University of Texas Southwestern Medical Center at Dallas

In Partial Fulfillment of the Requirements

For the Degree of

DOCTOR OF PHILOSOPHY

The University of Texas Southwestern Medical Center at Dallas

Dallas, Texas

December, 2006

DYNAMIC BEHAVIORS OF LANGERHANS CELLS *IN SITU*

Brant Russell Ward

The University of Texas Southwestern Medical Center at Dallas, 2006

Supervising Professor: Akira Takashima, M.D., Ph.D.

The epithelial surfaces of the body, being constantly exposed to both innocuous and potentially harmful substances and organisms, are protected by an array of immune cells called Langerhans cells (LCs). As a bridge between the innate (non-specific) and adaptive (specific) immune responses, LCs sense injurious stimuli and contribute to tissue inflammation as well as initiate the antibody- or cell-mediated specific responses to pathogenic organisms. These events represent pivotal occurrences in the instigation of the immune response, and thus are important targets for experimental investigation. To explore the dynamic

behaviors of LCs within the epithelial tissues, LCs in living corneal and epidermal tissue were examined *ex vivo* and *in vivo* by multiphoton and confocal laser scanning microscopy. LCs at baseline exhibit a unique behavior characterized by rhythmic extension and retraction of the dendritic processes. To explore the responses of LCs to tissue injury, LCs in the cornea and epidermis were examined after pinpoint thermal or diffuse chemical injury. After these stimuli, LCs displayed more active dSEARCH and lateral movement through the tissue. These behavioral responses were dependent on the inflammatory cytokines IL-1 and TNF α , suggesting a requirement for these cytokines in LCs responses to injury. After infection of the epidermis with pathogenic bacteria *in vivo*, LCs displayed similar responses, showing increased dSEARCH and lateral migration. These results indicate that LCs in different tissues react to varying pathogenic stimuli with common behavioral responses and add a new dimension to our understanding of LC biology.

TABLE OF CONTENTS

Dedication	ii
Abstract.....	iv
Table of Contents.....	vi
Prior Publications.....	xii
List of Figures	xiv
Abbreviations.....	xvii
Chapter 1: Introduction	
Dynamic Behaviors of Langerhans Cells <i>In Situ</i>	1
Specific Aims of This Work	1
To Study LC Behaviors Under Physiologic Conditions.....	1
To Study How Local Tissue Injury Affects LC Behaviors.....	2
To Study LC Behaviors During Infection by Pathogenic Organisms.....	2
Chapter 2: Background	
Basic Principles of Immunology	3
Innate Immune Responses	3
Adaptive Immune Responses.....	6
Antigen Presenting Cells.....	8
Dendritic Cells	9
Background.....	9
Danger Signals and DC Maturation.....	11

Antigen Presentation	13
Langerhans Cells	14
Background	15
Similarities to DCs	15
Differences from Other DC Subsets	17
LCs and Corneal Immunobiology	19
LCs in the Cornea and Ocular Immune Privilege	19
Migration of Corneal LCs	20
Imaging the Immune System	22
Imaging Technologies	22
Confocal Laser Scanning Microscopy	23
Multiphoton Laser Scanning Microscopy	24
Second Harmonic Generation	26
Detection of Light Emitted from Fluorescent Proteins	27
Chapter 3: Materials and Methods	
LC Behaviors Under Pathologic Conditions	30
Generation of EGFP+ Corneal LCs <i>In Situ</i>	30
Animals	30
Flow Cytometric Examination of Bone Marrow Chimerism	31
Static Imaging of Corneal LCs <i>In Situ</i>	33
Visualization of EGFP+ LCs in Living Corneal Tissue	35
Corneal Organ Culture	35

Time-Lapse Imaging Studies	36
Image Analysis and Quantification.....	37
Dynamic Behaviors of Epidermal LCs <i>Ex Vivo</i>	38
Animals	38
Characterization of LCs in the Epidermis of I-A β -EGFP Knock-in Mice	38
<i>Ex Vivo</i> Imaging of Ear Skin Samples by Confocal Microscopy	39
Observation of LC Behaviors in Living Animals	39
Intravital Imaging of Epidermal LC Behaviors	39
Quantification of Epidermal LC Behaviors Monitored <i>In Vivo</i>	40
LC Behavioral Responses to Local Tissue Injury.....	41
Corneal LC Responses to Pinpoint Thermal Injury	41
Infrared Pinpoint Thermal Injury.....	41
Quantification of LC Dendrite Activity	42
Quantification of LC Migration	42
Statistical Analyses	43
Mechanisms of Corneal LC Responses to Thermal Injury	43
Inhibition of LC Behavioral Responses to Pinpoint Thermal Injury	43
Provocation of LC Behavioral Responses by Cytokines	44
Epidermal LC Responses to Diffuse Inflammatory Stimuli <i>Ex Vivo</i>	44
Overnight Culture of Skin Samples	44
<i>Ex Vivo</i> Behaviors after Injection of TNF α	45
Quantification of LC Behaviors Monitored <i>Ex Vivo</i>	46

Epidermal LC Responses to Reactive Hapten <i>In Vivo</i>	46
Intravital Imaging of LCs After DNFB Application.....	46
LC Behavioral Responses to Pathogenic Organisms.....	48
Development of Fluorescent Bacterial Cells	48
Tn7 Transformation of Bacterial Cells	48
CMTMR Labeling of Bacterial Cells	49
Fluorescent Protein Expression in <i>Escherichia coli</i> Cells	50
Behavioral Responses of Epidermal LCs to Bacterial Cells <i>In Vivo</i>	51
EGFP and EYFP Spectral Characteristics	51
<i>In Vivo</i> Imaging of LCs.....	52
Tape-Strip Model of Infection	53
Quantification of LC Responses to Bacterial Organisms	53
Chapter 4: Results	
LC Behaviors Under Physiologic Conditions.....	55
Visualization of Corneal LCs <i>In Situ</i>	55
Reconstitution of Leukocyte Populations After Bone Marrow Transplantation .	55
Corneal LCs Interact With Their Environment Via dSEARCH.....	58
Lateral Migration by EGFP ⁺ Cells in the Cornea	59
Visualization of LC Behaviors in the Epidermis	61
Quantification of LC Populations in the Epidermis.....	61
Behaviors of Epidermal LCs <i>Ex Vivo</i>	62
Steady State Behaviors of Epidermal LCs <i>In Vivo</i>	63

LC Behavioral Responses to Local Tissue Injury.....	77
Behavioral Responses of Corneal LCs to Local Tissue Injury	77
Pinpoint Thermal Injury Elicits Rapid Changes in LC Behaviors.....	77
Role of IL-1 in Injury-Induced Behavioral Changes	79
Effect of TNF α on Dynamic LC Behaviors	82
Behavioral Responses of Epidermal LCs to Inflammatory Insults.....	83
LC Responses to Diffuse Inflammatory Stimuli <i>Ex Vivo</i>	83
LC Responses to Reactive Hapten Application <i>In Vivo</i>	85
LC Behavioral Responses to Pathogenic Organisms.....	118
Generation of Fluorescent Bacteria for <i>In Situ</i> Imaging	118
Transformation of <i>Pseudomonas aeruginosa</i> by the Mini-Tn7 Transposon.....	118
Labeling of <i>Pseudomonas aeruginosa</i> Cells by CMTMR.....	120
ECFP and EYFP Expression by Plasmid Vectors	122
LC Responses to Bacterial Cells <i>In Vivo</i>	122
Epidermal LCs Show Augmented dSEARCH in Response to Bacterial	
Infection	123
Epidermal LC Migration After Infection of the Skin	125
Chapter 5: Conclusions and Discussion	
Summary of Experimental Findings	138
LC Behaviors at Baseline.....	138
Baseline LC Behaviors Observed <i>Ex Vivo</i>	139
<i>In Vivo</i> Behaviors of LCs in the Steady State.....	140

LC Responses to Injury and Inflammatory Stimuli	140
Behavioral Responses After Pinpoint Thermal Injury	140
Responses to Diffuse Stimuli in the Epidermis	142
LC Responses to Pathogenic Organisms	142
Bacterial Infection of Skin <i>In Vivo</i>	142
Questions and Significance.....	143
Imaging the Immune System	143
Dynamic Behaviors of DCs	144
Dynamics of DC-T Cell Interactions	145
Imaging of Langerhans Cells in Living Tissues	147
Technical Significance of This Study	148
Implications of LC Behaviors	149
Differences in dSEARCH Between Tissue Preparations.....	149
Functions of Dynamic LC Behaviors	151
LCs in Corneal Pathology	153
Epidermal LCs in Cutaneous Disease.....	155
Prospects for the Future	156
Challenges to the Role of LCs as APCs.....	156
List of Works Cited.....	161
Vitae.....	191

PRIOR PUBLICATIONS

Taylor, M. A., B. Ward, J. D. Schatzle, and M. Bennett. 2002. Perforin- and Fas-dependent mechanisms of natural killer cell-mediated rejection of incompatible bone marrow cell grafts. *Eur. J. Immunol.* 32:793.

Kumamoto, T., D. Shalhevet, H. Matsue, M. E. Mummert, B. R. Ward, J. V. Jester, and A. Takashima. 2003. Hair follicle serves as a local reservoir of skin mast cell precursors. *Blood* 102:1654.

Nishibu, A.¹, B. R. Ward¹, J. V. Jester, H. Ploegh, M. Boes, and A. Takashima. 2006. Behavioral responses of epidermal Langerhans cells *in situ* to local pathological stimuli. *J. Invest. Dermatol.* 126:787.

Vishwanath, M., A. Nishibu, S. Saelend, B. R. Ward, N. Mizumoto, H. Ploegh, M. Boes, and A. Takashima. 2006. Development of intravital intermittent confocal imaging system for studying Langerhans cell turnover. *J. Invest. Dermatol.* (in press).

Ward, B. R.¹, J. V. Jester¹, A. Nishibu, M. Vishwanath, D. Shalhevet, T. Kumamoto, W. M. Petroll, H. D. Cavanagh, and A. Takashima. 2006.

Local thermal injury elicits immediate dynamic behavioral responses by corneal Langerhans cells. Submitted.

Nishibu, A., B. R. Ward, M. Boes, and A. Takashima. 2006. Roles for IL-1 and TNF α in dynamic behavioral responses of Langerhans cells to topical hapten application. Submitted.

¹Equal contribution was made by these authors.

LIST OF FIGURES

Figure 1. Schematic illustration of the confocal principle	28
Figure 2. Fluorescence by one- or two-photon excitation	29
Figure 3. EGFP expression by leukocytes in BM chimeric animals	65
Figure 4. LCs in the corneal epithelium express CD11c and exhibit a dendritic morphology	66
Figure 5. Schematic of the Delta T4 culture system for <i>in situ</i> imaging of LCs	68
Figure 6. Corneal LCs display a unique behavior termed dSEARCH.....	69
Figure 7. Dendrite length varies over time in LCs showing dSEARCH	70
Figure 8. Periodicity of the changes in dendrite length	71
Figure 9. Identification of EGFP ⁺ epidermal cells in the skin of I-A-EGFP knock-in mice.....	72
Figure 10. dSEARCH recorded <i>ex vivo</i> in EGFP ⁺ epidermal LCs	73
Figure 11. dSEARCH recorded in the steady state in living animals.....	74
Figure 12. Pinpoint thermal injury triggers augmented dSEARCH in nearby LCs.....	87
Figure 13. dSEARCH index values in corneal LCs are elevated after thermal injury	88
Figure 14. Pinpoint thermal injury induces lateral migration in corneal LCs	90
Figure 15. The mean velocity of corneal LCs per frame is increased after thermal injury. ..	91
Figure 16. Injury-induced dSEARCH augmentation is inhibited by IL-1Ra	92
Figure 17. IL-1Ra prevents injury-induced increase in dSEARCH index in corneal LCs	93
Figure 18. IL-1Ra prevents injury-induced lateral migration in corneal LCs	95

Figure 19. Exogenous IL-1 α induces transient augmentation of dSEARCH in EGFP+ corneal LCs	96
Figure 20. IL-1 α transiently elevates dSEARCH index values in corneal LCs	97
Figure 21. IL-1 α fails to induce an increase in lateral migration by corneal LCs.....	99
Figure 22. IL-1 α causes progressive dendrite elongation in corneal LCs at higher concentrations	100
Figure 23. Exogenous TNF α elicits augmented dSEARCH by EGFP ⁺ corneal LCs.....	103
Figure 24. Exogenous TNF α causes an elevation in dSEARCH index values in corneal LCs.....	103
Figure 25. Exogenous TNF α induces lateral migration by corneal LCs	105
Figure 26. LCs in the epidermis after diffuse inflammatory stimuli	106
Figure 27. dSEARCH recorded <i>ex vivo</i> in EGFP ⁺ epidermal LCs after diffuse inflammatory stimuli.....	107
Figure 28. dSEARCH index of epidermal LCs is elevated by inflammatory stimuli <i>ex vivo</i>	109
Figure 29. Inflammation-associated lateral migration of EGFP ⁺ epidermal LCs <i>ex vivo</i> ...	110
Figure 30. Inflammatory stimuli increase lateral migration of epidermal LCs <i>ex vivo</i>	111
Figure 31. Topical hapten application induces augmented dSEARCH by EGFP ⁺ epidermal LCs <i>in vivo</i>	112
Figure 32. dSEARCH index values of epidermal LCs are elevated after hapten application <i>in vivo</i>	113
Figure 33. Application of reactive hapten induces lateral migration of epidermal LCs	

<i>in vivo</i>	114
Figure 34. DsRed fluorescence emission by mini-Tn7-transformed <i>Pseudomonas</i>	
<i>aeruginosa</i>	126
Figure 35. Fluorescent protein expression in <i>Escherichia coli</i> vectors	128
Figure 36. Fluorescence in <i>Pseudomonas aeruginosa</i> cells labeled with CMTMR.....	130
Figure 37. Fluorescence by <i>Pseudomonas aeruginosa</i> cells expressing ECFP or EYFP....	131
Figure 38. dSEARCH activity in epidermal LCs is increased after tape-stripping <i>in vivo</i> .	132
Figure 39. dSEARCH index values are increased after tape-stripping and infection	
with <i>Escherichia coli</i>	133
Figure 40. Epidermal LCs display hyper-augmented dSEARCH after bacterial infection	
of taped-stripped skin.....	134
Figure 41. Lateral migration of epidermal LCs is seen after infection of tape-stripped	
skin <i>in vivo</i>	135
Figure 42. Tape-stripping and infection with <i>Escherichia coli</i> induces increased	
lateral migration by epidermal LCs <i>in vivo</i>	136

ABBREVIATIONS

Ab	antibody
Ag	antigen
Amp	ampicillin
APC	antigen presenting cell
BCR	B cell receptor
BMC	bone marrow cell
CFSE	5-(and-6)-carboxyfluorescein diacetate, succinimidyl ester
CHS	contact hypersensitivity
CMTMR	5-(and-6)-(((4-chloromethyl)benzoyl)amino)tetramethylrhodamine
CpG	unmethylated cytosine-guanine dinucleotide
cRPMI	complete Roswell Park Memorial Institute-1640 culture medium
DC	dendritic cell
DC-SIGN	dendritic cell-specific ICAM-grabbing non-integrin
DC-LAMP	dendritic cell lysosome-associated membrane protein
DNA	deoxyribonucleic acid
DNFB	dinitrofluorobenzene
dSEARCH	dendrite surveillance extension and retraction cycling habitude
DTR	diphtheria toxin receptor
EDTA	ethylenediaminetetraacetic acid

EGFP	enhanced green fluorescent protein
EYFP	enhanced yellow fluorescent protein
FACS	fluorescence activated cell sorting
FCS	fetal calf serum
HBSS	Hank's balanced salt solution
HSV	herpes simplex virus
ICAM	intercellular adhesion molecule
Ig	immunoglobulin
IL	interleukin
IL-1Ra	interleukin-1 receptor antagonist
IFN	interferon
i.p.	intraperitoneal
i.v.	intravenous
LB	Luria Bertani
LC	Langerhans cell
LCS	Leica Confocal Software
LPS	lipopolysaccharide
mAb	monoclonal antibody
MIP	macrophage inflammatory protein
MHC	major histocompatibility complex
MHC I	major histocompatibility complex class I (protein)

MHC II	major histocompatibility complex class II (protein)
NA	numerical aperture
OVA	ovalbumin
<i>P</i>	probability
PBS	phosphate buffered saline
PE	R-phycoerythrin
PMN	polymorphonuclear cell
RBC	red blood cell
RNA	ribonucleic acid
ROI	region of interest
s.c.	subcutaneous
SD	standard deviation
SEM	standard error of the mean
Ti:sapphire	titanium-doped sapphire
TCR	T cell receptor
TLR	Toll-like receptor
sTNFRSF1A	soluble tumor-necrosis-factor-receptor super family 1A
TNF α	tumor necrosis factor alpha

CHAPTER ONE

Introduction

DYNAMIC BEHAVIORS OF LANGERHANS CELLS *IN SITU*

Specific Aims of this Work

Unlike other types of dendritic cells (DCs), Langerhans cells (LCs) are found at the very forefront of the body's defenses against the external environment, within the outermost layers of tissues like the epidermis and corneal epithelium. While their functions as antigen presenting cells (APCs) have been inferred from conventional assays and immunohistochemistry in various experimental models, the dynamic behaviors of LCs within the tissues had yet to be directly observed. Since understanding such behaviors would potentially lead to a greater understanding of the complex and subtle nature of LC function, it was the goal of this work to examine the behaviors of LCs within their native environment where the critical steps in the initiation of immune responses occur.

To Study LC Behaviors Under Physiologic Conditions

To study LC behaviors, unique model systems were developed that allowed for the multidimensional observation of LCs within living tissues for extended time periods. Two-photon and confocal laser scanning microscopy were used to examine LCs within living cornea and skin organ cultures, as well as live

animals, and the resulting four-dimensional image sets were used to quantify the behaviors of the LCs using several different parameters.

To Study How Local Tissue Injury Affects LC Behaviors

Because LCs respond to tissue injury with alterations to their functional characteristics, it was thought that such injury would also result in changes in LC behaviors. Physical trauma was implemented to areas surrounding the LCs under observation, and the changes in LC behaviors were recorded and analyzed. As soluble mediators are thought to play a role in LC responses to injury, the roles of two prototypic inflammatory cytokines, IL-1 and TNF α , in the LC behavioral responses to pathologic tissue damage were examined.

To Study LC Behaviors During Infection by Pathogenic Organisms

One major role thought to be played by LCs is the initiation of immunologic responses to pathogenic organisms. To investigate the behaviors associated with LC responses to invading organisms, LCs were observed along with bacterial cells by confocal microscopy. The resulting behaviors were quantified using the parameters for dynamic movement as above.

CHAPTER TWO

Background

BASIC PRINCIPLES OF IMMUNOLOGY

The immune system is a complex collection of proteins, cells, and organs that through a combined effort act to protect the body from injuries and insults originating both from without and from within. It has evolved many arms to achieve this goal, both effector and sentry. Within the epithelial tissues at the external interfaces of the body, literally at the forefront of the immune system, are sentinel cells known as Langerhans cells, which serve to alert and coordinate the various effectors of the immune response. While much has been inferred regarding the biology and function of these cells from previous studies, the dynamic behaviors of these cells in their natural environs, which may be important to our greater understanding of their biology, remain unknown. This work will focus on the elucidation of the behaviors of Langerhans cells within the epithelium and the ways in which they respond to pathogenic insults.

Innate Immune Responses

Considered the first line of defense against the myriad dangers to the body, the innate arm of the immune response is evolutionarily very ancient, with

homologous components found across an incredibly diverse range of phyla and species. In mammals, physical barriers, such as the epithelial tissues and secreted antimicrobial compounds, make the most significant contribution, preventing the vast majority of external threats from gaining access to the internal tissues of the body. If a pathogen manages to circumvent these physical barriers, the immune system is able to bring to bear an array of cellular and extracellular components to contain and eliminate the incursion. Complement proteins present within the extracellular fluid can spontaneously or specifically polymerize on the surface of foreign particles, ranging from bacteria to viruses to the wooden fibers of a splinter. The resulting protein complexes can disrupt the membrane potential of bacterial cells and kill them directly, or, by coating their surface, make foreign bodies more susceptible to phagocytosis by macrophages and polymorphonuclear cells (PMNs). When viruses or certain bacteria enter the host cells, and thus shield themselves from the complement and phagocytic cell systems, natural killer (NK) cells are able to recognize the transgression and destroy the host cell to prevent further growth or replication of the pathogen (1).

While the complement cascade can begin spontaneously on any surface, the other important effector arms of the innate immune response are triggered when the immune system is alerted to the presence of an invader—something that is non-self. The ability of the immune system to distinguish self from non-self is

a central part of immunological dogma, and the innate immune response accomplishes this task mainly through the use of pattern recognition receptors. As life has evolved, certain classes of chemicals with unique structures have come to be produced by or associated with specific groups of organisms. Examples include lipopolysaccharide (LPS), a component of the outer membrane of Gram-negative bacteria; CpG motifs, regions of unmethylated DNA found predominantly in prokaryotic-, but not eukaryotic-, genomes; and double-stranded RNA, the genetic component of some viruses. Such compounds are recognized by families of proteins, including Toll-like receptors and C-type lectin scavenger receptors, which bind to unique structural elements of the foreign material (2-4). These receptors can be found on immune cells and non-immune cells, alike, and upon binding their ligand can lead to or directly trigger the various effector functions of the innate immune response, such as increased phagocytosis, cytotoxicity, and cytokine and chemokine secretion (1).

As pathogens often bypass the physical barriers via physical disruption of the tissues, we have evolved mechanisms by which injuries to the tissues alert the immune system to possible incursion. The disruption of cellular membranes that happens during acute trauma causes the release of intracellular materials into the extracellular space, and both immune and non-immune cells possess receptors capable of recognizing these unusual “danger signals.” Molecules like ADP,

ATP, and uric acid bind to cell surface receptors on neighboring healthy cells and very rapidly trigger the release of proinflammatory cytokines like interleukin (IL)-1 and tumor necrosis factor alpha (TNF α) (5-12). Moreover, many tissues, especially the epithelial tissues where injury is likely to occur, contain pre-made stores of inflammatory cytokines that are released upon injury (13-21). These cytokines act in many ways to unleash the immune response—increasing blood flow to the area, inducing the production of chemokines and adhesion proteins to draw out leukocytes, activating immune cells, and causing a feed-forward production of more inflammatory cytokines. These mechanisms act in concert to draw the immune system to the site of injury and activate the effector cells so as to destroy the invaders.

Adaptive Immune Responses

Over millions of years, the innate immune mechanisms have been honed to recognize and destroy classes of potentially harmful organisms. Those bacteria, viruses, and parasites did not sit idly by, however, and many have evolved complex means to bypass, disrupt, or protect themselves from our innate defenses. In turn we have developed a response to the increased threat posed by these organisms—the adaptive immune response. Whereas the innate response was characterized by germline-encoded receptors that recognize broad classes of

pathogen-associated molecules, the adaptive response employs polymorphic gene segments that are rearranged to generate an incredibly diverse repertoire of potential antigen (Ag) receptors. In addition, the rearrangement occurs in a clonal manner, in that each cell possesses a single specific receptor, and only those cells that possess a receptor recognizing the invading pathogen will divide and become activated during the immune response. Thus the adaptive response is just that, suiting the need of the immune system to specifically target and eliminate a specific pathogen as the need arises (1).

Action on behalf of the adaptive immune response is carried out by two families of cells, B cells and T cells, which differ in the type of specific Ag receptors they express. The B cell receptor (BCR) is a membrane-bound form of the immunoglobulin (Ig) protein, which in its secreted form becomes the antibody that is in fact the ultimate effector mechanism of the activated B cell. Antibodies (Ab) are bivalent proteins composed of two identical heavy chains and two identical light chains, each derived from a rearrangement of gene segments, and are capable of initiating the complement cascade to kill pathogens, opsonizing particles to make them better targets for phagocytosis, and blocking the active sites of toxic proteins or viral attachment proteins. The T cell receptor (TCR) is a monovalent protein that, unlike the BCR, can only recognize Ags when they are present within specialized grooves in particular cell surface proteins called major

histocompatibility complex (MHC) proteins. T cells with the CD4 coreceptor protein recognize Ags in the context of MHC class II (MHC II) proteins; T cells possessing the CD8 coreceptor recognize Ag within MHC class I proteins. This difference in coreceptor expression amongst T cell subpopulations correlates with the effector functions of the cells, in that CD4 T cells produce factors that recruit other leukocytes to the sites of infection and license their effector function, while CD8 T cells possess the capacity to directly kill virus-infected or cancerous target cells. Thus, once activated, the cells of adaptive immunity will respond in a manner resulting in the specific neutralization of invasive particles or the destruction of host cells harboring them (1).

ANTIGEN PRESENTING CELLS

The activation and expansion of the adaptive immune response takes time, and thus it still falls on the innate response to rapidly meet the invading organisms and defend the body against the attack. If the innate response is unable to clear the infection, the increased Ag load and prolonged inflammation will eventually result in the activation of T cells and B cells, the effectors of the adaptive response. This activation is critically dependent upon the sentinels that coordinate the innate response—the so-called antigen presenting cells (APCs)—principally the tissue dendritic cells (DCs) and epithelial Langerhans cells (LCs), but in some

cases macrophages and B cells, as well. Once activated by their cytokine or pattern recognition receptors, these cells develop the unique ability to present Ags to the adaptive immune cells and activate them, and thus they serve as a crucial link between the innate and adaptive immune responses.

Dendritic Cells

Background

The dendritic cell family comprises what many consider the prototypic APC. DCs are found scattered throughout the body; in any tissue in which one will find leukocytes there will undoubtedly be DCs, ready to take up Ags and alert the rest of the immune system to arising threats. Like other leukocytes, they are derived from CD34⁺ hematopoietic stem cell progenitors and are continuously generated throughout life (22-25). Anecdotal evidence from our lab, supported by several recently published studies, indicates that the life span for DCs is relatively short, with reconstitution of DC populations by donor-derived cells within a matter of weeks after bone marrow transplantation (26,27). Some evidence has suggested that DCs may arise from two different stem cell progenitors, the granulocyte/monocyte progenitor and the lymphoid progenitor, and thus can be described as myeloid DC and lymphoid DC, respectively (24,28-30). The evidence for this division suggested that lymphoid DCs were more closely related

to T cells than B cells and NK cells and that myeloid DCs could arise from committed precursors or differentiated monocytes, suggesting a great deal of plasticity in the DC lineage.

The hallmark identifiers of DCs have traditionally been the surface molecules CD11c (DC-associated integrin- α_x chain) and MHC II, although recent efforts by investigators studying gene expression in DCs have identified proteins such as DC-SIGN and DC-LAMP that are specifically expressed by DCs (22-24,31). Moreover, investigators have discovered that DC can be divided into subpopulations, each with unique functional characteristics, based on the expression of key surface molecules. The CD8 surface protein, once thought to be expressed exclusively by a subset of T cells, is expressed on a key subset of DCs that are generally considered to induce TH1-type responses in T cells, versus the TH2 phenotype induced by CD8⁻ DCs (32,33). Plasmacytoid DCs are identified as cells expressing traditional DC markers that also express the B cell marker B220 and the granulocyte marker Gr-1 (Ly-6C/G) (34-36). These plasmacytoid DC were found to be extremely potent producers of the type-1 interferons (IFNs), IFN- α and - β , during certain viral infections. Since it was later demonstrated that they express the TLRs for ligands expressed during infection, these DCs most likely represent the primary source of the anti-viral interferon produced in response to viral infection (37-40).

Danger Signals and DC Maturation

As the sentinel cells of the immune system, DCs are well equipped to monitor the tissues for the first signs of infection, inflammation, or injury. Although there is currently still some discussion within the scientific community regarding the extent of TLR expression by DCs between different species and even between subpopulations within an individual organism, it is clear that DCs as a whole possess a wide variety of TLRs recognizing many different classes of pathogen-associated molecules (24,41-43). In addition, DCs express an array of different cytokine receptors that enable DCs to detect inflammatory changes in the tissues, of which IL-1 receptors and TNF α receptors are particularly important, as these are the primary cytokines released by cells during acute inflammation and tissue injury (22-24). Moreover, DCs are able to detect damage to neighboring cells via receptors specific for proteins and compounds normally found only in the intracellular space—*exempla gratis*, ATP and ADP by purinergic type 2 receptors and uric acid by an as-yet unidentified mechanism (5,44-46).

Ligation of any of these receptors results in a cascade of changes in the gene expression and cellular behaviors of DCs that is designed to augment the cells' ability to regulate the innate and adaptive immune responses (47). One of

the first changes that take place is the secretion of inflammatory cytokines such as IL-1 β , IL-6, TNF α , and the type-1 interferons, as well as chemokines like IL-8 (22-24,48). This has the effect of propagating the inflammatory state, leading to an autocrine activation of individual DCs and paracrine activation of DCs nearby. It also ensures that the effectors of the innate response will arrive at the site of inflammation, via increased blood flow and leakiness of the vasculature caused by IL-1 and TNF α in addition to the direct chemotactic effect of IL-8 (1).

Activation of DCs increases the capability of the innate response, but importantly also provokes the initiation of the adaptive immune response (23,24). When activated, DCs downregulate their ability to internalize Ags and instead shuttle the Ags they have already internalized to the cell surface in context with MHC molecules. Cellular motility is provoked concurrently with decreased expression of the cellular adhesion molecules that bind them to the tissues in which they reside. These changes coincide with upregulation of chemokine receptors like CCR7 (49). This in turn draws the DCs to the lymphoid organs through the lymphatics due to the constitutive expression of the chemokines CCL19 and CCL21 by the cells of the lymphatic vessels and by stromal cells in the T cell areas of the lymphoid organs. All the while, DCs begin to express surface markers that are characteristic of the activated or “mature” state, notably

CD40, CD80, and CD86. As a result, activation primes and relocates DCs for the stimulation of the adaptive immune response (23,24).

Antigen Presentation

When at rest in the peripheral tissues, DCs are considered to be in an immature state, in that their function as sentinels and coordinators of the immune response has not been triggered. In this state, DCs are especially capable of internalizing Ags, be they host proteins, innocuous environmental compounds, or potentially harmful bacterial products. Antigens are internalized through phagocytosis, pinocytosis, and/or receptor mediated endocytosis, after which they are processed in specialized vesicular compartments and loaded onto either MHC II molecules or, through a process called cross-presentation, onto MHC I molecules (23,24,50-54). In the steady state, small numbers of immature DCs trickle into the lymphoid organs, where presentation of the MHC/Ag complexes by the immature cells to naïve T cells is thought to result in tolerance to those Ags (55,56). Thus, this represents one way by which the immune system learns not to attack targets, such as the body's own cells or beneficial bacterial flora, to which a response would be detrimental to the organism.

After activation, antigen presentation becomes the *sine qua non* of DC function, and is absolutely crucial for the effective generation of adaptive immune

responses. As stated above, the expression of Ag/MHC complexes on the surface of DCs is increased post-activation. Drawn by chemokines, DCs enter areas rich in T cells and are there scanned by the numerous lymphocytes for expression of Ag/MHC complexes that are recognizable by the specific TCRs of those cells. If a suitably specific TCR is present, the receptor, as well as the CD4 or CD8 coreceptor, depending on the type of T cell, binds to the antigen/MHC complex. Ligation of CD80 or CD86 molecules on the DCs to CD28 on the T cells occurs concomitantly with MHC/TCR binding, and, it should be noted, is essential for T cell activation, for without the costimulatory signal generated through CD28 the T cell will likely become unresponsive to antigenic stimulation. These two signals are sufficient to activate CD4 T cells, which consequently express CD40 ligand on their surface (57,58). This activating ligand binds to CD40 on the DCs and triggers their utmost activation state, in which 4-1BB ligand and OX-40 ligand expressed by fully mature DCs license the activation and expansion of the B cell and CD8 T cell arms of the adaptive immune response (1,22-24).

LANGERHANS CELLS

The outermost tissues of the body, those exposed to the external environment, develop with significant physical and biological differences from the other somatic tissues of the body. While separated from the blood and lymph circulation by a basement membrane, the epithelial tissues nonetheless represent

the primary setting for immune responses to foreign invaders, for it is primarily in these tissues that the body first contacts potentially harmful materials or organisms. The immune cells in the epithelium must therefore be especially vigilant against pathogenic insults. On the other hand, these leukocytes must also be especially discerning, as the body contacts untold numbers of innocuous and/or potentially helpful materials and organisms via the epithelium. DCs, as sentinels and coordinators of the immune response, are especially important at these interfaces with the environment, and it is the LC, a subtype of DC found exclusively in the epithelial tissues, that carries this burden.

Background

Similarities to DCs

LCs were first discovered in 1868 after the staining of skin samples with gold chloride by Paul Langerhans, who believed the cells to be neurons based on their shape. Langerhans cells were later shown not to be neurons, but in fact represent a prototypic immature DC subset that is characterized by localization within epithelial tissues such as the cornea, skin, and mucosa and by extension of long dendritic processes (23,24,59-61). Like other DCs, LCs are considered to have an immature phenotype while in the tissues and are capable of internalizing a variety of Ags, from pathogenic microbes to innocuous melanin granules (62-

64). Moreover, LCs express many of the same cell surface receptors as DCs, including CD11c and MHC II, and undergo a functional and phenotypic maturation process in response to danger signals released by pathogenic organisms or inflamed tissues. In fact, the concept of DC maturation was first proposed based on the observation that LCs begin to exhibit the characteristic immunostimulatory features of splenic DCs after short term culture (65). As do other DCs, LCs upregulate expression of the costimulatory molecules CD40, CD80, and CD86 upon maturation, and are known to migrate out of the epithelia and into the draining lymph nodes after receiving inflammatory signals (66-70). Thus it seems that the maturation of LCs is the initial and critical event in the innate and adaptive immune responses in the epithelial tissues.

In addition to sharing similar phenotypes and functions to those of mature DCs, LCs appear to possess the same ability to silence immune responses by T cells to Ags presented when in an immature state. In mice expressing ovalbumin (OVA) under the control of the keratin 14 (K14) promoter, the immune system failed to mount responses to this foreign Ag in the steady state, despite its abundant expression in the epidermis. After injection of T cells expressing a transgenic TCR specific for OVA, however, the mice began exhibiting symptoms of graft-versus-host disease, indicating that OVA was not merely sequestered away from the immune responder cells (71). Together, these results imply that

presentation of the OVA by LCs in the steady state resulted in peripheral tolerance to the Ag. Additionally, the idea that LCs traffic to the draining lymph nodes in the steady state is supported by two recent findings. In K14 promoter-driven steel factor transgenic mice, in which hyperpigmentation caused by abundant melanocytes is restricted to the epidermis, LCs were found to capture and transport melanin granules to the skin draining lymph nodes in the steady state (72). Finally, subpopulations of DCs expressing LC-specific markers were discovered in the steady state in skin-draining lymph nodes, but not mesenteric lymph nodes, implying that LC migration occurs at some basal rate without maturation-associated migration signals (73).

Differences from Other DC Subsets

While there are many similarities between LCs and other DCs in terms of phenotype and function, there are important intrinsic differences between these DC subpopulations. The most obvious difference comes in terms of distribution within the tissues of the body; LCs are by definition located within the epithelial tissues, whereas other DCs are found in the more internal compartments of the body. The reasons for this localization to the epidermis highlight additional features that set LCs apart from other DCs. LCs and their precursors, which have recently been shown to be cells of the monocyte lineage, express the chemokine receptor CCR6, the ligand of which, macrophage inflammatory protein (MIP)-3 α ,

is expressed profusely by epithelial cells (24,74). Uniquely among DCs, LCs express the cellular adhesion molecule, E-cadherin. Expressed by many cell types, especially cells in the epithelial tissues, E-cadherin is utilized by LCs as an anchor to maintain their positions within the epithelium (75,76). Expression of these proteins results in the recruitment of LCs precursors to the epithelial tissues and the retention of differentiated immature LCs therein.

The localization within the epithelium notwithstanding, LCs possess several unique features that set them apart from other DCs. Classically, the hallmark feature identifying LCs was the presence of so-called Birbeck granules in transmission electron micrographs of the skin (77). These cytoplasmic inclusions, which have a characteristic tennis-racquet shape, are now believed to be subcompartments of recycling endosomes that attain their shape after the accumulation of langerin, a LC-specific endocytic receptor (78-80). A member of the C-type lectin family, langerin has been shown to bind to various carbohydrate substrates, with a preference for mannosyl residues (81,82). While the loss of langerin expression in knock-out mice did not contribute to an overt change in LC function, it was recently discovered that langerin cooperates with another LC-specific protein in humans, CD1a, in the presentation of mycobacterial Ag to T cells. In these experiments, it was demonstrated that binding of non-peptide Ag to langerin on the surface of LCs resulted in their internalization and processing

for presentation on CD1a molecules to T cells (83). Thus, LCs possess unique characteristics that not only differentiate them from other DCs, but also allow them to perform distinctive functions in their role as sentinels of the environmental interfaces.

LCs and Corneal Immunobiology

As an epithelial tissue at the external interface with the environment, the cornea is protected against infectious pathogens and inflammatory insults by a network of immature LCs. However, the cornea has evolved to execute specialized functions that other epithelial tissues need not perform. Therefore, while they share to a great extent the biology of epidermal LCs, corneal LCs differ in the tissue microenvironment, developmental regulation, and physiologic and pathologic functions compared to other LC populations. As such, special note must be made regarding how the biology of the cornea could affect LC behaviors.

LCs in the Cornea and Ocular Immune Privilege

The immune system in the cornea has the dual task of protecting the tissues from external pathogenic insults while at the same time tempering immune responses that could potentially negatively affect vision. Similar to other

epithelial tissues, the first line of defense consists of physical barriers, such as the eye lids, lashes, and tear fluid, which prevent invading pathogens from gaining access to the underlying tissues. Beyond these defenses, the ocular tissues maintain a status of immune privilege, in which the immune system remains detached and uninvolved so as not to inadvertently initiate destructive responses. Multiple mechanisms have been elucidated that help contribute to this effect, including isolation of tissues via the blood-eye barrier and the avascular state of the cornea, constitutive expression of CD95 ligand, and the presence of immunomodulatory factors like transforming growth factor- β_2 in the aqueous humor (84,85). Finally, one mechanism believed to be important for the maintenance immune privilege in the cornea is the relative absence of APCs in that tissue, particularly the paucity of LCs within the central corneal epithelium (21,85-92).

Migration of Corneal LCs

In the steady state, LCs in the corneal epithelium are found within the peripheral regions of the cornea where transparent tissue of the cornea converges with the sclera, an area known as the limbus. Identifiable by the hallmark features of LCs, *id est*, the expression of CD11c and MHC II and the characteristic dendritic morphology, LCs in the cornea are believed to migrate into the central cornea in response to various inflammatory stimuli including thermal cautery

wounds, primary infection or reactivation of latent herpes simplex virus (HSV)-1, instillation of latex beads or formalin-killed *Staphylococcus aureus* into shallow incisions in the tissue, and even conjunctival inflammation or extended wear of contact lenses (21,93-99). Experimental evidence suggests that this centripetal migration is mediated by proinflammatory cytokines released by injured epithelial cells in the central cornea, for LC migration can be abrogated by anti-IL-1 Abs or IL-1 receptor antagonist (IL-1Ra) (21,100,101). Furthermore, mice lacking either TNF receptor I or II showed markedly impaired LC migration in response to inflammatory stimuli (102).

While the appearance of LCs in the central cornea in fixed time-course samples was traditionally thought to be the result of physical migration of cells from the limbus, recent evidence suggests that LCs may arise from precursor cells distributed throughout the corneal epithelium. Unlike the conventional LCs that express CD45, CD11c, and MHC II and are restricted to the limbus, the precursor cells express only CD45 and CD11c in the steady state and acquire MHC II expression after inflammatory stimuli (103,104). These observations challenge the idea of centripetal migration of LCs during corneal inflammation, implying instead a maturation of cells into MHC II-expressing LCs.

IMAGING THE IMMUNE SYSTEM

In recent years, an explosion of technological breakthroughs has occurred that has opened the door to waves of innovative experimentation that have greatly expanded the bounds of our scientific knowledge. Milestone achievements like the development of the polymerase chain reaction, high-throughput nucleotide sequencing, and gene chips have enabled investigators to make incredible strides in fields such as molecular biology, genomics, biophysics, and immunology. The development of new imaging modalities has, in particular, facilitated a renaissance in our understanding of cellular behaviors and interactions and of how essential these phenomena are to biological processes.

Imaging Technologies

While video microscopy and bright field imaging remain staples of microscopic examination, the majority of current imaging techniques rely on the emissions of fluorescent chemicals or proteins to track species within the imaging field. The discovery and development of protein fluorophores and microscopic apparatus that can image three-dimensional structures at high resolutions has above all facilitated the observation of specific structures cells or cells within living tissues.

Confocal Laser Scanning Microscopy

Though the theory was first postulated by Marvin Minsky in 1953, the use of confocal microscopes was not practical until the development of efficient lasers towards the end of the 1980s. The strength of the confocal microscope lies in its ability to create optical sections, blur-free images taken at the exact focal plane of the optics, through the use of a series of tiny apertures, or pinholes, within the light collection path. Laser light shone through the excitation pinhole is focused onto the sample via an objective lens, where it is absorbed by fluorophores in the sample and elicits fluorescent emission. Fluorescent light is collected by the same objective lens and focused back through a second pinhole to a detector such as a photomultiplier tube. As the two pinholes are aligned at the same focal length from the objective lens (hence, confocal), only fluorescence from focal point of the objective is collected by the detector; the remaining light from fluorescence above and below the focal point is descanned, or blocked from the detector by the pinhole aperture (Figure 1). As a consequence of the confocal principle, fluorescence is detected only at a very tiny point, and therefore the focal point is moved in a scanning motion through the sample to generate an image of the entire microscopic field.

Interestingly, by moving the sample in relation the focal point, an image can be acquired of an optical section at a different depth in the tissue, and thus confocal microscopy can be used to generate high resolution, three-dimensional images of tissue samples (105-108). The mechanical movements that regulate the scanning pattern and imaging depth represent the technological roadblock in terms of the speed at which images can be acquired, but after years of development, the speed of confocal microscope has increased to the point that it is well suited for time-lapse imaging of living cells (109,110). Even more impressively, some investigators have even used confocal microscopy to explore the biology of cells within living subjects (111-114).

Multiphoton Laser Scanning Microscopy

First proposed by Maria Göppert-Mayer in her doctoral dissertation, the theory of multiphoton fluorescence excitation is similar in character to that of standard fluorescence excitation. Wherein a photon of light at a given energy is absorbed by a fluorophore to induce fluorescent emission by conventional illumination, two or more photons of lower energy are absorbed at the same time by the same electron to produce fluorescent emission with multiphoton excitation (Figure 2). Because the absorbing electron will return to its unexcited state fairly quickly after absorption of low energy photons, the window in which the two or more photons must be absorbed is exceedingly small and necessitates an

enormous flux of photons to increase the probability for this absorption to occur. For many years, however, a laser source capable of generating that kind of output was not practically available. The breakthrough came in the development of pulsed lasers, such as the Ti:sapphire tunable lasers, which generate brief (on the order of femtoseconds) pulses of intense laser light between periods of inactivity at a rate of approximately 80 Hz. While the overall output is modest, the photon flux during the pulses is sufficient to induce multiphoton absorption. Moreover, the flux of photons is high enough for excitation only at the focal point of the objective lens, where the laser light is focused and concentrated. This property results in inherent optical slicing, as fluorescence only occurs at the focal point, and was utilized to generate three-dimensional microscopic images for the first time in the early 1990s (115).

By its nature, multiphoton microscopy is well suited to the examination of biological processes. First, because of the intrinsic optical sectioning, the fluorescence emissions need not be descanned at the detector by a pinhole, and thus all the emitted light can be collected, resulting in little loss of information. Also, the longer wavelength light used in multiphoton excitation penetrates farther into the tissues, allowing for deeper imaging of structures than is possible with conventional fluorescence or even confocal microscopy. Lastly, the low energy photons of the excitation light transfer less energy to the sample being

examined, and thus result in less tissue damage and photobleaching (116).

Indeed, investigators have utilized this technique to observe the interaction of living cells in culture, as well as in living organisms (117-124).

Second Harmonic Generation

Taking advantage of a unique property of non-linear crystalline structures, second harmonic generation (SHG), or frequency doubling, has become a useful tool for the study of biological systems. For instance, collagen bundles, owing to their repetitious, highly crystalline triple helix structures, possess the ability to retransmit photons at exactly half the wavelength of the original incident light (125). As such, it has provided investigators with a means to locate and delineate specific tissues and regions within the body (126-128). Since the frequency-double light is detected principally in light transmitted through the sample, the utility of SHG was basically limited to ex vivo preparations. However, several breakthroughs and innovations in illumination and detection have facilitated the examination of frequency-double light reflected back from biological samples. Thus, investigators now use SHG as an important tool in the examination of living tissues (129,130).

Detection of Light Emitted from Fluorescent Proteins

The advent of fluorescent proteins has revolutionized the field of microscopic examination of biological specimens. First isolated from the jellyfish *Aequorea victoria* in early 1960s, the green fluorescent protein started a transformation in the way proteins and cells are studied and has served as the basis for the development of further fluorescent proteins for biological experiments (131). Currently, fluorescent proteins are available that emit light in the blue, cyan, green, yellow, orange, red, and far red spectrums of visible light. Even after development and modification of these proteins through mutational analysis, it remains that the proteins in the cyan, green, and yellow spectra exhibit the best biological, spectral, and quantum features for use in microscopic studies. However, the overlapping nature of their emission spectra makes the use of these proteins in the same sample problematic for detection by conventional means. To compensate for this, detection of the entire emission spectrum for each protein can be used to distinguish between them (132,133). By analyzing the emission spectrum for each pixel scanned with a confocal or multiphoton microscope, computer software is able to separate the fluorescence signals of multiple spectrally-similar fluorophores using an algorithm called “linear unmixing” (134-136). Therefore, the simultaneous use of multiple fluorescent proteins or dyes has allowed investigators to fully explore multiple, complex biological interactions.

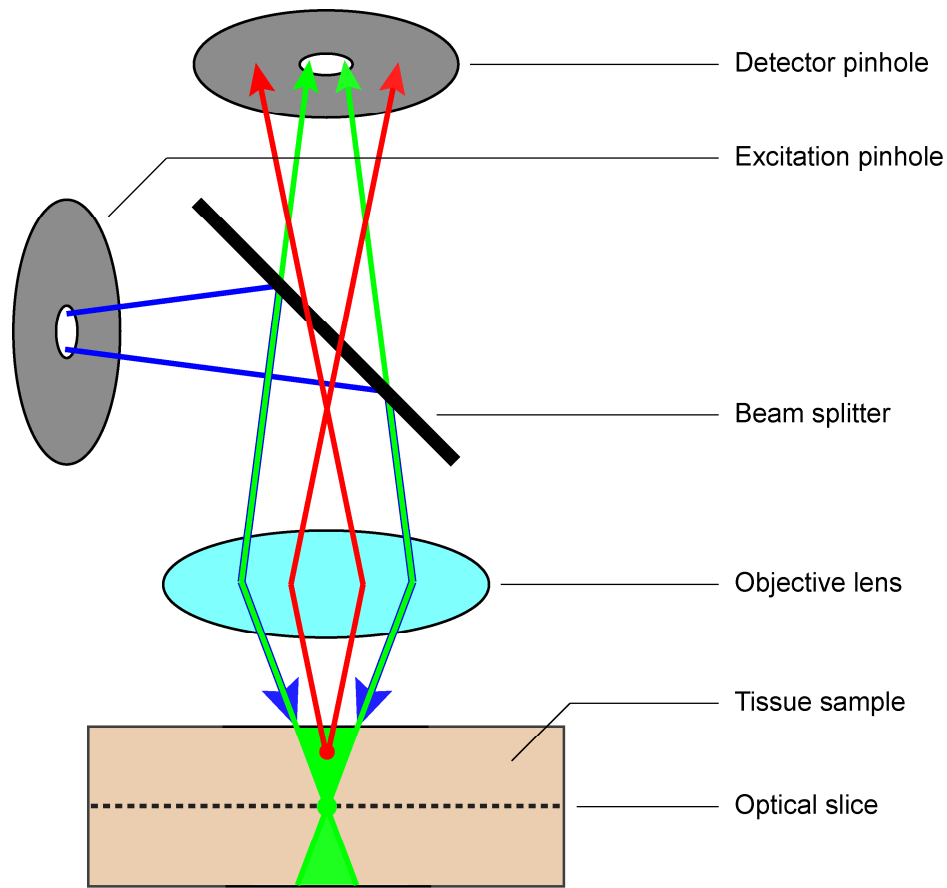


Figure 1. Schematic illustration of the confocal principle.

Light from an excitation source such as an ArKr laser (blue arrows) is shown through the excitation pinhole and focused onto the sample via an objective lens. Fluorescent light emitted from the sample is focused back through the same objective lens to a beam splitter, which allows the emitted light (and not the excitation light) to reach the detector pinhole. Light emitted at the focal point (green arrows) passes through the pinhole and is detected by a photomultiplier tube. Fluorescence from above or below the focal point (red arrows) arrives at the detector pinhole out-of-focus, and thus is blocked from passing through aperture. Fluorescence from the entire sample is collected by moving the focal point through the tissue in a scanning motion. Since only information at the focal point is acquired, the resulting image represents a single plane, or optical slice, within the tissue.

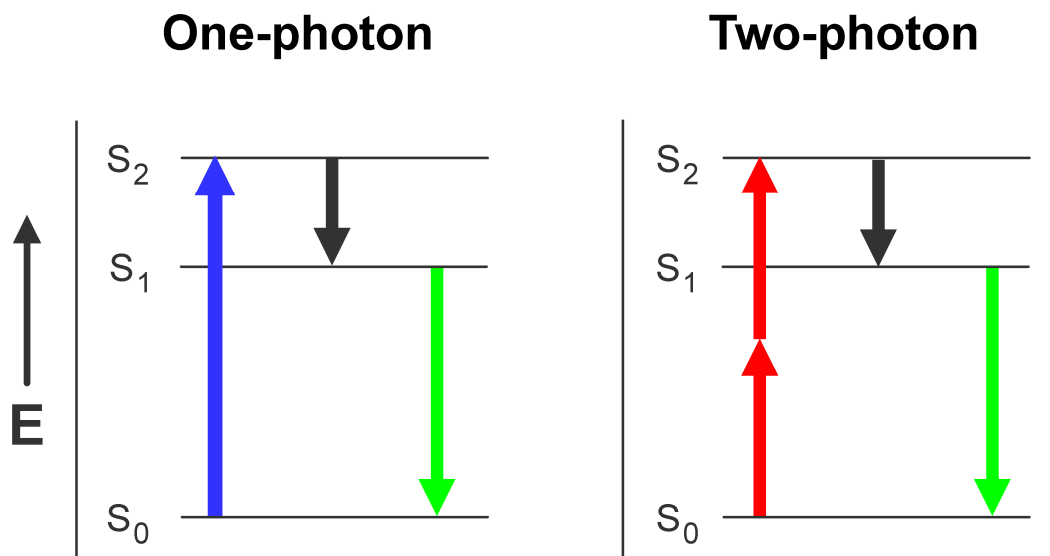


Figure 2. Fluorescence by one- or two-photon excitation.

In conventional one-photon fluorescence excitation, a single high energy photon (blue arrow) is absorbed by an electron in the fluorophore. The energy imparted by the photon causes the electron to jump from the ground state (S_0) to a high energy excited state (S_2). Some of the energy is released by the electron back to the environment in a process known as non-radiative relaxation (black arrow), and the electron reaches a medium-energy excited state (S_1). The electron then falls back to the ground state, releasing the remaining energy as a photon of slightly less energy (green arrow) as the original excitation light. In two-photon excitation, two low energy photons (red arrows) are absorbed at the same time by a single electron. As the electron falls back to the ground state, a single higher-energy photon is released.

CHAPTER THREE

Materials and Methods

LC BEHAVIORS UNDER PHYSIOLOGIC CONDITIONS

Generation of EGFP⁺ Corneal LC *In Situ*

Animals

Mice expressing the enhanced green fluorescent protein (EGFP) under the control of the chicken β -actin promoter and cytomegalovirus enhancer on a C57Bl/6 background (137) were purchased from Jackson Laboratories (Bar Harbor, ME), and breeding colonies were established at the University of Texas Southwestern Medical Center (Dallas, TX). Tibias and femurs were surgically excised from a pair of mice, and all tissue was removed from the bone shafts using a scalpel blade under aseptic conditions. The ends of the bones were removed, and the marrow cavity was lavaged using a 3 ml syringe with a 27 gauge needle filled with Hank's balanced salt solution (HBSS). Bone marrow cells (BMCs) were resuspended by repeated pipetting and then spun down for 10 minutes at 400 x g at 4° C. Supernatants were removed and the cells were resuspended in 3 ml red blood cell (RBC) lysing buffer (Sigma Aldrich, St. Louis, MO), and then 3 ml fetal calf serum (FCS) were underlaid beneath the BMC suspension. The cells were allowed to incubate on ice for 3-4 minutes, at which

point the cell suspension was spun down as above. The cell suspension was washed twice in HBSS, and then finally resuspended in 3.5 ml of HBSS.

Ten sex-matched, 8-10 week old wild-type C57BL/6 recipient mice were prepared for the bone marrow transplant by administration of 500 rads of γ -radiation. After a 3-hour rest period, the mice were given an additional 450 rads of radiation. Each animal was then given 300 μ l of BMC suspension ($\sim 10^7$ cells) via tail-vein injection with a 27 gauge needle. The animals were allowed to recover and were watched closely for the next several days.

Flow Cytometric Examination of Bone Marrow Chimerism

In order to confirm the successful engraftment of the EGFP⁺ hematopoietic stem cells and the resultant reconstitution of the immune system, various tissues in the recipient mice were examined for EGFP expression 10-12 weeks after BMC transplantation. To obtain peripheral blood leukocytes, several drops of blood were collected in heparinized capillary tubes from the lateral tail vein of chimeric mice. Blood samples were added to microcentrifuge tubes containing 70 μ l heparin sodium solution (Pharmacia & Upjohn, Kalamazoo, MI) and kept on ice until all samples were collected. Into each tube, 500 μ l of RBC lysing solution were added, and the tubes were incubated at room temperature for 10 minutes. Cells were spun down for 1.5 min at 800 x g at room temperature in a

tabletop microcentrifuge. Supernatants were removed, and the cells were then washed twice in 500 μ l HBSS + 2% FCS.

To collect splenocyte samples, EGFP chimeric mice were sacrificed, and the spleens were removed via a small incision in the left flank. The spleens were dissociated by pressing the organ between the frosted ends of two autoclaved microscope slides in 35 mm Petri dish containing HBSS. The cells were resuspended by repeated pipetting, and then passed through nylon mesh into microcentrifuge tubes. The samples were spun down for 10 minutes at 400 x g at room temperature, after which the supernatants were removed. The samples were then washed twice in 500 μ l HBSS + 2% FCS.

Peripheral blood leukocyte and splenocyte suspensions were resuspended in HBSS + 2% FCS and stained with R-phycoerythrin (PE)-conjugated monoclonal antibodies (mAb) against CD45, CD3, B220, CD11b, or CD11c (all from BD Biosciences – Pharmingen, San Diego, CA) at a 1:200 dilution. After 30 minutes incubation at 4° C, the samples were spun down and washed twice with HBSS + 2% FCS. Cells were resuspended in 500 μ l HBSS + 2% FCS, passed through nylon mesh into plastic FACS tubes, and then examined using a FACSCaliber flow cytometer (BD Biosciences – Immunocytometry Systems, San Jose, CA). Populations were gated on live cells using forward scatter and side

scatter, and the relative expression of both EGFP and the above cell surface proteins was collected. Analysis of the flow cytometry data was carried out using the CellQuest (BD Biosciences – Immunocytometry Systems) and WinMDI (The Scripps Research Institute, La Jolla, CA) software packages.

Static Imaging of Corneal LCs in Situ

The extent of reconstitution and the distribution of immune cells within the cornea were examined by whole mount immunofluorescent staining. Bone marrow (BM) chimeric and wild-type mice were sacrificed, and enucleated eyes were immersed in 4% paraformaldehyde in PBS for 2 minutes at room temperature. Corneas were then excised by carefully cutting around the corneal-scleral border with microdissection scissors. The lens, iris, and any remaining extraneous tissues were removed, and four small, radial cuts were made along the edge of the cornea, equidistant to one another, to better allow the cornea to lay flat. The samples were fixed in 4% paraformaldehyde for an additional 15 minutes at room temperature, and then washed in PBS on a table-top rocker. The corneas were blocked with 1% bovine serum albumin in PBS with or without goat serum diluted 1:50, stained overnight with mAb against CD45, MHC II, CD11b, CD3, B220, or Gr1 (BD Biosciences – Pharmingen), or F4/80 (Serotec, Raleigh, NC), and washed extensively. The samples were then mounted to microscope slides using gel/mount mounting medium and examined using a Zeiss LSM 510

META confocal microscope with a Zeiss 10x Plan-NEOFLUAR objective (numerical aperture (NA) 0.30). Overlapping fields of view covering the entire cornea were collected. Maximum intensity projections of these data sets were created, and the numbers of cells expressing the above cell surface markers were counted using the MetaMorph (Molecular Devices, Downingtown, PA) and ImageJ (National Institutes of Health, Bethesda, MD) software packages.

To quantify the distribution and phenotype of LCs in the corneal epithelium of chimeric mice, enucleated eyes were incubated in 20 mM EDTA in PBS for 3 hours at 37° C, causing the corneal epithelium to dislodge from the underlying stroma. Four small cuts were made to the periphery of the resulting corneal epithelial sheets, as above, in order for them to lay flat. The samples were then fixed in 4% paraformaldehyde for 20 minutes at 4° C, and washed as above. Samples were then stained with PE-conjugated mAb against CD11c or MHC II (BD Biosciences – Pharmingen), washed, and mounted to microscope slides for examination under an Olympus BX60 fluorescence microscope with 10x or 20x Olympus UPlan FI objectives (NA 0.30 or 0.50, respectively) using a Sensys digital camera system and MetaVue software (Molecular Devices). Cells expressing EGFP, CD11c, and/or MHC II were then quantified using MetaVue.

To examine the spacial relationships of LCs to epithelial cells in the cornea, whole corneal samples, prepared as above, were fixed in 4% paraformaldehyde in PBS, washed, labeled with propidium iodide, and mounted to microscope slides. Three-dimensional image data sets of the samples were then collected using a Leica TCS SP2 confocal microscope with a Leica 40x air objective and a 63x water immersion objective (NA 0.85 and 1.20, respectively). Maximum intensity projections and three-dimensional reconstructions of the data sets were created using the Leice Confocal Software (LCS, Leica Microsystems, Exton, PA) software package.

Visualization of EGFP⁺ LCs in Living Corneal Tissue

Corneal Organ Culture

A 1 mm wide anterior-posterior slice was made through a freshly enucleated eye using a specially constructed knife consisting of two parallel razor blades. The slice was centered so as to incorporate the maximum possible area of the cornea. The sample was rid of the lens and iris and then cut at the posterior pole. The resulting strip of corneal tissue was draped over the aperture of a Tissue Slice Adapter (Bioptechs, Butler, PA), centered with the cornea within the aperture, and secured in place with a rubber washer. The sample was placed into a Delta T4 culture dish (Bioptechs) and perfused by microperfusion pump at 200-

300 μ l/min with complete RPMI 1640 medium (cRPMI, supplemented with 20 μ M L-glutamine, 100 μ M nonessential amino acids, 100 U/ml penicillin, 100 μ g/ml streptomycin, 0.25 μ g/ml amphotericin B, 10 μ M sodium pyruvate, and 50 mM HEPES) aerated with 5% CO₂ in air. Temperature in the culture dish was maintained at 37° C using a Delta T4 Controller (Bioptechs).

Time-lapse Imaging Studies

Corneal samples in Delta T4 culture dishes were secured via a T4 adapter plate (Bioptechs) to a Leica TCS SP2 multiphoton microscope equipped with a Mira 900F Ti:sapphire laser (Coherent, Santa Clara, CA). Two-photon excitation was achieved at a wavelength of 860 nm, and images were collected using non-descan detectors and 10x or 20x Leica Plan Apo objectives (NA 0.40 or 0.70, respectively). Three-dimensional image stacks (~20 sequential axial images with an average x-y-z voxel size of approximately 460 nm x 460 nm x 1.5-5.0 μ m) were collected every 2 minutes for up to 5 hours. The z-axis range was chosen to include all the dendritic processes of the LCs that may have extended upward (up to 10-20 μ m) from the cell bodies. Additionally, the number of planes was chosen so as to minimize the scan time (~1 min/stack), preventing excess photobleaching and allowing the tissue to recover between scans.

Image Analysis and Quantification

Maximum intensity projections of the time-lapse data sets were created using the LCS and MetaMorph software packages. Using the known x-y voxel distance for each data set, the lengths of the LCs' dendrites were calculated from the maximum intensity projections. Dendrite length was defined as the linear distance from the tip of a dendrite to the point of attachment at the cell body. For observations of lateral migration by LCs, each data set was corrected for any x-y drift using the Align Stack command in MetaMorph with a ' $n-1$ ' reference plane. To analyze the periodicity of LC dendrite movement, data were subjected to Fourier analysis using MATLAB software (The Math Works, Natick, MA). Briefly, the lengths of individual dendritic processes over time were normalized about zero, and a fast Fourier transform was then applied to the data set. Power spectra were created by multiplying the transforms by their conjugates and dividing by the number of data points. A weighted mean period was calculated for each cell by dividing the sum of (period x power) values for all dendrites on that cell by the sum of the power values.

Dynamic Behaviors of Epidermal LCs *Ex Vivo*

Animals

To visualize LC in the epidermis, I-A β -EGFP knock-in mice (138) were obtained from Dr. Hidde Ploegh at the Massachusetts Institute of Technology, and breeding colonies were established at the University of Texas Southwestern Medical Center.

Characterization of LCs in the Epidermis of I-A β -EGFP Knock-in Mice

To determine the identity of the EGFP⁺ cell populations in the skin of knock-in mice, epidermal sheets were prepared from ear skin samples by 60 min incubation in 20 mM EDTA in PBS at 37° C, fixed in 4% paraformaldehyde for 30 min at room temperature, and then stained overnight with PE-conjugated anti-CD11c mAb (BD Biosciences – Pharmingen) or anti-langerin hybridoma supernatant (clone 929F3, kindly provided by Dr. Nikolaus Romani at Innsbruck Medical University). The numbers of cells expressing EGFP, CD11c, and/or langerin were counted under an Olympus BX60 fluorescence microscope with an Olympus 40x UPlan Fl objective (NA 0.75) using a Sensys digital camera system and MetaVue software.

Ex Vivo Imaging of Ear Skin Samples by Confocal Microscopy

To observe the behaviors of epidermal LCs, ear skin samples were harvested from I-A β -EGFP knock-in mice 3 days after removal of the hair with Nair® (Church & Dwight, Princeton, NJ) and separated into dorsal and ventral halves with forceps. The dorsal halves were draped over the aperture of the tissue slice adapter (Biopetechs) and secured in place with a rubber o-ring, then placed into a Delta T4 culture dish. The temperature of the sample was controlled by the Delta T4 Controller via an electrically conductive coverslip bottom on the culture dish, which was continuously perfused with aerated cRPMI. Three-dimensional image sets, consisting of 20 sequential x-y images separated by 1.0 to 2.6 μ m, were acquired every 5 minutes for up to 4 hours using a Leica TCS SP2 confocal microscope with a Leica 20x Plan Apo objective (NA 0.70) and 488 nm excitation.

Observation of LC Behaviors in Living Animals

Intravital Imaging of Epidermal LC Behaviors

To assess the behaviors of epidermal LCs in living animals, EGFP⁺ LCs in the ear skin of anesthetized mice were examined by time-lapse confocal microscopy. I-A β -EGFP knock-in mice were anesthetized by intraperitoneal (i.p.) injection of the mouse anesthetic cocktail (ketamine 100 mg/kg, xylazine 10

mg/kg, and acepromazine 1 mg/kg) and placed onto the stage of a Zeiss LSM 510 META confocal microscope with the dorsal side of the ear, which was held in place with a microscope slide, facing down. The temperature of the mouse was maintained while anesthetized via a surgical heating pad, and oxygen was administered via an inhaler throughout the duration of the experiment. Three-dimensional image sets of EGFP⁺ within the ear skin were then recorded every 2 min for up to 2 hours.

Quantification of Epidermal LC Behaviors Monitored In Vivo

Using the ImageJ software, maximum intensity projections were created of the time-lapse three-dimensional data sets. As a measure of the total activity of dSEARCH, the dSEARCH index was calculated for EGFP⁺ epidermal LCs in I- β -EGFP knock-in mice. The dSEARCH index was defined as the total change in dendrite length for a given cell over a 6 minute period, chosen arbitrarily. First, the lengths of all dendrites for a given cell were measured using ImageJ. Next, the lengths of the same dendrites were measured again after advancing the projection 6 min. Finally, the absolute values of the changes in length were calculated, and then summed to obtain the dSEARCH index value for that cell over that 6 min interval, and the process was repeated for the entire imaging period. The size and EGFP fluorescence intensity for each LC were measured using MetaMorph. A Pearson correlation test was applied to the data to determine

the significance of the correlation between dSEARCH index and LC size or EGFP fluorescence intensity.

LC BEHAVIORAL RESPONSES TO LOCAL TISSUE INJURY

Corneal LC Responses to Pinpoint Thermal Injury

Infrared Pinpoint Thermal Injury

To observe the responses of LCs to local tissue injury, corneal samples from EGFP BM chimeric mice were prepared and cultured as above. Multiphoton excitation at a wavelength of 860 nm was used to record three-dimensional image stacks every 2 minutes for 1 hour on a Leica TCS SP2 microscope with a Leica 20x Plan Apo objective (NA 0.70). At this point, an appropriate LC target was chosen and a single x-y plane image was scanned to mark the state before injury. The infrared laser of the multiphoton system was then set to maximum output, and the bleach function of the LCS software was used to expose a single-pixel region of interest (ROI) to the laser for 1 minute. With these settings, >23 joules of energy were delivered to an area of approximately $0.25 \mu\text{m}^2$ over the 1 minute span. A single x-y plane image was scanned to judge the effectiveness of the injury. Three-dimensional image stacks were then recorded every 2 minutes for an addition 3 hours.

Quantification of LC dendrite activity

To quantify changes in dendrite activity, the dSEARCH index was calculated for each cell before and after injury. To calculate this value, maximum intensity projections of the data sets were created, and all the dendrites of a given LC (including branches) were traced at time 0 using the LCS software. The projection was advanced 6 minutes, and the distances between the ends of the tracings and the tips of the dendrites and/or the border of the cell body at the current time point were recorded. The sum of these distances is equivalent to the dSEARCH index for that cell at $t = 6$ minutes. The procedure was then repeated until the dSEARCH index had been calculated for the entire data set.

Quantification of LC migration

The migration of LCs in response to thermal injury was examined in a similar fashion as above. Maximum intensity projections of the data sets were created using the LCS software. The projections were aligned to correct for lateral drift using the Align Stack command in MetaMorph. The Track Points command was then used to manually mark the center of the cell body at all time points. Finally, the coordinates of the cell body positions were used to calculate the distances traveled between frames (i.e., every 2 minutes) for each cell.

Statistical Analyses

The data for dSEARCH index and traveled distance per frame for each cell were split into four groups: before injury, the first hour after injury, the second hour after injury, and the third hour after injury. Mean dSEARCH index and mean traveled distance values were then calculated for each cell for each category. As the data represented repeated measures of the same cells before and after injury, paired Student's *t*-tests were used to compare the mean values before injury to those in the three post-injury phases.

Mechanisms of Corneal LC Responses to Thermal Injury

Inhibition of LC behavioral responses to pinpoint thermal injury

To explore the mechanisms behind the injury-provoked behavioral responses by LC, IL-1Ra was used to block IL-1 signaling. Mouse recombinant IL-1Ra (R&D Systems, Minneapolis, MN) was added to 15 ml complete RPMI 1640 to achieve a final concentration of 200 ng/ml. Corneal organ cultures were prepared using the IL-1Ra-containing media, which was recirculated between the Delta T4 culture dish and a 15 ml culture tube using the microperfusion pump. Multiphoton excitation was used to collect 3D image stacks every 2 minutes for 1 hour. The infrared laser was used to deliver a pinpoint thermal injury to a LC

target as above. Three-dimensional data sets were collected every 2 minutes for an additional 3 hours, all in the presence of IL-1Ra.

Provocation of LC Behavioral Responses by Cytokines

Corneal samples were prepared as normal and imaged by multiphoton microscopy every 2 minutes for 1 hour. At this point, the microperfusion pump supplying medium to the culture dish was turned to the maximum and the medium perfusing the organ culture was purged from the system. Complete RPMI 1640 containing mouse recombinant IL-1 α at final concentration of 5 pg/ml or 100 pg/ml was then circulated through the culture system, and 3D image stacks were collected every 2 minutes for an additional 3 hours. In a different set of experiments, corneal samples were observed for 1 hour as normal. After purging the medium from the system, complete RPMI 1640 containing 50 pg/ml mouse recombinant TNF α was pumped through the culture system, and the samples were imaged for an additional 3 hours.

Epidermal LC responses to Diffuse Inflammatory Stimuli *Ex Vivo*

Overnight culture of Skin Samples

As one model of diffuse inflammation that causes LC maturation, ear skin samples were collected from I-A β -EGFP knock-in mice and cultured overnight

(139-141). Samples were harvested from the mice and separated into dorsal and ventral halves using forceps. The dorsal-side samples were floated on cRPMI and cultured at 37° in a tissue culture incubator for 16 hours. To observe the behaviors of EGFP⁺ LC in the ear skin, the samples were mounted onto the tissue slice adapter (Biopetechs) and placed into the Delta T4 culture system, with constant circulation of aerated medium and temperature control, as above. Three-dimensional data sets (20 sequential axial planes separated by 1.0 to 2.6 μm) were collect every 5 minutes for up to 4 hours using a Leica TCS SP2 confocal microscope with a Leica 20x Plan Apo objective (NA 0.70) and 488 nm excitation.

Ex Vivo Behaviors After Injection of TNF α

To mimic an inflammatory response, the ears of I-A β -EGFP knock-in mice were injected with 50 ng mouse recombinant TNF α (R & D Systems) in 40 μl PBS (142). Ear skin samples were harvested 16 hours after injection, placed into the Delta T4 organ culture system, and immediately imaged by confocal microscopy. Three-dimensional data sets were collected every 5 min for up to 4 hours, and analysis of the LC behaviors in the sample was carried out on maximum intensity projections of the image sets.

Quantification of LC Behaviors Monitored Ex Vivo

As a measure of total dendrite activity, the dSEARCH index was calculated for each LC. Maximum intensity projections of the data sets were created and the lengths of all the dendrites of a given LC were measured using LCS. The lengths of the dendrites were measured again after advancing the data set 5 min. The absolute values of the changes in dendrite length over the 5 min period were summed to obtain the dSEARCH index value. The procedure was repeated over the entire imaging period for each cell. To measure the extent of lateral migration, the maximum intensity projections were aligned to correct for lateral drift using the Align Stack command in MetaMorph. The Track Points command was then used to manually mark the center of the cell body at all time points. Finally, the coordinates of the cell body positions were used to calculate the distances traveled between frames (i.e., every 5 minutes) for each cell. Statistical differences in the dSEARCH index values and lateral migration values between groups were calculated by Mann-Whitney *U*-test.

Epidermal LC Responses to Reactive Hapten *In Vivo*

Intravital Imaging of LCs After DNFB Application

To investigate the *bona fide* behavioral responses to inflammatory stimuli in living animals, a reactive hapten was applied to the ears of I-A β -EGFP knock-

in mice (143-145). To reduce the autofluorescence and light scattering associated with the hair shafts and follicles in the skin, the ventral ear skin of knock-in mice were treated with Nair (Church & Dwight) three days prior to imaging experiments. Using a sterile pipet tip, 20 μ l of a 0.5% dinitrofluorobenzene (DNFB) solution in 3:1 mixture of acetone and olive oil were applied to the ventral surfaces of the ears. After 30 hours, the mice were anesthetized by i.p. injection of the anesthetic cocktail, and the ears were mounted to the microscope stage, as above. Three-dimensional data sets of EGFP⁺ epidermal LCs were collected every 2 min for up 2 hours, with the temperature of the mice regulated by a heating pad and oxygen delivered via an inhaler throughout the imaging period. In some experiments, ears were imaged without any treatment or 30 hours after application of 20 μ l vehicle alone. The dSEARCH index values for the EGFP⁺ LCs were calculated as described for the observation of LC behaviors in the steady state *in vivo*, and lateral migration was quantified as described above. Statistical differences between treatment groups were determined by Mann-Whitney *U*-test.

LC BEHAVIORAL RESPONSES TO PATHOGENIC ORGANISMS

Development of Fluorescent Bacterial Cells

Tn7 Transformation of Bacterial Cells

Pseudomonas aeruginosa, an easily cultured bacterial species that is able to infect various epithelial tissues, was chosen as a model bacterium for infection of both the cornea and epidermis. In order to observe the interactions of EGFP⁺ LCs with bacterial cells, the *P. aeruginosa* strain PA01 was transformed to express fluorescent proteins using the mini-Tn7 transposon system (146). The component plasmids for the mini-Tn7 transposon system, developed for use in *Pseudomonas* species by Søren Molin and colleagues, were obtained by Kevin McIver in the Department of Microbiology at the University of Texas Southwestern Medical Center. The delivery plasmids miniTn7(Km,Sm)*P*_{A1/03/04}—*ecfp*-a, miniTn7(Km,Sm)*P*_{A1/03/04}—*eyfp*-a, and miniTn7(Km,Sm)*P*_{A1/03/04}—DsRedExpress-a were harbored in *Escherichia coli* strains MT102 (ECFP and EYFP) and JM105 (DsRedExpress). The helper plasmid pUX-BF13 and the conjugation plasmid pRK-2013 were contained in the *E. coli* strains SM10/*λpir* and MM294, respectively.

The Tn7 transposon was introduced into the PA01 cells using the conjugation reaction developed by Lambertsen, et al (147). Briefly, cultures of the recipient strain, helper strains, and delivery strain were grown overnight in Luria Bertani (LB) broth cultures. After a short growth period in fresh media, the cultures were mixed together and filtered onto a 25 mm polycarbonate conjugation filter (0.22 μm pore size). The filters were placed onto an LB agar plate and incubated overnight at 37° C. The next day, the bacteria were resuspended in PBS by vortexing the filter disks and then plated on *Pseudomonas* conjugation agar plates and cultured overnight. Fresh overnight LB broth cultures using kanamycin at 150 $\mu\text{g/ml}$ were made from colonies isolated off the conjugation agar plates to select for cells containing the transposon, and sterile glycerol was added to a final concentration of 20% by volume to create a stock culture that was stored at -80° C. Fresh liquid cultures were made from the frozen stock culture in LB broth.

CMTMR Labeling of Bacterial Cells

To generate bacterial cells that could be detectable by the confocal microscope, cells of the *P. aeruginosa* strain PA01 were labeled with the cell tracking dye, 5-(and-6)-(((4-chloromethyl)benzoyl)amino)tetramethylrhodamine (CMTMR). Normal PA01 cells were grown in overnight LB broth cultures from the frozen stock culture. The bacterial cells were resuspended in PBS containing

0.5 mM EDTA and 100 μ M CMTMR and incubated for 45 min at 37° C. After being resuspended in fresh LB broth and incubated an additional 30 min at 37° C, the cells were extensively washed in PBS before being used for experiments.

Fluorescent Protein Expression in Escherichia coli Cells

Escherichia coli strains containing the enhanced cyan fluorescent protein or the enhanced yellow fluorescent protein genes under the control of the Plac promoter in the *Pseudomonas aeruginosa* shuttle vector pUCP18, DH5 α (pUCP18-CFP $_{+++}$) and DH5 α (pUCP18-YFP $_{+++}$), was developed by Søren Molin and colleagues and obtained via Dr. Kevin McIver. An overnight culture was grown in LB broth containing 100 μ g/ml ampicillin (to maintain plasmid selection pressure) at 37° C with shaking. Sterile glycerol was then added to achieve a final concentration of 20% by volume, and this solution was frozen and maintained at -80° C to create a stock culture. For all experiments, a small amount of frozen stock culture was inoculated directly into a sterile plastic culture tube containing 5 ml LB broth with 100 μ g/ml Amp, which was then incubated 18 hours at 37° C with shaking. Fresh cultures were made from the frozen stock each day so as to maintain consistent culture conditions across experiments.

Behavioral Responses of Epidermal LCs to Bacterial Cells *In Vivo*

EGFP and EYFP Spectral Characteristics

Because the emission spectra of EGFP and EYFP overlap extensively, the spectral characteristics of the EGFP-expressing mice and EYFP-expressing bacteria were examined. An overnight culture of DH5 α (pUCP18-YFP $^{+++}$) was grown, as above, and 5 μ l of culture were mounted to a microscope slide. Additionally, the hair on the ears of an I-A β -EGFP knock-in mouse was removed with Nair. The mouse was then sacrificed and the ears removed. Ears were split into dorsal and ventral halves with forceps, and the ventral halves were discarded. One dorsal ear skin sample was mounted epidermal-side up to a microscope slide using gel/mount tissue mounting medium. The second sample was also mounted onto a microscope slide, epidermal-side up, after 5 μ l of bacterial culture had been placed onto the skin surface.

The samples were then examined under a Zeiss LSM 510 META confocal microscope using a Zeiss 40x Apoplan water dipping objective (NA 0.80). A lambda scan was collected from 494 nm to 719 nm at 10 nm intervals for the skin sample without bacteria, using 488 nm excitation. A single-pixel ROI was selected within a LC, and the spectral profile for that point was saved. A lambda scan was collected for the bacterial culture using the same excitation wavelength

and settings as above, and a spectral profile was saved from an ROI located within a bacterial cell. Finally, to ensure adequate spectral information was collected, a lambda scan of the sample containing skin plus bacteria was collected with the same excitation and settings as above. Linear unmixing was performed on the resultant lambda scan using the spectral profiles collected for the EGFP and EYFP, and good separation was noted between the two fluorophores.

In Vivo Imaging of LC

I-A β -EGFP knock-in mice were anaesthetized by i.p. injection of the anesthetic cocktail. To enhance the quality of the confocal images, hair was removed from the dorsal sides of the ears with Nair at least 48 hours beforehand. The animals were placed onto the stage of a Zeiss LSM 510 META confocal microscope with the dorsal side of the ear down, and the ear was held in place with a microscope slide. Confocal images were acquired using 488 nm excitation via a Zeiss 40x Apoplan water dipping objective (NA 0.80). Three-dimensional image stacks (consisting of 20 sequential axial scans with an x-y-z voxel size of 450 nm x 450 nm x 1.0-2.0 μ m) were collected every 4 minutes for up to 3 hours. The body temperature was maintained using a surgical heating pad (Gaymar, Orchard Park, NY), and half- or full-dose administrations of anesthetic cocktail were given every hour or as needed via i.p. injection.

Tape Strip Model of Infection

A culture of DH5 α (pUCP18-YFP $_{+++}$) was started as above. After 18 hours, 1 ml of culture was spun down at 16,000 x g for 5 minutes in a tabletop centrifuge. The supernatant was removed, and the cells were resuspended in 40 μ l PBS. Scotch tape was applied and removed from the dorsal surface of the ear of an I-A β -EGFP knock-in mouse a total of 15 times, using a new piece of tape each time, and then 10 μ l of bacterial suspension (approximately 5×10^8 colony-forming units) were painted over the ear surface with a pipet. Hair had been removed from the dorsal sides of the ears with Nair at least 24-48 hours before tape stripping. Eighteen hours later, the mouse was sedated and imaged by confocal microscopy as above.

Quantification of LC Responses to Bacterial Organisms

Maximum intensity projections of the confocal image sets were created using the Z-Project command in ImageJ. The dSEARCH index values calculated using a method similar to the procedure described for epidermal LC responses to reactive hapten application. The lengths of all dendrites for a given cell were calculated by tracing the dendrites with the line segment ROI using the MultiMeasure plugin for ImageJ. The lengths of the same dendrites were then recorded again after advancing the projection by 8 min. The absolute values of the changes in dendrite length were summed to arrive at the dSEARCH index

value for that cell over that 8 min period. The procedure was repeated until the dSEARCH index had been calculated over the entire imaging period. Likewise, the extent of lateral migration was calculated in a manner similar to that described above. The maximum intensity projections were aligned to account for drift during acquisition using the StackReg plugin for ImageJ. The x-y positions of the cell bodies were tracked over the entire imaging period using the Manual Tracking plugin for ImageJ, and the data were used to determine the mean distance moved per image (i.e., 4 min). Statistical differences between the mean dSEARCH index values or mean migration rate values among the different treatment groups were determined by Mann-Whitney *U*-test.

CHAPTER FOUR

Results

LC BEHAVIORS UNDER PHYSIOLOGIC CONDITIONS

Visualization of Corneal LCs *In Situ*

When this project was begun, we chose to monitor LC behaviors in the cornea, considering its two major advantages for *ex vivo* imaging studies. First, as an optically transparent organ, the cornea is an ideal tissue from which fluorescence data can be obtained at high resolutions even at a significant depth beneath the surface of the tissue. Second, the cornea is an avascular organ, receiving oxygen and nutrients from the fluids that bathe it, and as such would maintain a more physiologic state when introduced into an organ culture system. As we later found, an additional feature of corneal LCs is that they seem to be replaced by bone marrow derived precursors with greater proclivity than epidermal LCs, and thus could be effectively studied using a bone marrow transplantation protocol.

Reconstitution of Leukocyte Populations After Bone Marrow Transplantation

To visualize LCs in the absence of tissue fixation or staining, bone marrow cells harvested from EGFP-transgenic mice were transplanted into γ -

irradiated wild-type C57BL/6 mice, with the assertion that leukocytes originating from the donor stem cells would fluoresce under the proper stimulation and thus be distinguishable from the somatic tissues of the recipient. After six to eight weeks, allowing for engraftment of the bone marrow cells, the extent of reconstitution in the spleen and peripheral blood were determined by flow cytometric analysis. Reconstitution ranged from 67% to 84% for each of the CD45⁺ leukocyte, CD3⁺ T cell, B220⁺ B cell, and CD11c⁺ DC populations, determined by calculating the percentage of cells expressing EGFP within each population as defined with fluorescently-labeled mAbs (Figure 3). In experiments performed with the help of Akiko Nishibu, a post-doctoral fellow, reconstitution of immune cells in the cornea was found to be comparable to that observed in splenocyte and peripheral blood leukocyte samples, with EGFP expression detected in a majority of CD45⁺ leukocytes (76%), CD3⁺ T cells (53%), F4/80⁺ macrophages (67%), and Gr-1⁺ granulocytes (56%); very few, if any, B220⁺ B cells were found in the corneal samples.

Within the corneal epithelium were found many EGFP⁺ cells, primarily distributed in the peripheral regions near the corneal-scleral border, in an area known as the limbus. After isolation of the epithelium by EDTA treatment and consequent staining of the samples with mAb, CD11c expression was detected in $82.2 \pm 8.0\%$ (mean \pm SD, $n = 215$) of the EGFP⁺ cells (Figure 4A), while $91.9 \pm$

1.9% ($n = 391$) expressed MHC II. Virtually all the cells showing the classic dendritic morphology of LCs (Figure 4, Movies 1-2) were located within the epithelium in the limbal areas of the cornea and expressed the classic LC markers CD11c (Figure 4A) and MHC II (data not shown). The surface densities of the MHC II⁺ cells in the limbus were comparable ($P > 0.1$) between the EGFP bone marrow chimeric mice (37.5 ± 16.3 cells/mm²) and untreated, wild-type C57BL/6 control mice (48.3 ± 11.4 cells/mm²). Moreover, no significant differences were observed in the morphology or distribution of MHC II⁺ cells in the epithelium between the transplant recipients and normal controls. Finally, EGFP⁺ cells lacking the characteristic LC morphology were observed, but they resided mainly in the stromal compartment of the cornea and predominantly expressed CD3, CD11b, F4/80, or Gr1, markers of T cells, macrophages or PMNs.

Owing to its high crystalline triple helix structure, collagen is capable of second harmonic generation (SHG), or frequency doubling, a physical phenomenon in which the wavelength of electromagnetic waves encountering the collagen are precisely halved. SHG during two-photon excitation of the corneal samples resulted in visible wavelength emission that could be monitored concurrently with EGFP fluorescence, and as a result the presence or absence of collagen in the tissues could be used to identify cells in the corneal stroma and epithelium, respectively (Figure 4C and Movie 3). Since LCs are by definition

located within the epithelium, for all further experiments LCs were defined as intraepithelial EGFP⁺ cells showing the characteristic dendritic morphology. It should be noted, however, that EGFP expression was detected in only $91.1 \pm 2.0\%$ of CD11c⁺ cells and $86.1 \pm 8.2\%$ of MHC II⁺ cells. Thus, a small fraction of LCs, presumably of recipient origin, remained invisible to detection by *in situ* microscopy.

Corneal LCs Interact With Their Environment Via dSEARCH

In order to visualize the dynamic behaviors of LCs *in situ*, corneal samples from EGFP bone marrow chimeric mice were harvested and placed into a specialized organ culture system designed to maintain the tissue via temperature control and constant circulation of aerated culture medium (Figure 5). LCs in the limbus of the corneal samples were then immediately imaged using two-photon laser microscopy. When imaged in this manner, an overwhelming majority of LCs displayed an intriguing behavior characterized by repetitive extension of dendritic process in random directions between adjacent corneal epithelial cells, followed by retraction of those processes through the same paths (Figure 6 and Movie 4 & 5). This behavior, which we termed dendrite surveillance extension and retraction cycling habitude, or dSEARCH, occurred in a regular manner with a mean period of 32 ± 8 min (mean \pm SD, $n = 40$), a mean speed of extension of

$1.5 \pm 0.2 \mu\text{m}/\text{min}$, and a mean speed of retraction of $2.0 \pm 0.6 \mu\text{m}/\text{min}$, as measured from maximum intensity projections of the data sets (see Figure 7).

In order to claim that the dSEARCH consisted of true periodic movements, the data were subjected to a more quantitative analysis. Fast Fourier transforms are used in numerous disciplines as a means to analyze complex signals (for example, to extract information from carrier waves), and as such are powerful tools for the decryption of convoluted data sets. Power spectra were created for each cell analyzed in order to extract frequencies from the transforms, and these spectra nicely illustrate that the lengths of the dendrites of cells displaying dSEARCH are in fact cyclical and do not represent random variation in dendrite length (Figure 8). Weighted mean periods, which include the contributions of small fluctuations in length within the greater pattern, were calculated for the dSEARCH displayed by the corneal LCs. The weighted periods of the three cells shown in Figure 7 were 40.0, 38.5, and 36.4 min, which approximate the analog mean period estimated above.

Lateral Migration by EGFP⁺ Cells in the Cornea

Although dSEARCH was the primary dynamic behavior noted in EGFP⁺ LCs in the cornea, populations of cells were observed that migrated laterally through the corneal tissue. While the vast majority of LCs remained sedentary,

with the cell body centroids moving very little over the course of the experiments, occasionally a LC was seen to move slightly in an amoeboid fashion in the x-y plane. Given the extent to which the dendrites moved, it was surprising to note that overall little lateral movement was observed in LCs.

The majority of the movement observed in EGFP⁺ cells in the cornea occurred in the stromal compartment, and was exhibited by cells lacking the morphological characteristics of LCs. Smaller, fast moving cells with a polygonal shape were observed throughout the stroma, some reaching a speed of approximately 10 $\mu\text{m}/\text{min}$. While *post hoc* identification of specific cells within the cultured samples was not practical, these small, fast moving cells resembled the CD3⁺ or Gr-1⁺ cells seen in the fixed corneal preparations in terms of morphology and location within the stroma. Additionally, slower migration was seen in larger, amorphously shaped cells that resembled the F4/80⁺/CD11b⁺ macrophages seen in the fixed samples. Thus, it seems reasonable to speculate that the cornea is constantly patrolled by migratory T cells and/or granulocytes, in addition to the tissue-resident macrophages.

Visualization of LC Behaviors in the Epidermis

In the process of characterizing the EGFP bone marrow chimeric mice, it became evident that epidermal LCs are not replaced by bone marrow precursors after γ -irradiation, even several months after the transplantation procedure. In our mice, isolated patches of skin could be found that contained EGFP⁺ cells within the epidermal compartments, but these represented a very small fraction of the total skin surface area. Further experiments by other investigators confirmed these observations, suggesting that LCs self-propagate within the epidermis except in states of extreme inflammation (148,149). Thus, the EGFP bone marrow chimeric mice could not be used to study epidermal LC behavior, and we instead opted to employ I-A β -EGFP knock-in mice developed by our collaborator, Dr. Hidde Ploegh. In these mice, the endogenous *I-A β* gene has been replaced by a construct encoding an I-A-EGFP fusion protein, and thus all cells expressing MHC II, including LCs, concomitantly express EGFP. With these mice, experiments were performed with the cooperation of Akiko Nishibu to elucidate the behaviors of epidermal LCs in the physiologic state.

Quantification of LC Populations in the Epidermis

The ear skin was chosen as the location for all subsequent imaging studies in these mice because it possessed several advantages for experimental

assessment of epidermal LC behaviors. In particular, the ear skin is readily accessible for the application of treatments, the collection of samples, and even the direct observation of cells within the animal. Furthermore, the ear skin is thinner and relatively hairless when compared to the footpad or abdominal skin, respectively. In ear skin samples freshly harvested from the knock-in mice, many EGFP⁺ cells extending long dendritic processes in the classic manner of LCs were observed in the epidermal compartment. After immunofluorescent staining and examination by epifluorescence and confocal microscopy, CD11c and langerin expression were detected in all tested EGFP⁺ cells ($n = 1670$). Conversely, all tested CD11c⁺ or langerin⁺ cells exhibited EGFP fluorescence, and all possessed the characteristic dendritic morphology of LCs (Figure 9). Thus, epidermal LCs in the I-A β -EGFP knock-in mice can be visualized as EGFP⁺ cells in the epidermis of intact skin, even in the absence of tissue fixation or staining.

Behaviors of Epidermal LCs Ex Vivo

Based on the results discovered during examination of corneal LCs, one could assume that epidermal LCs would also be prone to display the same repetitive dendrite movement. The difference between corneal and epidermal LCs in terms of repopulation after bone marrow transplantation, however, gave us pause since the precursor populations and/or biology of these populations theoretically could be very different. Therefore we set out to investigate the

behaviors of epidermal LCs. To determine whether EGFP⁺ epidermal LCs might exhibit any baseline motility, ear skin samples freshly harvested from I-A β -EGFP knock-in mice were placed into organ culture in a manner very similar to that used for the corneal samples above. As the abundant keratin content of the epidermis and the presence of melanin within the hair follicles made the detection of EGFP fluorescence by two-photon excitation problematic, the skin samples were examined by conventional confocal microscopy. In a manner similar to that of corneal LCs, EGFP⁺ epidermal LCs exhibited movement characterized by repetitive extension and retraction of the long dendritic processes through spaces between adjacent keratinocytes (Figure 10 and Movie 6). Of a total of 205 EGFP⁺ epidermal LCs monitored, this behavior was detected in 198 cells (97%), and thus dSEARCH seems to represent an inherent behavior of epithelial-residing LCs.

Steady State Behaviors of Epidermal LCs In Vivo

With the advantages of avascularity and optical transparency, the cornea is well suited to microscopic investigation in organ culture. However, examination of corneal tissue by laser scanning microscopy in living animals is impractical at best, due to minute involuntary eye movements that disrupt the field of view during scanning, even in anesthetized animals. The skin on sites such as the ear, however, can be isolated and secured in living, anesthetized animals, and

therefore has no such disadvantages for *in vivo* imaging. Consequently, we decided to examine the epidermis of living I-A β -EGFP knock-in mice in order to visualize the *bona fide* steady state behaviors of LCs.

While nearly all the LCs in the corneal and skin organ cultures display noticeable dSEARCH, substantial dSEARCH was detectable in only a small fraction (5-10%) of epidermal LCs in living animals (Figure 11 and Movies 7 & 8). Interestingly, the population of LCs displaying dSEARCH was discernible from the more sessile LCs by the distinguishing features of larger cell size and elevated I-A β -EGFP expression. Since it is not necessarily the absolute dendrite length, but rather the total amount of change in dendrite length, that fluctuates with increased dSEARCH activity, a more quantitative indicator of augmented dendrite activity was computed. The dSEARCH index values, a measure of the total change in dendrite length for a cell over a given time, of the LCs in live animals showed statistical correlation with their x-y plane areas ($P < 0.05$, $n = 79$), as well as their EGFP fluorescence intensities ($P < 0.01$, $n = 79$). With the modest dSEARCH activity found in only a small fraction of epidermal LCs, it was not surprising to note that little or no lateral movement by EGFP⁺ LCs in the epidermis was observed throughout the imaging periods.

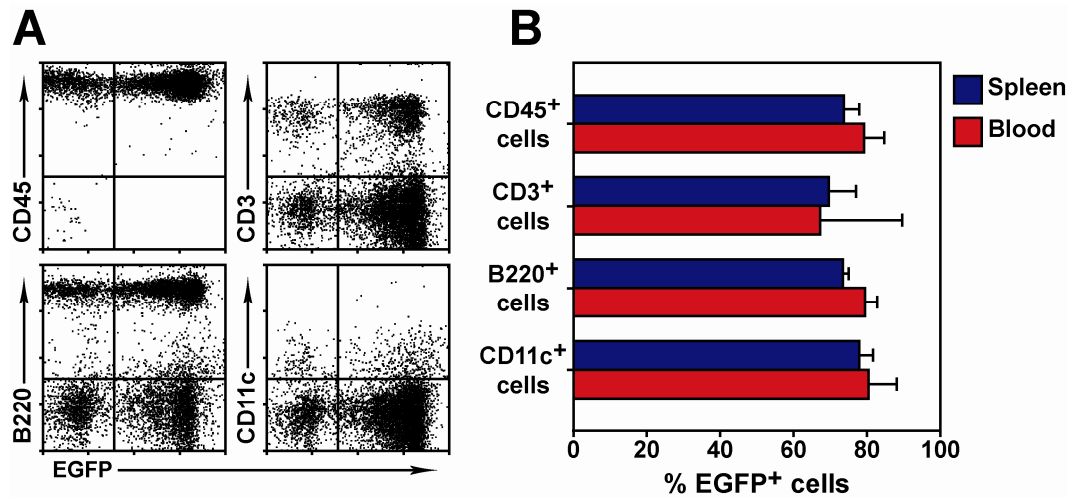


Figure 3. EGFP expression by leukocytes in BM chimeric animals.

C57BL/6 mice received 950 rads of γ radiation followed by i.v. injection of bone marrow cells isolated from EGFP transgenic mice. (A) Peripheral blood leukocytes isolate from the recipient mice 10 weeks after bone marrow transplantation were labeled with PE-conjugated mAb against CD45, CD3, B220, and CD11c and examined for EGFP expression by flow cytometry. (B) Spleen cell and peripheral blood leukocyte suspensions collected from chimeric mice 10-12 weeks after transplantation were labeled with PE-conjugated mAb against the indicated leukocyte markers. Data shown are the means \pm SD (spleen, $n = 3$; blood, $n = 6$) of the percent EGFP⁺ cells within in leukocyte subset, as determined by FACS.

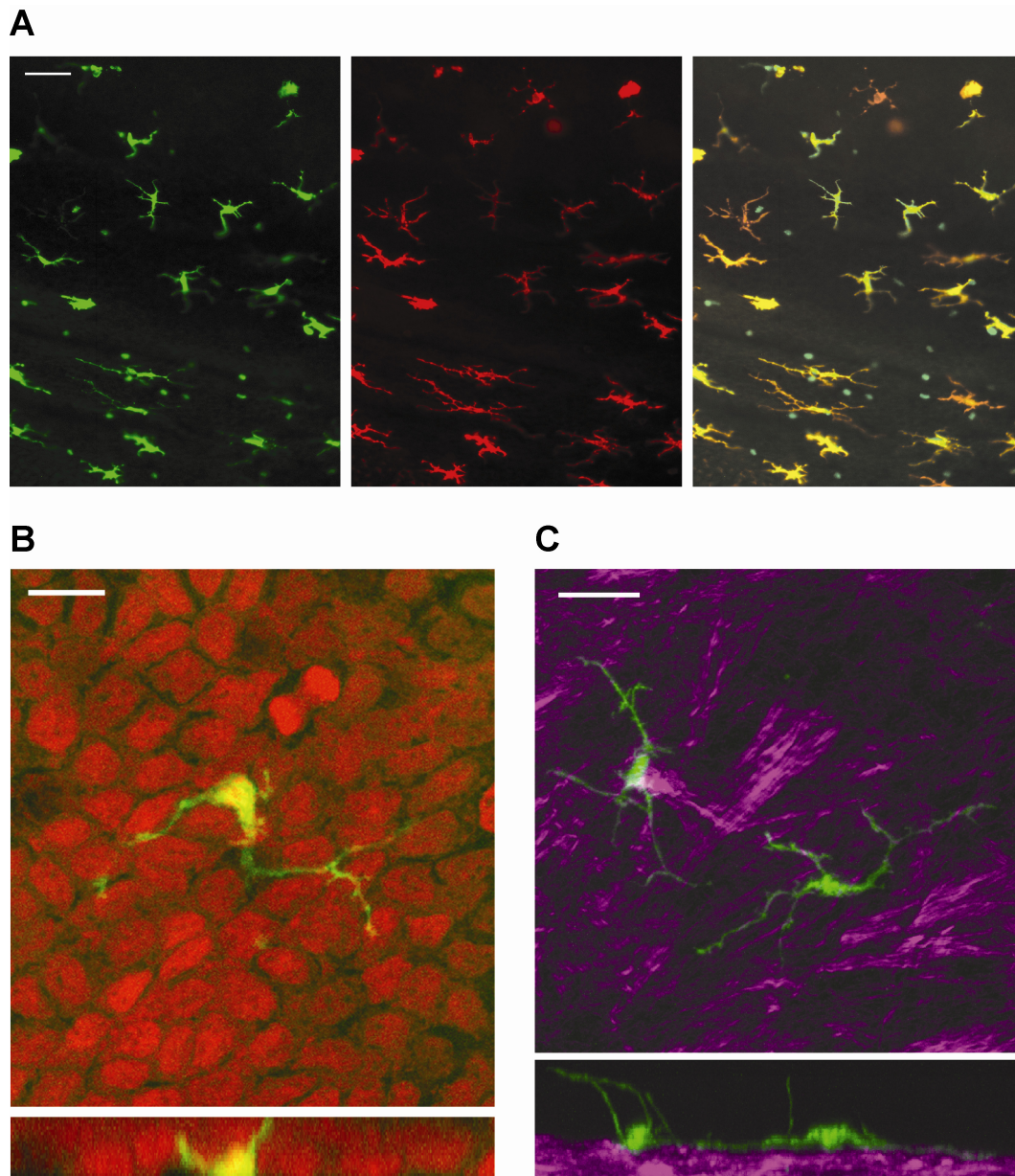


Figure 4. LCs in the corneal epithelium express CD11c and exhibit a dendritic morphology.

LCs were examined in fixed cornea samples from EGFP BM chimeric mice. (A) Corneal epithelial sheets harvested 10 weeks after bone marrow transplantation

were labeled with PE-conjugated anti-CD11c mAb and examined by conventional fluorescence microscopy. Panels show EGFP (green), CD11c (red), and overlay. Scale bar, 50 μm . (B) Whole corneal samples harvested from EGFP chimeric mice were fixed, stained with PI, and then examined under single-photon confocal microscopy. Green fluorescence signals demarcate the three-dimensional structure of an intraepithelial EGFP⁺ LC extending long dendritic processes through intercellular spaces between epithelial cells, visualized by red fluorescence signals. Scale bar, 10 μm . Rotational images and Z-axis stack can be viewed in Movies 1 and 2, respectively. (C) Corneal sample harvested from EGFP chimeric mice was fixed and then examined by two-photon laser scanning microscopy for the spatial relationship of EGFP⁺ LCs (green) to collagen bundles detected *via* second harmonic generation (magenta). Scale bar, 20 μm . Rotation images are shown in Movie 3.

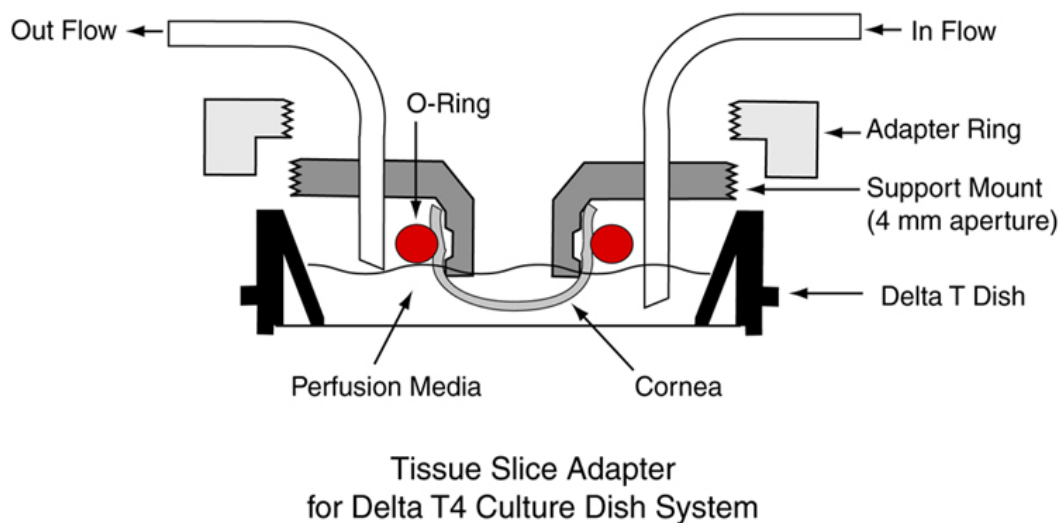


Figure 5. Schematic of the Delta T4 culture system for *in situ* imaging of LCs.

Corneal samples were prepared from the freshly enucleated eyes of EGFP bone marrow chimeric mice using a specially-fabricated double bladed knife. Samples were secured with a rubber O-ring to the tissue slice adapter, which was placed into a Delta T4 culture dish. Aerated culture medium was circulated through the culture dish throughout the imaging period via a microperfusion pump. The temperature of the sample was maintained by means of an electrically conductive coverslip bottom on the culture dish, regulated by the Delta T4 Controller.

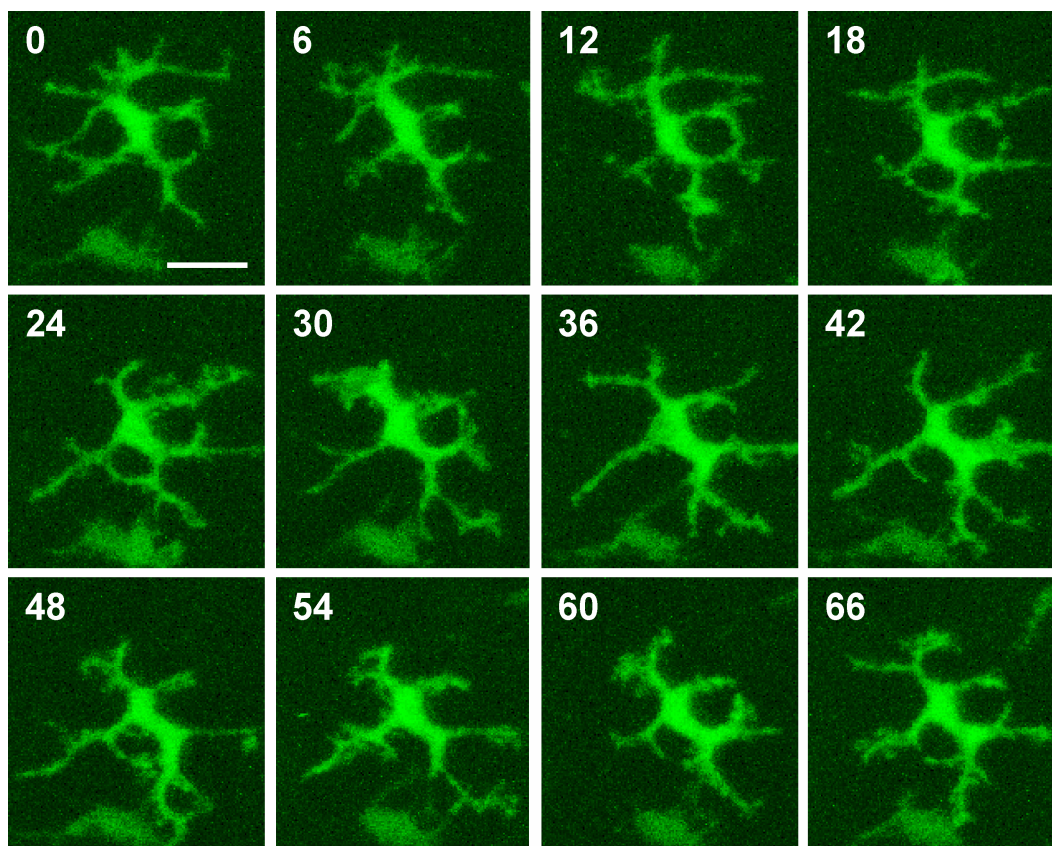


Figure 6. Corneal LCs display a unique behavior termed dSEARCH.

Corneal samples freshly harvested from EGFP bone marrow chimeric mice were imaged by two-photon microscopy. LCs displayed a characteristic behavior comprised of extension of the dendritic processes, retraction of the dendrites through the same path, and repetition of the extension/retraction cycle. dSEARCH by a representative LC is shown in static images. Panels show maximum intensity projections of three-dimensional data sets collected with a 6 min interval. Scale bar, 20 μm .

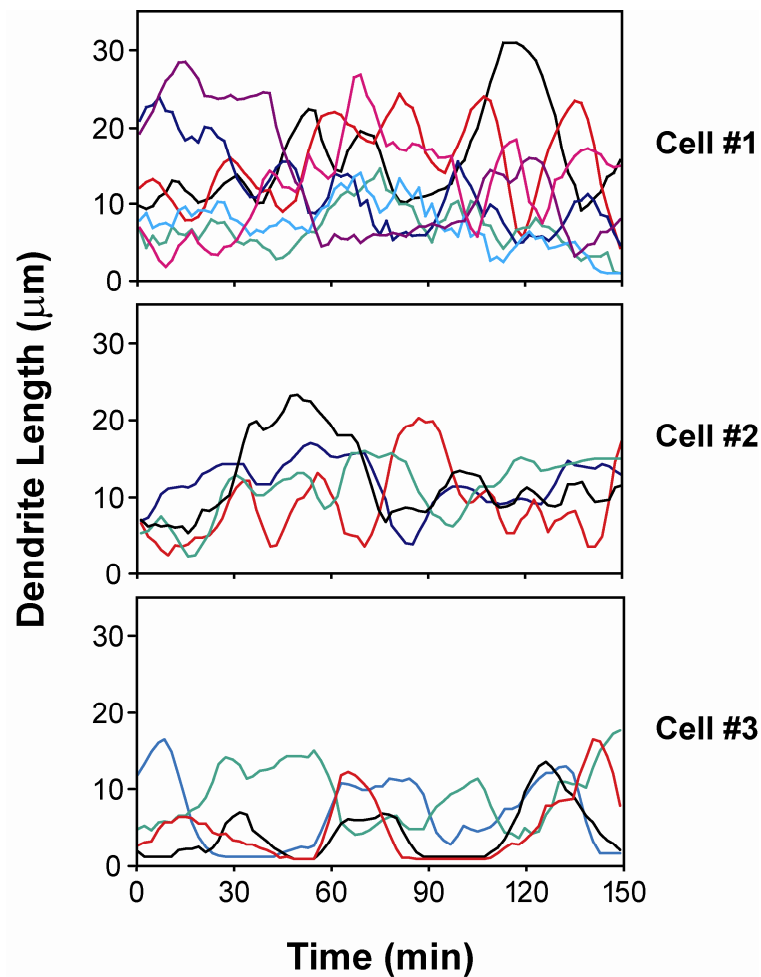


Figure 7. Dendrite length varies over time in LCs showing dSEARCH.

EGFP⁺ LCs in corneal samples were imaged by two-photon microscopy and displayed a unique behavior characterized by rhythmic extension and retraction of dendritic processes. To explore this behavior, the lengths of individual dendrites were measured over time. The panels display the lengths of multiple dendrites for three representative cells measured over the 150 min imaging period. Dendrite length was defined as the linear distance from the tip to the junction with the cell body. Data shown have been smoothed using a moving average with a period of 4.

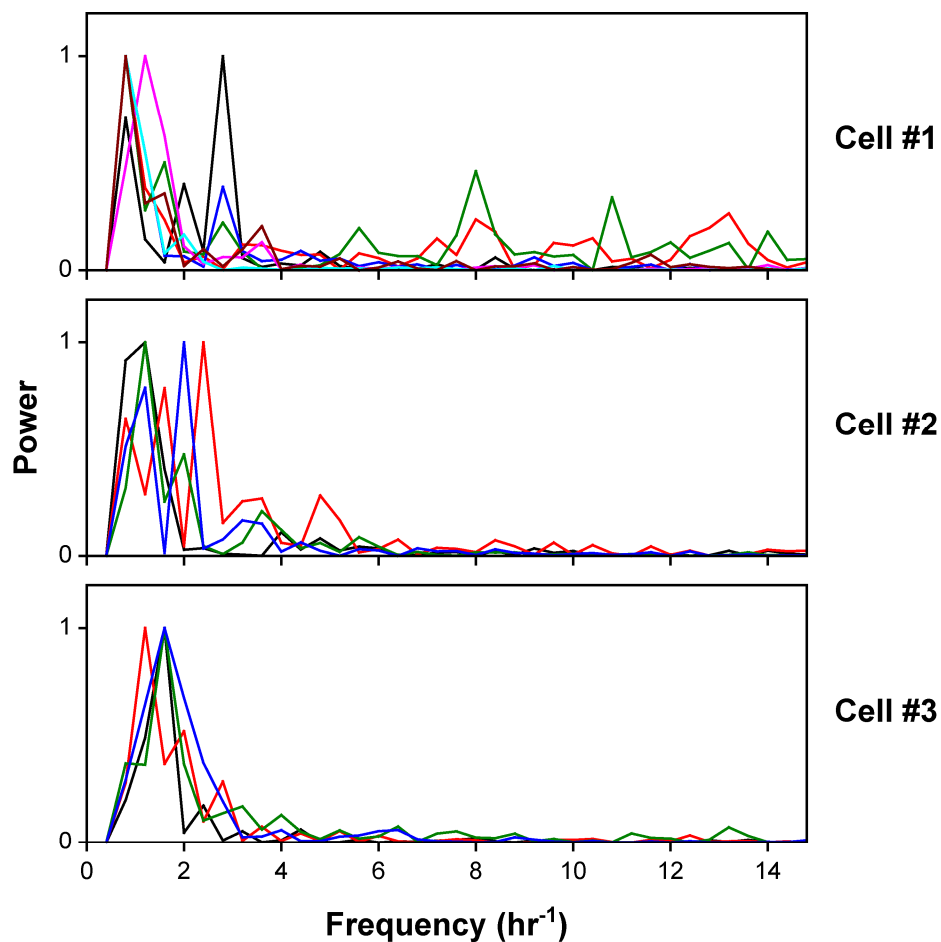


Figure 8. Periodicity of the changes in dendrite length.

The periodicity of dSEARCH by the same cells as in Figure 5 was assessed by Fourier analysis. Fast Fourier transforms were applied to data sets plotted in Figure 5, and power spectra were created by multiplying the transforms by their conjugates. Each line represents the normalized power spectrum of a given dendritic process over the indicated frequencies. For reference, the colors of individual lines correspond to dendrites plotted in Figure 7.

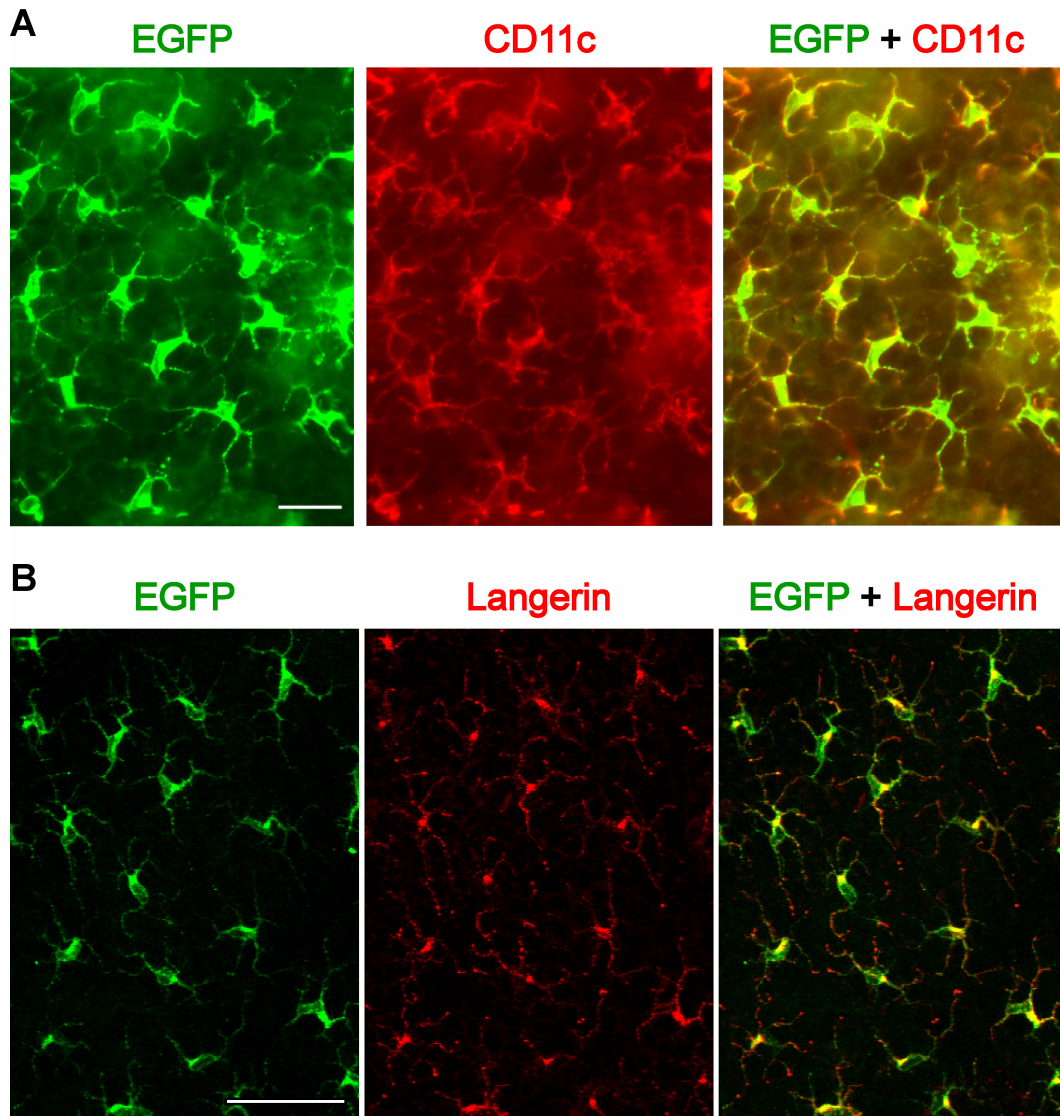


Figure 9. Identification of EGFP⁺ epidermal cells in the skin of I-A β -EGFP knock-in mice.

Epidermal sheets were prepared from ear skin samples freshly harvest from I-A β -EGFP knock-in mice. The preparations were labeled with PE-conjugated anti-CD11c mAb (A) or anti-langerin hybridoma supernatant (B) and then examined by conventional fluorescence microscopy. All examined EGFP⁺ cells expressed CD11c or langerin, and vice versa. Scale bars, 20 μ m (A), 50 μ m (B).

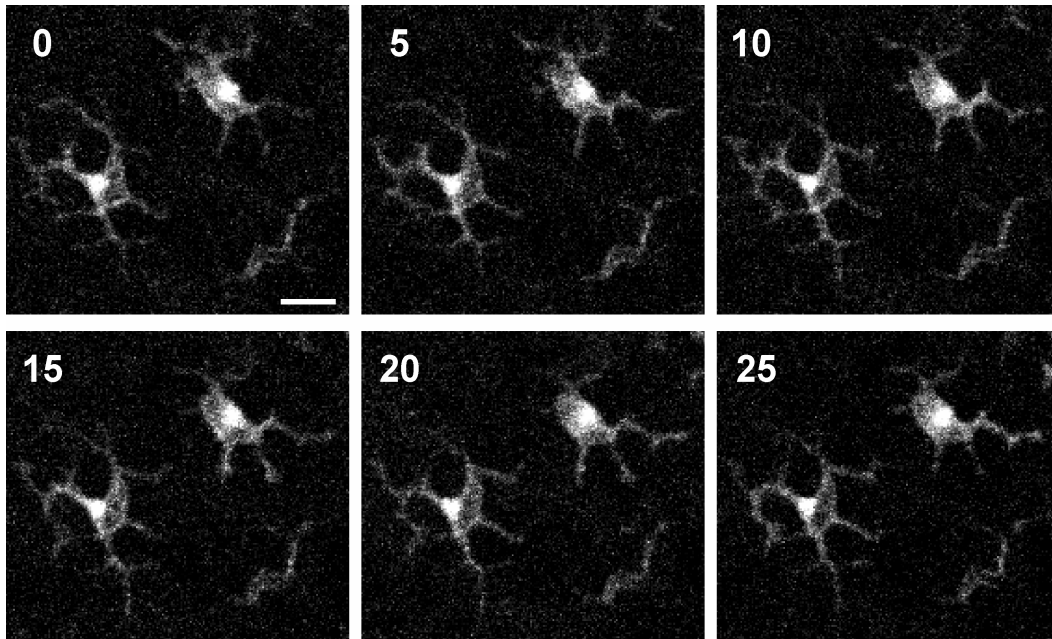


Figure 10. dSEARCH recorded *ex vivo* in EGFP⁺ epidermal LC.

Ear skin samples freshly harvested from I-A β -EGFP knock-in mice were placed into a specialized organ culture system and imaged by confocal microscopy. Representative cells demonstrating the characteristic dendrite activity known as dSEARCH are shown. While not as active as corneal LCs, epidermal LCs exhibit similar repetitious movements of the dendrites. The panels display maximum intensity projection of three-dimensional data sets collected at 5 min intervals. Scale bar, 10 μ m.

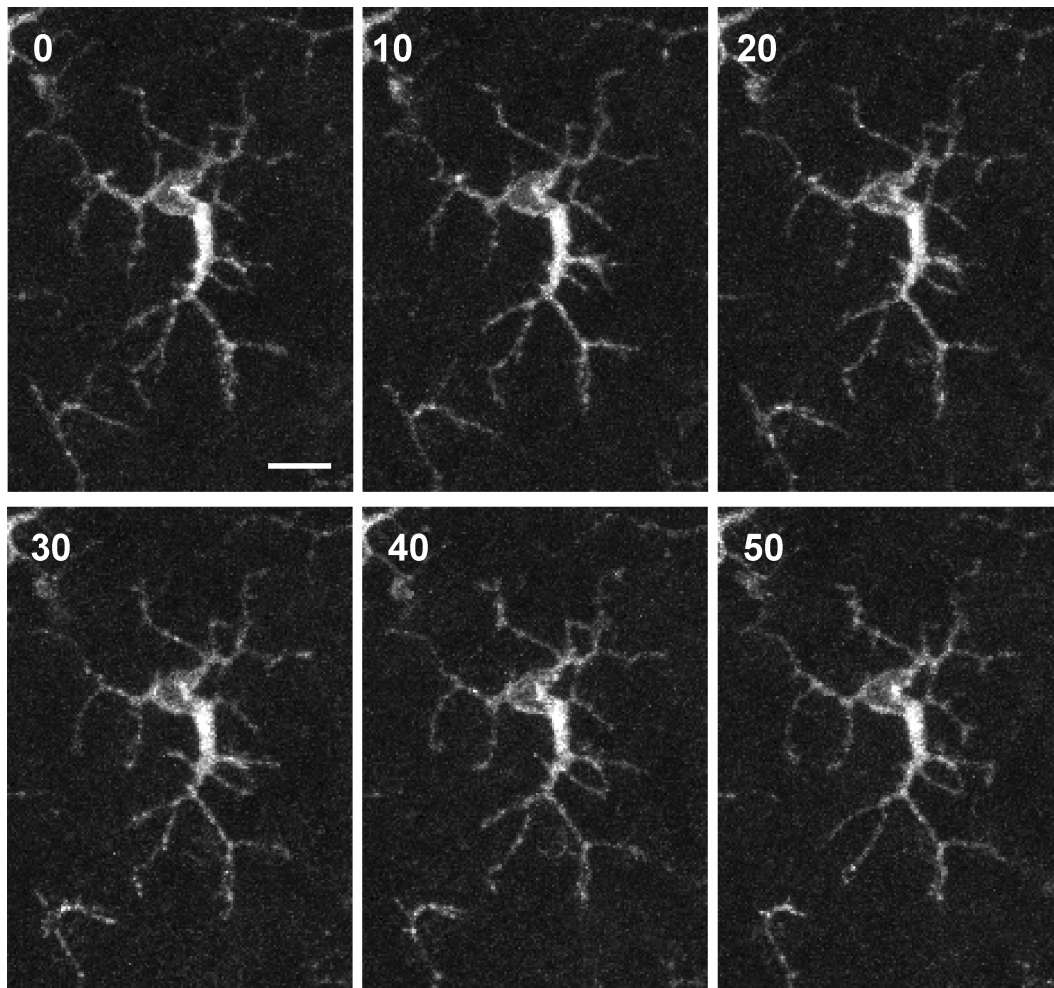


Figure 11. dSEARCH recorded in the steady state in living animals.

Anesthetized I-A β -EGFP knock-in mice were examined by intravital confocal microscopy for dynamic movement of EGFP⁺ epidermal LCs. LCs in the steady state in live animals overall show minimal dSEARCH when compared to corneal and epidermal LCs imaged *ex vivo*. However, the magnitude of dSEARCH is increased in a small population of cells showing increased cell size and upregulated MHC II expression (i.e., increased EGFP fluorescence intensity). The panels display maximum intensity projections of three-dimensional data sets collected at 10 min intervals of a representative LC. Scale bar, 20 μ m.

*Legends to Supplemental Movies***Movie 1. Three-dimensional images of an EGFP⁺ corneal LC.**

A three-dimensional data set similar to that shown in Figure 4B (without counter-staining with PI) was reconstructed along the x-z plane, followed by rotation about the z-axis (180°) and the x-axis (360°). Note that while some of the fine dendritic processes extend upward in the z-axis, the LC occupies a much greater area in the x-y plane.

Movie 2. Spatial relationship of an EGFP⁺ corneal LC to neighboring epithelial cells.

The data set shown in Figure 4B was processed to display 46 sequential x-y images separated by 0.5 μm spanning a total z-axis depth of 24 μm . The series begins superficially in the epithelium and proceeds towards to the stroma.

Movie 3. The spatial relationship of EGFP⁺ corneal LCs to collagen bundles.

The data set shown in Figure 4C was processed to show rotation about the z-axis (360°). Note the location of the EGFP⁺ LCs slightly above the collagen signals. This places the LCs within the epithelium, which lacks the abundant collagen bundles seen in the stroma.

Movies 4-5. Time-lapse images of baseline dSEARCH performed by multiple corneal LCs.

The data set shown in Figure 6 (Movie 4) and the data set from an independent experiment (Movie 5) were compiled to show dynamic movement of EGFP⁺ corneal LCs. Note that most of the EGFP⁺ LCs with the characteristic dendritic morphology exhibit dSEARCH in the epithelial compartment, while rapid migration is observed in smaller EGFP⁺ cells possessing a polygonal shape primarily in the stromal compartment.

Movie 6. Time-lapse images of baseline behaviors of epidermal LCs *ex vivo*.

Confocal images recorded every 5 min in a skin sample freshly harvested from an I-A β -EGFP knock-in mouse were compiled to show the dynamic movement of EGFP⁺ epidermal LCs.

Movies 7-8. Time-lapse images of *in vivo* behaviors of epidermal LCs in the steady state.

The data set shown in Figure 11 and the data set from an independent experiment were compiled to show steady state dSEARCH detectable in some of the EGFP⁺ epidermal LCs in anesthetized mice. dSEARCH was noticeable in EGFP⁺ LCs characterized by larger cell size and higher EGFP signal intensity.

LC BEHAVIORAL RESPONSES TO LOCAL TISSUE INJURY

Behavioral Responses of Corneal LC to Local Tissue Injury

Having discovered the baseline behaviors of corneal LCs in our organ culture system, the next step in elucidating the behavioral biology of LCs was to observe their responses to localized tissue injury. As sentinel cells protecting and watching the epithelial tissues of the body, LCs are acutely sensitive to pathogenic injury to the tissues in which they reside and undergo a functional reprogramming upon injury that allows them to initiate and modulate the immune response. We reasoned that this change in LC function would be accompanied by corresponding changes in LC behaviors, and thus we set out to observe LCs in the cornea continuously before and after acute injury.

Pinpoint Thermal Injury Elicits Rapid Changes in LC Behaviors

Because of the inherent variability in dSEARCH and the notion that harvesting and culturing corneal tissue could influence the LCs in varying ways, a system was developed in which the same LCs from corneal samples could be observed before and after injury to the tissue. Additionally, it was decided that pinpoint injury to an area localized within the field of view of the microscope

during image acquisition would be ideal, since the effect of the injury on the cells in the immediate surroundings could be studied. To this end, we produced pinpoint thermal injury to LC targets using the Ti:sapphire laser of the two-photon microscope. Operating in the near-infrared portion of the spectrum, the laser transmits electromagnetic radiation that is absorbed by water molecules in the sample, causing an increase in the total thermal energy. By parking the laser at maximum output on one specific spot of the corneal sample with the point bleach function of the microscope, at least 23 joules of energy can be delivered to an area no bigger than $0.25 \mu\text{m}^2$ over one minute. LCs were chosen as targets simply because effective energy delivery could be assessed in images taken before and after by the disappearance of EGFP signals from the field of view.

Using this technique, LCs could be effectively targeted, and thus tissue injury inflicted, during the course of an imaging experiment without disrupting the imaging volume or significantly interrupting image acquisition. Corneal samples were observed for an hour under normal culture conditions before injury, and then were observed for an additional three hours. Almost immediately, i.e., within 2-10 min of injury, LCs in the proximity of the injury site (within approximately $100 \mu\text{m}$) began to exhibit augmented dSEARCH (Figure 12 and Movies 9-11) that was discernable with the naked eye. Indeed, the overall dSEARCH activity, quantitatively assessed by measuring the dSEARCH index,

was significantly ($P < 0.01$, $n = 24$) elevated in the early (0-60 min), middle (60-120 min), and late (120-180 min) phases after injury (Figure 13).

In addition to augmented dSEARCH, local thermal injury also provoked lateral movement in nearby LCs, a feature seldom seen in LCs at baseline (Figure 14 and Movies 9-12). The increase in lateral movement was noticeable forthwith after injury, and thus paralleled the rapidity in which dSEARCH augmentation occurred. To quantitatively assess the migratory activity, we calculated the mean traveled distance, or the mean distance in which the cell body centroid of individual LCs moved between image frames (2 min interval). Thermal injury was found to increase this parameter significantly ($P < 0.05$, $n = 28$) in all three post-injury phases (Figure 15). While in some instances the neighboring LCs were remarkably drawn to the site of injury, migration by corneal LCs after local injury primarily occurred in random paths without an apparent directional bias toward the injury site. Thus, LCs are capable of acutely responding to local tissue injury with two unique behaviors, augmented dSEARCH and increased lateral migration.

Role of IL-1 in Injury-Induced Behavioral Changes

Since corneal epithelial cells and LCs are known to release IL-1 in response to various pathologic stimuli (including tissue injury) and rapid and

profound IL-1 release occurs after thermal injury, we chose to examine the roles of IL-1 in corneal LC responses to injury (150-154). Therefore, IL-1Ra, a protein that binds to circulating IL-1 and thereby antagonizes the binding to and consequent signaling by IL-1 receptors, was added to the circulating culture medium 60 min before injury as a means to disrupt the inflammatory signals generated by this cytokine (Figure 16 and Movies 13 & 14). IL-1Ra treatment did not appreciably affect the baseline dSEARCH of the LCs, as the dSEARCH index values before injury in the presence of IL-1Ra (Figure 17) were comparable ($P > 0.1$) to those in its absence (Figure 13, before injury). Strikingly, IL-1Ra completely abrogated ($P > 0.1$, $n = 20$) the increase in dSEARCH index after pinpoint thermal injury (Figure 17). In addition to its effects on dSEARCH, IL-1Ra treatment affected the ability of local injury to provoke lateral migration of LCs, for no apparent lateral movement was seen in the presence of IL-1Ra, and the mean traveled distance values were not significantly elevated after injury (Figure 18). These results imply that rapid release of IL-1 is required for both forms of LC behavioral responses to local thermal injury.

With evidence suggesting a role for IL-1 as provided by the treatment of corneal samples with IL-1Ra, we next sought to recapitulate the injury-induced changes in LC behaviors with exogenous IL-1. The addition of recombinant mouse IL-1 α to the circulating culture medium, to a final concentration of 5

pg/ml, caused augmented dSEARCH by corneal LCs in the absence of tissue injury (Figure 19 and Movie 15 & 16). However, this increase was transient, as the dSEARCH index was significantly elevated ($P < 0.05$, $n = 18$) only in the early (0-60 min) phase after IL-1 α addition (Figure 20). In addition, exogenous IL-1 α failed to cause noticeable lateral movement, and the mean traveled distance values remained unchanged ($P > 0.1$, $n = 24$) after treatment (Figure 21).

The concentration of IL-1 α used in the above experiments (5 pg/ml) was chosen to approximate the ED₅₀ of the recombinant cytokine given by the manufacturer, but we did consider the possibility that concentration of IL-1 α that diffuses into the tissues could be significantly lower than in the circulating medium. Therefore, several experiments were conducted in the presence of significantly higher concentrations of recombinant protein in the circulating medium. After exposure to medium containing IL-1 α at 100 pg/ml, LCs began to progressively extend their dendrites, with some eventually exceeding 100 μ m in length, yet never showed dramatic lateral movement (Figure 22 and Movie 17). Thus, IL-1 most likely acts as one, but not the only, factor mediating injury-induced LC behavior responses.

Effect of TNF α on Dynamic LC Behaviors

The inflammatory response that occurs after tissue injury involves release of multiple factors, including IL-1. TNF α , another factor critical to the inflammatory response, is also released by cells in the corneal epithelium (155-157). Moreover, TNF α has been reported to mediate IL-1-dependent migration of corneal LCs and trigger IL-1 production by corneal epithelial cells, and thus we examined the effect of TNF α on LC behaviors (158,159). Addition of recombinant mouse TNF α to the circulating medium, to a final concentration of 50 pg/ml, appeared to augment dSEARCH in corneal LCs (Figure 23 and Movies 18 & 19). In fact, LCs showed a significant ($P < 0.01$, $n = 26$) increase in dSEARCH index values in all phases of TNF α treatment (Figure 24). Furthermore, lateral movement of LCs became detectable after TNF α treatment, with a significant ($P < 0.05$, $n = 29$) increase in the mean traveled distance values in all phases after treatment (Figure 25). Together, these observations suggest the potential of TNF α to induce sustained augmentation of both dSEARCH and lateral migration of corneal LCs, and imply that the release of TNF α after injury can result in these behavioral responses.

Behavioral Responses of Epidermal LC to Inflammatory Insults

The data obtained when using the infrared laser to injure the tissue samples demonstrated that corneal LCs could respond to pathogenic insults, and this response was most likely mediated by inflammatory mediators like IL-1 and TNF α . With this in mind, it was hypothesized that epidermal LCs would behave in a similar manner when an inflammatory stimulus was introduced into the skin. To this end several models of inflammation were used to test the responses of LCs in the skin, both *ex vivo* and *in vivo*, in experiments performed along with Akiko Nishibu.

LC Responses to Diffuse Inflammatory Stimuli Ex Vivo

By using the infrared laser to deliver thermal energy to the cornea, we were able to produce pinpoint injury to the tissue and observe the acute response of LCs in the immediate vicinity. The limitations that prevented the use of two-photon excitation in the skin, however, also precluded the use of the laser to induce pinpoint thermal injury in that tissue. Therefore, diffuse inflammatory stimuli were given, and the LC responses measured after an extended period in cultured skin samples. In the first model, ear skin samples harvested from I-A β -EGFP knock-in mice were placed in organ culture for 16 hours before acquisition of time-lapse images by confocal microscopy (160-162). In the second model,

TNF α was injected s.c. into the ears, and after 16 hours, ear skin samples were harvested and immediately imaged as described previously (163). As expected, EGFP⁺ epidermal LCs showed a marked increase in size and elongation of the dendritic processes (Figure 26), two morphological changes known to accompany the in situ maturation of LCs during inflammation (144,164,165). The injection of PBS alone did not reproduce these changes, and, importantly, even after explant culture or TNF α injection, virtually all EGFP⁺ epidermal cells were confirmed to express CD11c, and vice versa (Figure 26). This indicated that the EGFP⁺ cells within the epidermis were indeed LCs.

The EGFP⁺ LCs in the epidermis appeared to exhibit exacerbated dSEARCH when monitored after skin organ culture or after TNF α injection (Figure 27 and Movies 20-22). In fact, the dSEARCH index values were significantly elevated after both organ culture ($P < 0.01$, $n = 20$) and TNF α injection ($P < 0.05$, $n = 20$), demonstrating that similar to corneal LCs, epidermal LCs respond to inflammatory signals by amplifying the magnitude of dSEARCH (Figure 28). Additionally, LCs were remarkably motile after these two treatments (Figure 29 and Movies 20-22), demonstrating amoeba-like movement through the intercellular spaces between adjacent keratinocytes, and as in corneal LCs, the migratory behavior occurred without an apparent directional bias. By measuring the distances traveled by individual LCs every frame throughout the imaging

period, it was shown that skin organ culture and $\text{TNF}\alpha$ injection significantly ($P < 10^{-6}$, $n = 57$, and $P < 10^{-11}$, $n = 61$, respectively) increased the lateral movement of LCs over baseline (Figure 30). Thus, LCs display the same basic dynamic response phenotypes in both the cornea and the epidermis in response to inflammatory stimuli.

LC Responses to Reactive Hapten Application In Vivo

Having discovered common behavioral responses of LCs in corneal and skin organ cultures to tissue injury and inflammatory stimuli, the key question then concerned whether LCs in living animals would respond in the same way. To answer this question, a standard hapten, dinitrofluorobenzene (DNFB), was applied topically to the ear of I-A β -EGFP knock-in mice, and the motile activities of EGFP⁺ LCs were recorded by intravital confocal microscopy (144,145,166). LCs exhibited not only an increase in size and elongation of the dendrites, but also a dramatic increase in the apparent magnitude of dSEARCH (Figure 31 and Movie 23). Indeed, the dSEARCH index values measured 30 hours after DNFB application were significantly elevated over those in the steady state ($P < 0.001$, $n = 20$) and over those measured 30 hours after application of the 3:1 acetone:olive oil vehicle alone ($P < 0.01$, $n = 20$) controls (Figure 32). Substantial lateral migration of EGFP⁺ cells became readily detectable in the epidermis after DNFB application, and the traveled distance values were significantly elevated above

steady state ($P < 0.001$, $n = 89$) and vehicle-alone ($P < 0.001$, $n = 206$) controls (Figure 33). Taken together, these intravital imaging experiments confirmed the *ex vivo* observations that injury or inflammation induces dynamic behavioral responses by LCs.

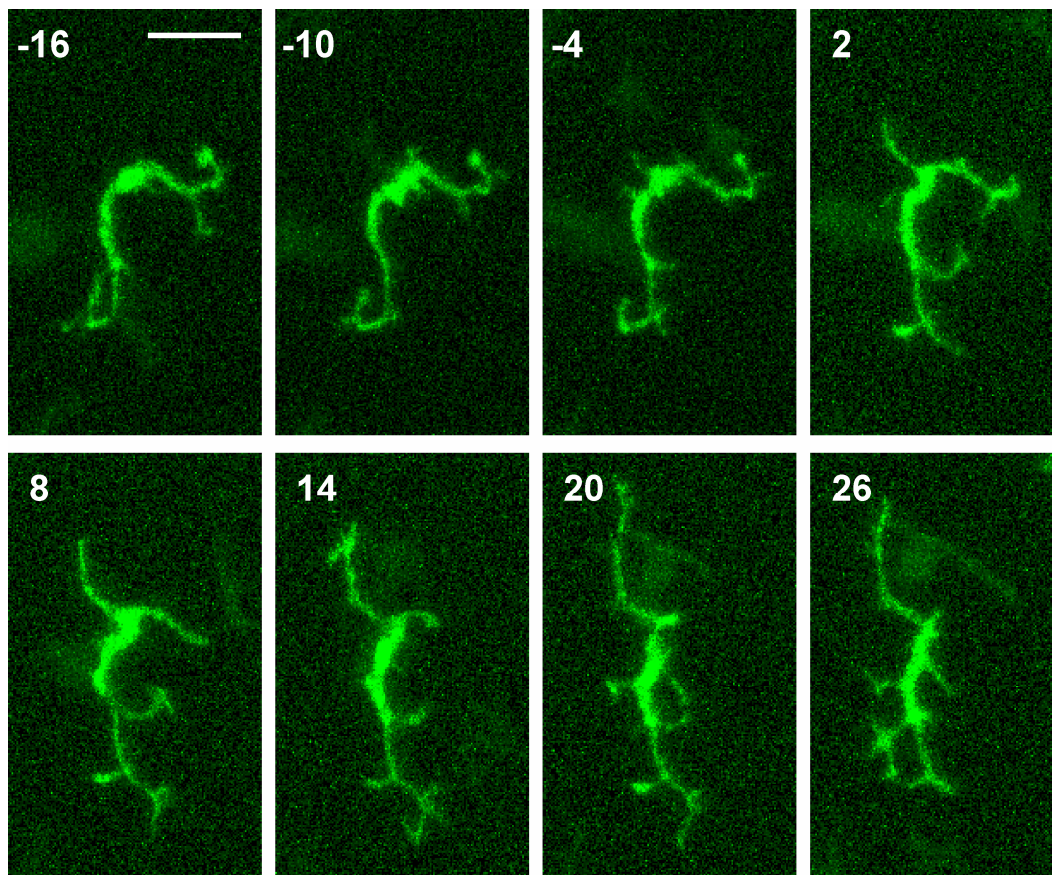


Figure 12. Pinpoint thermal injury triggers augmented dSEARCH in nearby LCs.

After 60 min recording of the baseline behaviors of corneal LCs, pinpoint injury was produced by infrared laser to a targeted LC at time 0. Panels show the changes in dSEARCH of a representative LC adjacent to the injury site. The images are maximum intensity projections of three-dimensional data sets collected every 6 min. Scale bar, 20 μm .

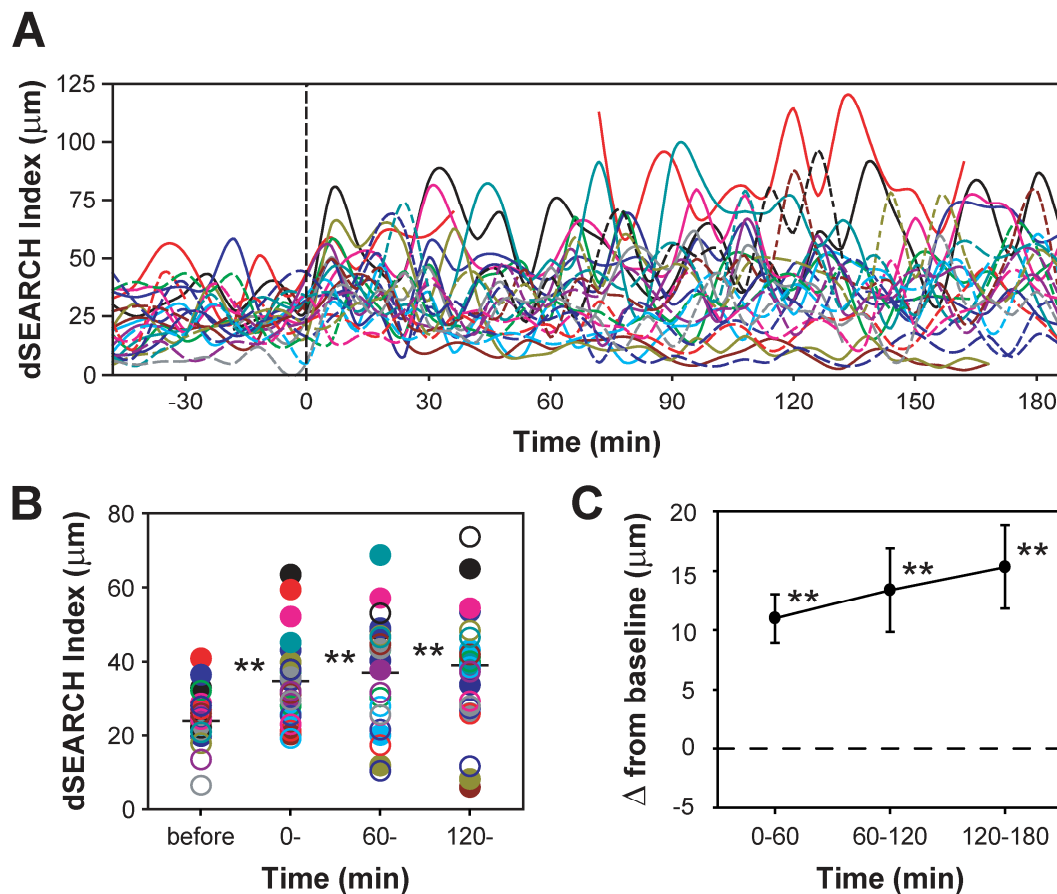


Figure 13. dSEARCH index values in corneal LC are elevated after thermal injury.

Pinpoint thermal injury was inflicted to a target LC, and the dSEARCH index values were calculated for neighboring LC by measuring the total change in dendrite length over a 6 min period. (A) The values for 24 LCs from 8 independent imaging experiments are shown over time, with each line representing the dSEARCH index values of a single LC. Thermal injury was inflicted using the infrared laser at time 0, indicated with a dashed vertical line. (B) Mean dSEARCH index values were calculated for each LC before injury (**before**, -60 to 0 min) and during the early (**0-**, 0 to 60 min), middle (**60-**, 60 to 120 min), and late (**120-**, 120 to 180 min) phases after injury. The filled and open circles correspond to the solid and dashed lines, respectively, in (B). The mean values among all LCs are shown with bars, and statistically significant differences

compared with baseline (**before**) are indicated with asterisks (** $P < 0.01$). (C) To account for the variability in the starting activity of different cells, the change in dSEARCH index over baseline was calculated for the data shown in (B). For each cell, the mean dSEARCH index value at baseline (-60 to 0 min) was subtracted from those values computed for the early (0 to 60 min), middle (60 to 120 min), and late (120 to 180 min) phases after injury. Data shown represent the mean \pm SEM for all cells. For reference, those groups in (B) that showed significant differences to baseline are indicated with asterisks.

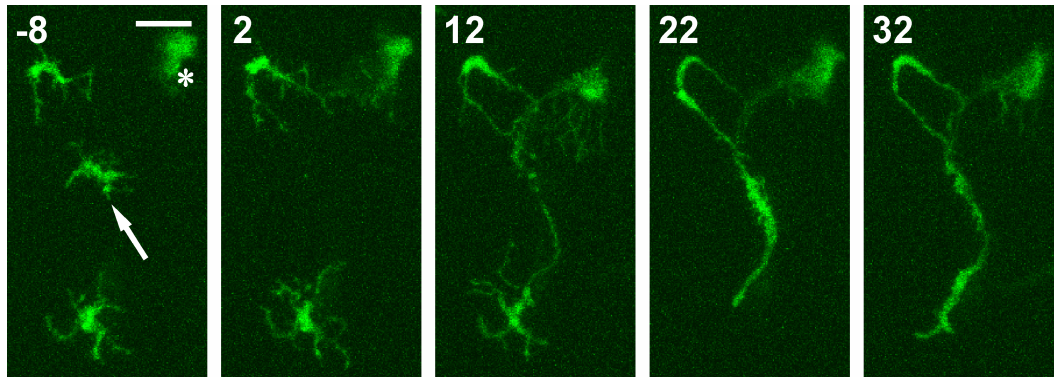


Figure 14. Pinpoint thermal injury induces lateral migration in corneal LCs.

After 60 min recording of baseline behaviors, pinpoint thermal injury was inflicted to a target LC using the infrared laser of the two-photon microscope. After injury, EGFP⁺ LCs in the vicinity of the injury showed increased lateral migration. The panels show the movement of two LCs after injury to a neighboring LC, indicated with an arrow. While these LCs move toward the site of injury, in general LCs showed no particular directional bias toward the injury and instead traveled in random directions. A large EGFP⁺ cell in the stroma is indicated with an asterisk. The images are maximum intensity projections of three-dimensional data sets acquired at 10 min intervals. Scale bar, 20 μ m.

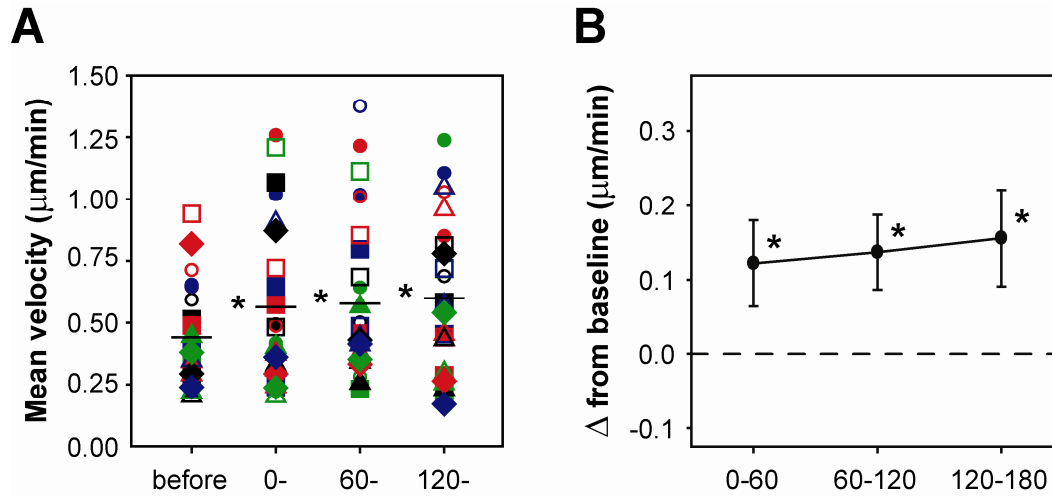


Figure 15. The mean velocity of corneal LCs per frame is increased after thermal injury.

After 60 min recording of baseline behaviors, pinpoint thermal injury was inflicted to a target LC using the infrared laser of the two-photon microscope. (A) The mean distance each LC traveled per image set (i.e., every 2 min) was calculated from the x-y positions of the cell bodies before thermal injury (**before**, -60 to 0 min) and in the early (**0-**, 0 to 60 min), middle (**60-**, 60 to 120 min) and late (**120-**, 120 to 180 min) phases after injury. From these values, the mean rate of lateral movement for each cell was calculated. Mean values among all LCs are shown with bars, and statistically significant differences compared to baseline (**before**) are indicated with asterisks (* $P < 0.05$). (B) To account for the variability in the starting activity of different cells, the change in mean velocity over baseline was calculated for the data shown in (A). For each cell, the mean velocity at baseline (-60 to 0 min) was subtracted from those values computed for the early (0 to 60 min), middle (60 to 120 min), and late (120 to 180 min) phases after injury. Data shown represent the mean \pm SEM for all cells. For reference, those groups in (A) that showed significant differences to baseline are indicated with asterisks.

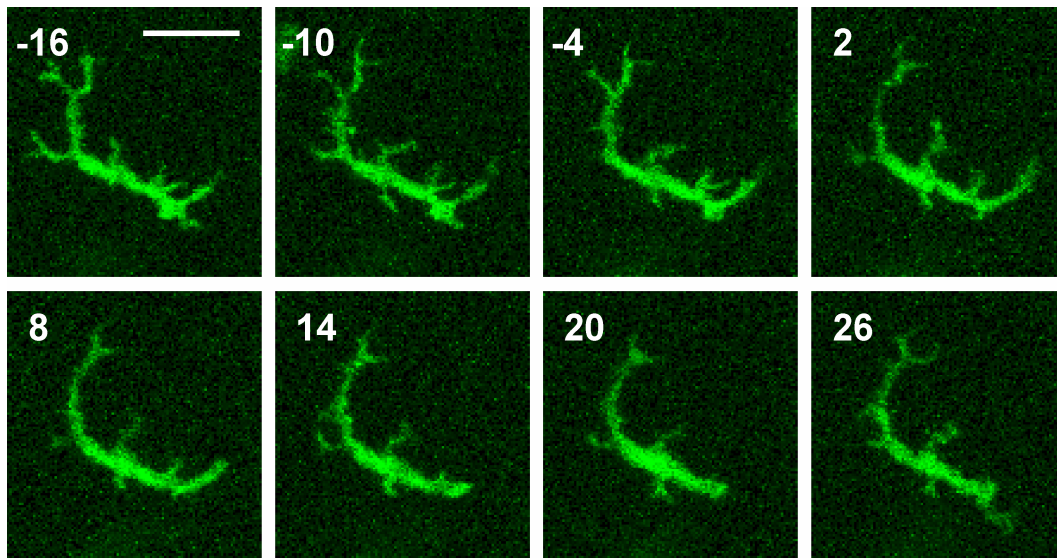


Figure 16. Injury-induced dSEARCH augmentation is inhibited by IL-1Ra.

After 60 min recording of the baseline behaviors of corneal LCs in the continuous presence of IL-1Ra (200 ng/ml), pinpoint injury was produced by infrared laser to a targeted LC at time 0. The panels demonstrate the lack of drastic changes in dSEARCH of a representative LC adjacent to the injury site. The images are maximum intensity projections of three-dimensional data sets collected every 6 min. Scale bar, 20 μ m.

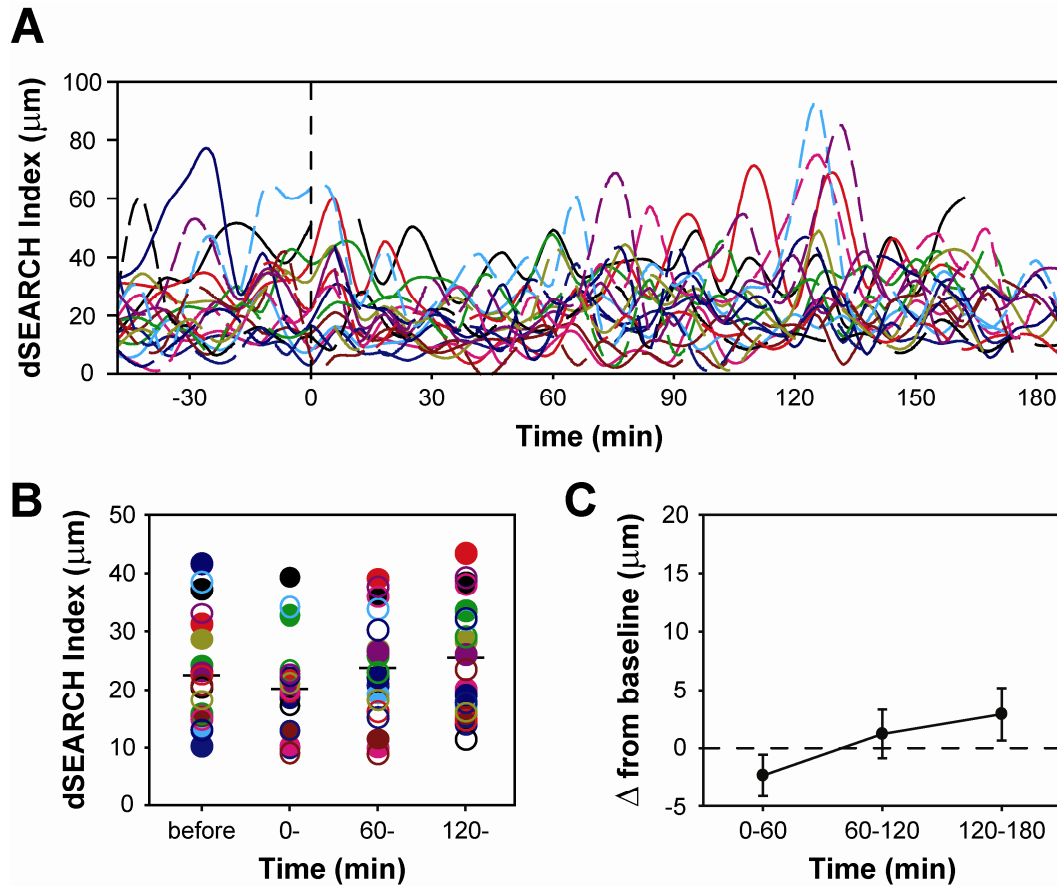


Figure 17. IL-1Ra prevents injury-induced increase in dSEARCH index in corneal LCs.

IL-1Ra was added to the circulating culture medium to achieve a concentration of 200 ng/ml, and the behaviors of corneal LCs were monitored before and after pinpoint thermal injury. (A) dSEARCH index values were calculated for 20 LCs in six independent experiments and plotted over time, with each line representing a single LC. Thermal injury was inflicted using the infrared laser at time zero, indicated with a dashed vertical line. (B) Mean dSEARCH index values were calculated for each LC before injury (**before**, -60 to 0 min) and during the early (**0-**, 0 to 60 min), middle (**60-**, 60 to 120 min), and late (**120-**, 120 to 180 min) phases after injury. The filled and open circles of a given color correspond to the solid and dashed lines, respectively, in (A). Mean values for all examined LCs are indicated with bars. No statistically significant differences from the baseline values (-60 to 0 min) were noted in any post-injury phase ($P >$

0.2). (D) To account for variability in the starting activity of different cells, the change in dSEARCH index over baseline was calculated for the data shown in (B). For each cell, the mean dSEARCH index value at baseline (-60 to 0 min) was subtracted from the mean values calculated for the early (0 to 60 min), middle (60 to 120 min), and late (120 to 180 min) phases after injury. The data shown represent the mean \pm SEM for all LCs.

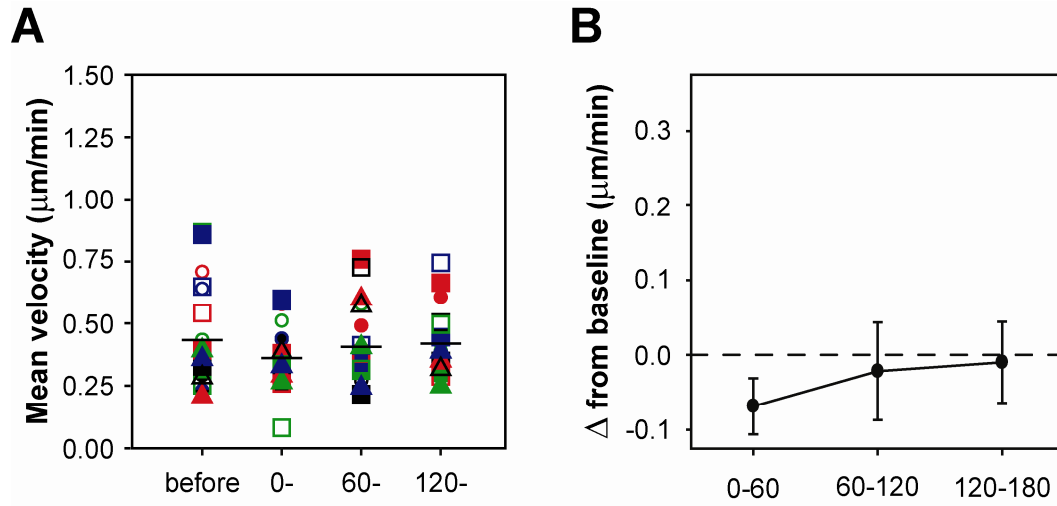


Figure 18. IL-1Ra prevents injury-induced lateral migration in corneal LCs.

After 60 min recording of baseline behaviors in the continuous presence of IL-1Ra (200 ng/ml) in the circulating culture medium, pinpoint thermal injury was inflicted to a target LC using the infrared laser of the two-photon microscope. (A) The mean distance each LC traveled per image set (i.e., every 2 min) was calculated from the x-y positions of the cell bodies before thermal injury (**before**, -60 to 0 min) and in the early (**0-**, 0 to 60 min), middle (**60-**, 60 to 120 min) and late (**120-**, 120 to 180 min) phases after injury. From these values, the mean rate of lateral movement for each cell was calculated. Mean values among all LCs are shown with bars. No statistically significant differences compared to baseline (**before**) were observed in any post-injury phase while in the presence of IL-1Ra ($P > 0.1$). (B) To account for the variability in the starting activity of different cells, the change in mean velocity over baseline was calculated for the data shown in (A). For each cell, the mean velocity at baseline (-60 to 0 min) was subtracted from those values computed for the early (0 to 60 min), middle (60 to 120 min), and late (120 to 180 min) phases after injury. Data shown represent the mean \pm SEM for all cells.

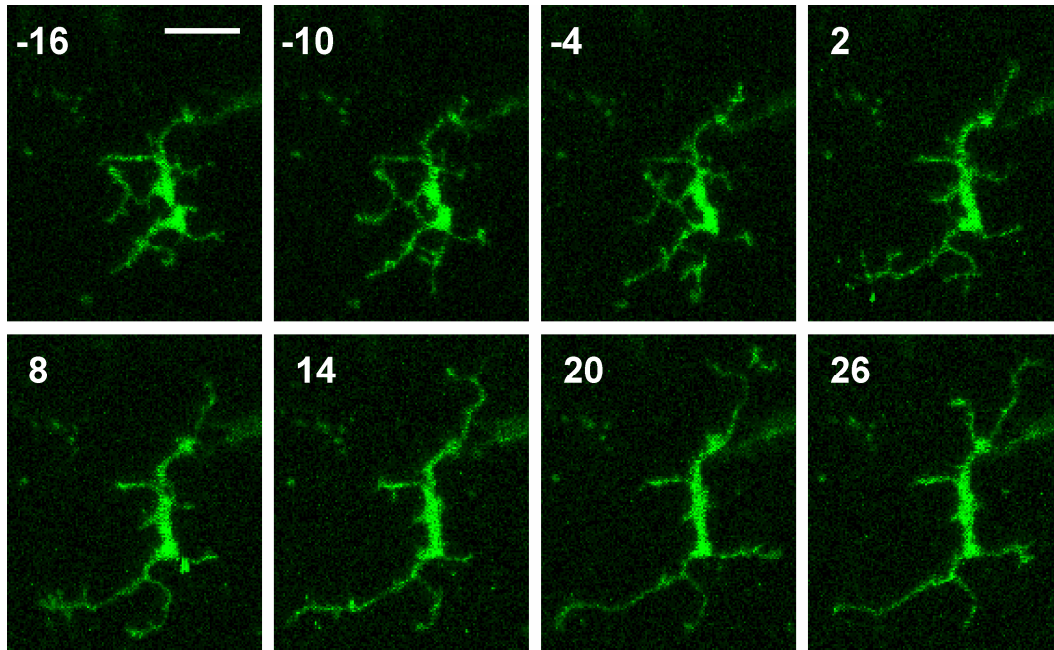


Figure 19. Exogenous IL-1 α induces transient augmentation of dSEARCH in EGFP⁺ corneal LCs.

After 60 min recording of the baseline behaviors of corneal LCs, mouse recombinant IL-1 α (5 pg/ml) was added to the circulating culture medium at time 0. The panels show the changes in dSEARCH of a representative LC. The images are maximum intensity projections of three-dimensional data sets collected every 6 min. Scale bar, 20 μ m.

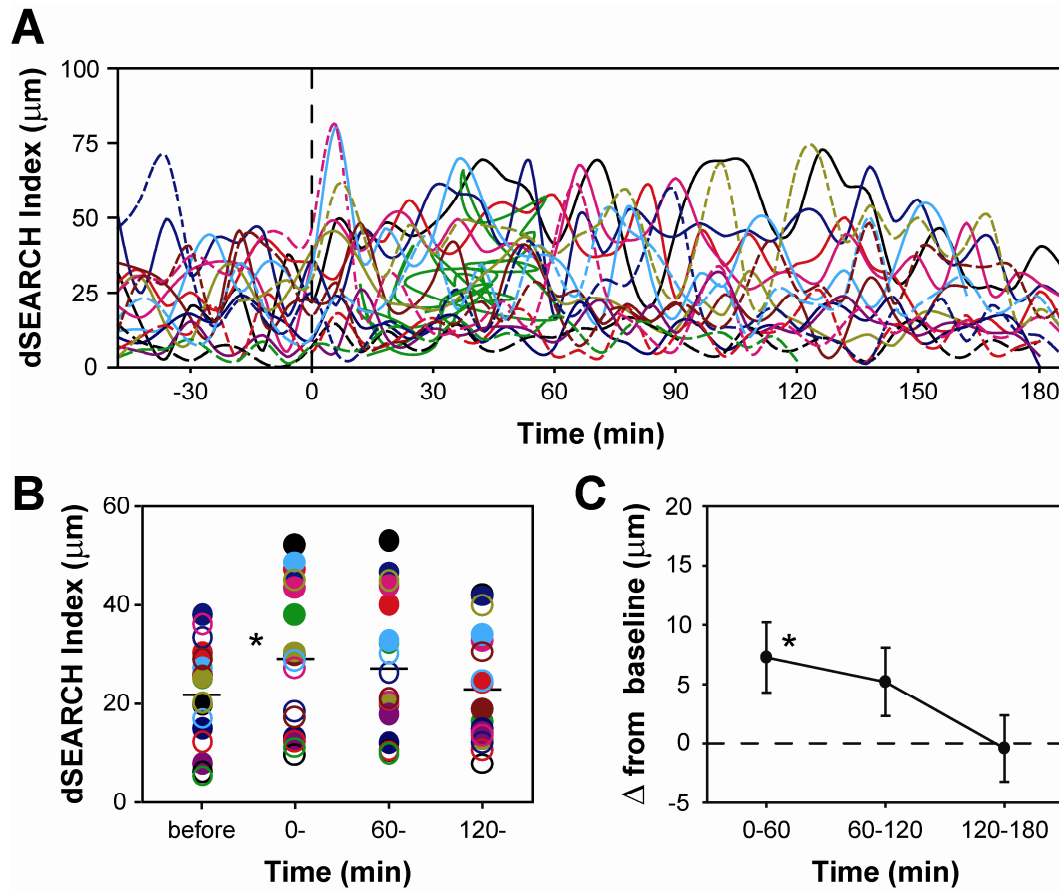


Figure 20. IL-1 α transiently elevates dSEARCH index values in corneal LCs.

Following 60 min recording of baseline behaviors, IL-1 α was added to the circulating medium to achieve a final concentration of 5 pg/ml. (A) dSEARCH index values were calculated for 18 LCs in 4 different experiments and plotted over time, with each line representing a single LC. IL-1 α was added to the medium at time 0, indicated with a dashed vertical line. (B) Mean dSEARCH index values were calculated for each LC before injury (**before**, -60 to 0 min) and during the early (**0-**, 0 to 60 min), middle (**60-**, 60 to 120 min), and late (**120-**, 120 to 180 min) phases after injury. The filled and open circles of a given color correspond to the solid and dashed lines, respectively, in (A). Mean values among LCs are shown with bars, and statistically significant differences compared with baseline (-60 to 0 min) are indicated with asterisks (* $P < 0.05$). (C) To account for variability in the starting activity of different cells, the change

in dSEARCH index over baseline was calculated for the data shown in (B). For each LC, the mean dSEARCH index value at baseline (-60 to 0 min) was subtracted from the mean values calculated for the early (0 to 60 min), middle (60 to 120 min), and late (120 to 180 min) phases after the addition of IL-1 α . Data shown represent the mean \pm SEM for all LCs. For reference, those groups in (B) that showed significant differences to baseline are indicated with asterisks.

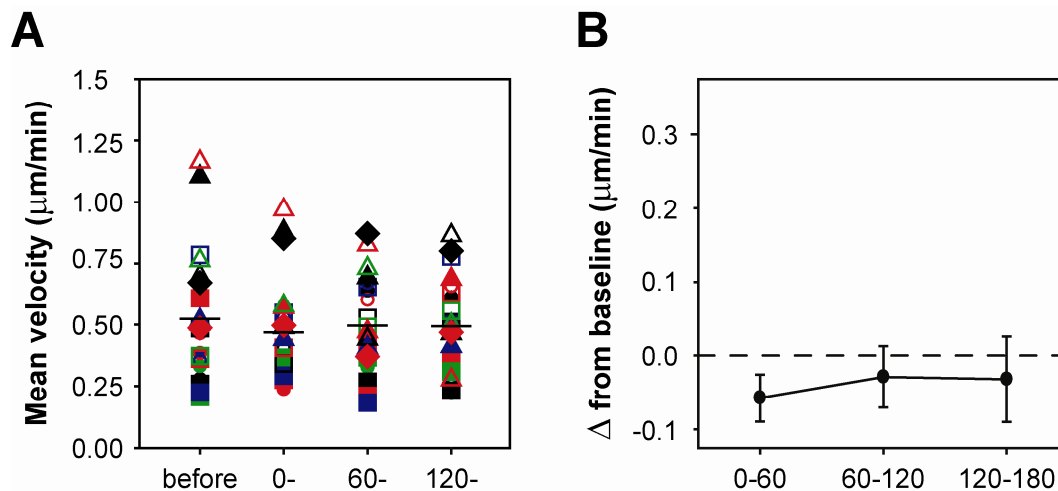


Figure 21. IL-1 α fails to induce an increase in lateral migration by corneal LCs.

After 60 min recording of baseline behaviors, mouse recombinant IL-1 α was added to the circulating culture medium to achieve a final concentration of 5 pg/ml. (A) The mean distance each LC traveled per image set (i.e., every 2 min) was calculated from the x-y positions of the cell bodies before the addition of IL-1 α (**before**, -60 to 0 min) and in the early (**0-**, 0 to 60 min), middle (**60-**, 60 to 120 min) and late (**120-**, 120 to 180 min) phases of treatment. From these values, the mean rate of lateral movement for each cell was calculated. Mean values among all LCs are shown with bars. No statistically significant differences compared to baseline (**before**) were observed after IL-1 α treatment ($P > 0.1$). (B) To account for the variability in the starting activity of different cells, the change in mean velocity over baseline was calculated for the data shown in (A). For each cell, the mean velocity at baseline (-60 to 0 min) was subtracted from those values computed for the early (0 to 60 min), middle (60 to 120 min), and late (120 to 180 min) phases of IL-1 α treatment. Data shown represent the mean \pm SEM for all cells.

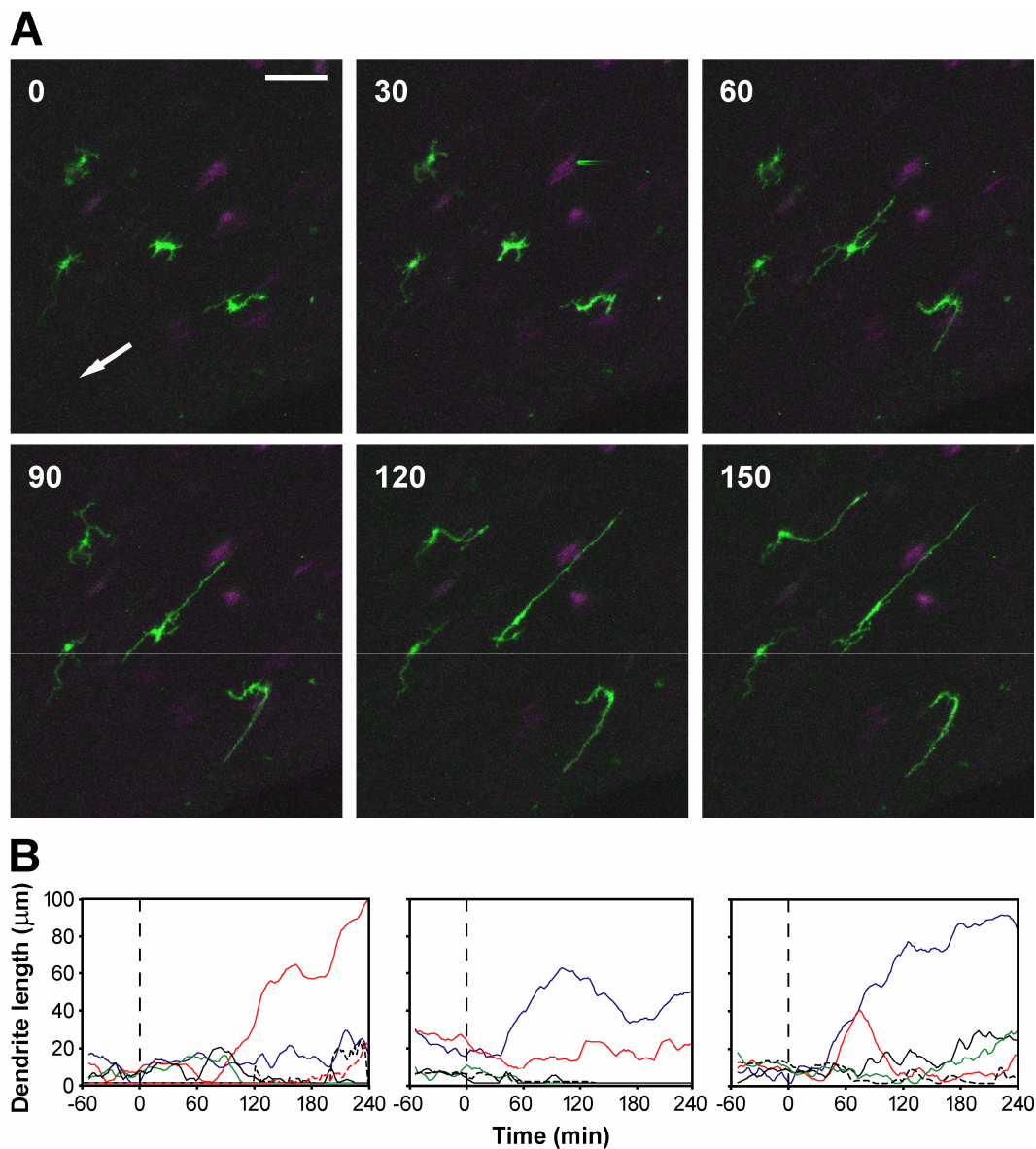


Figure 22. IL-1 α causes progressive dendrite elongation in corneal LCs at higher concentrations.

After 60 min recording of baseline behaviors, IL-1 α (100 pg/ml) was added to the circulating culture medium at time 0. (A) Panels show the maximum intensity projections of three-dimensional data sets collected at 30 min intervals, starting at time 0. Several intraepithelial EGFP⁺ LCs exhibit progressive elongation of their

dendrites in two opposing directions (the direction of the central cornea is indicated with an arrow). EGFP signals from cells in the stromal compartment are pseudo-colored in magenta. Scale bar, 50 μm . (B) The lengths of multiple dendrites of three representative EGFP⁺ LCs showing progressive dendrite elongation were measured at the indicated time points. Each line represents the length of a given dendrite measured every 2 min.

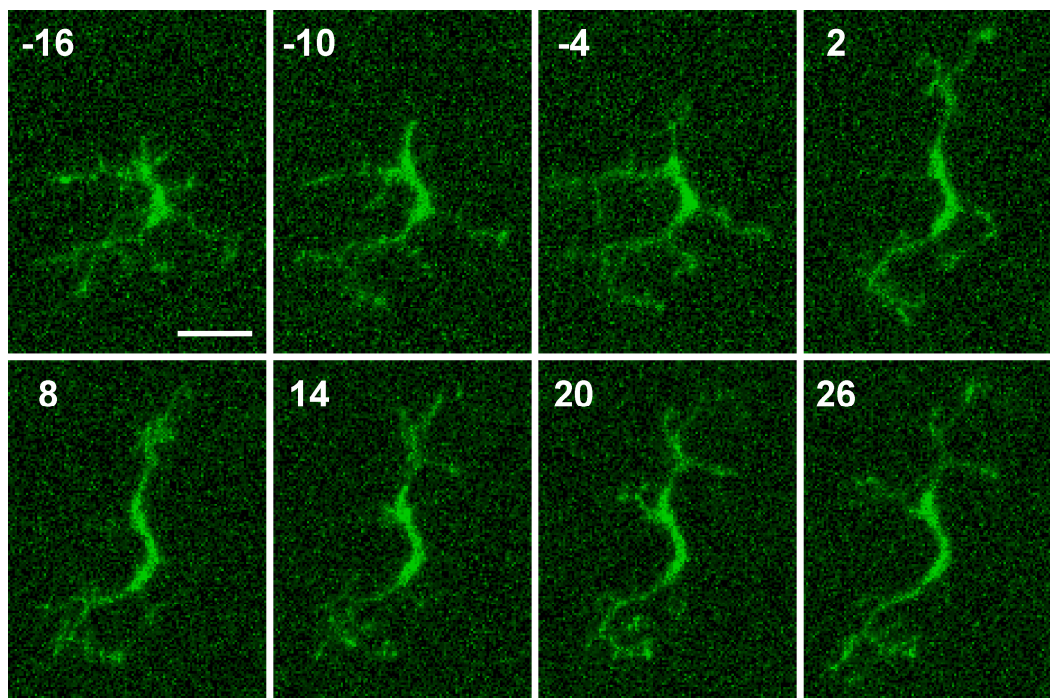


Figure 23. Exogenous TNF α elicits augmented dSEARCH by EGFP⁺ corneal LCs.

After 60 min recording of the baseline behaviors of corneal LCs, mouse recombinant TNF α (50 pg/ml) was added to the circulating culture medium at time 0. The panels demonstrate increase in dSEARCH activity of a representative LC. The images are maximum intensity projections of three-dimensional data sets collected every 6 min. Scale bar, 20 μ m.

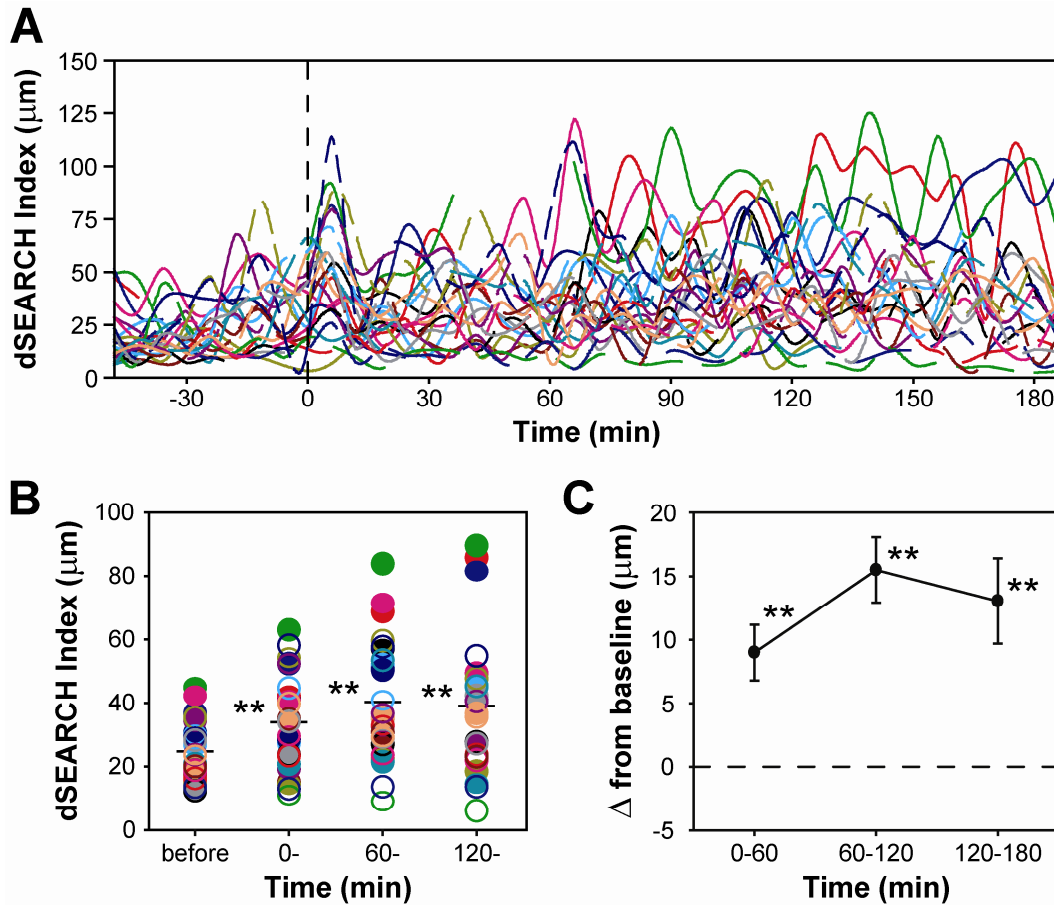


Figure 24. Exogenous $\text{TNF}\alpha$ causes an elevation in dSEARCH index values in corneal LCs.

Following 60 min recording of baseline behaviors, $\text{TNF}\alpha$ was added to the circulating culture medium to achieve a final concentration of 50 pg/ml. (A) dSEARCH index values were calculated for 26 LCs in 4 independent imaging experiments and plotted over time, with each line representing the values for a single LC. $\text{TNF}\alpha$ was added to the culture medium at time 0, indicated with a dashed vertical line. (B) Mean dSEARCH index values were calculated for each LC before injury (**before**, -60 to 0 min) and during the early (**0-**, 0 to 60 min), middle (**60-**, 60 to 120 min), and late (**120-**, 120 to 180 min) phases after injury. The filled and open circles correspond to the solid and dashed lines, respectively, in (B). The mean values among all LCs are indicated with bars, and statistically significant differences compared with baseline (-60 to 0 min) are indicated with

asterisks (** $P < 0.01$). (C) To account for variability in the starting activity of different cells, the change in dSEARCH index over baseline was calculated for the data shown in (B). For each LC, the mean dSEARCH index value at baseline (-60 to 0 min) was subtracted from the mean values calculated for the early (0 to 60 min), middle (60 to 120 min), and late (120 to 180 min) phases after the addition of TNF. Data shown represent the mean \pm SEM for all LCs. For reference, those groups in (B) that showed significant differences to baseline are indicated with asterisks.

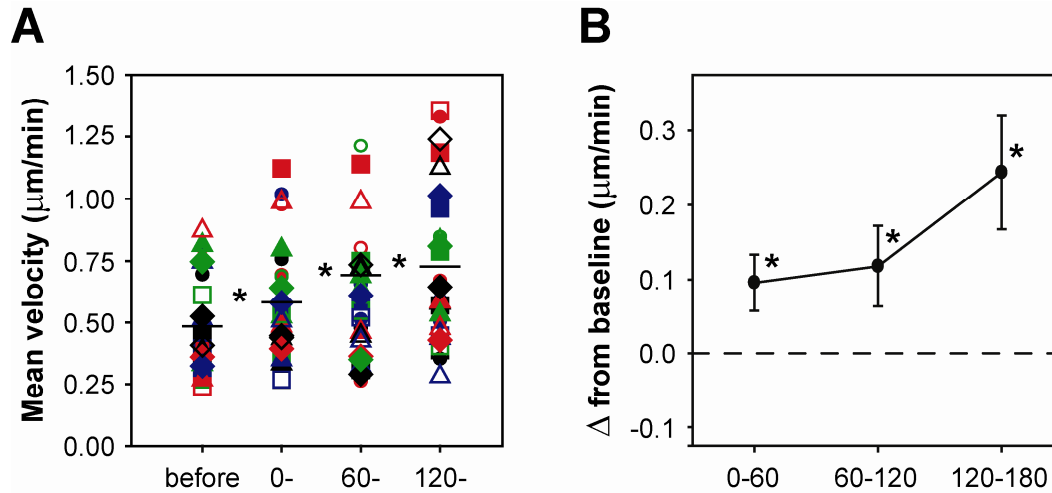


Figure 25. Exogenous TNF α induces lateral migration by corneal LCs.

After 60 min recording of baseline behaviors, mouse recombinant TNF α was added to the circulating culture medium to achieve a final concentration of 50 pg/ml. (A) The mean distance each LC traveled per image set (i.e., every 2 min) was calculated from the x-y positions of the cell bodies before the addition of TNF α (**before**, -60 to 0 min) and in the early (**0-**, 0 to 60 min), middle (**60-**, 60 to 120 min) and late (**120-**, 120 to 180 min) phases of treatment. From these values, the mean rate of lateral movement for each cell was calculated. Mean values among all LCs are shown with bars, and statistically significant differences compared to baseline (**before**) are indicated with asterisks (* $P < 0.05$). (B) To account for the variability in the starting activity of different cells, the change in mean velocity over baseline was calculated for the data shown in (A). For each cell, the mean velocity at baseline (-60 to 0 min) was subtracted from those values computed for the early (0 to 60 min), middle (60 to 120 min), and late (120 to 180 min) phases of IL-1 α treatment. Data shown represent the mean \pm SEM for all cells. For reference, those groups in (A) that showed significant differences to baseline are indicated with asterisks.

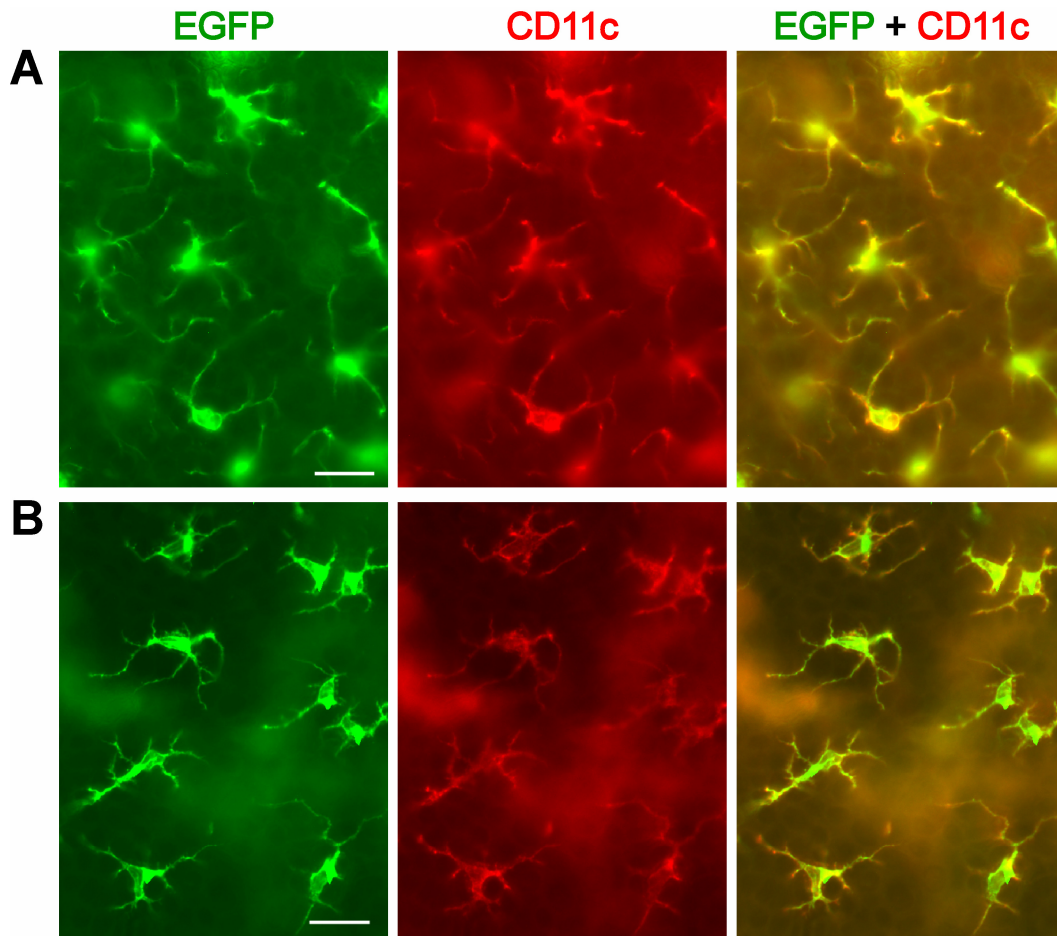


Figure 26. LCs in the epidermis after diffuse inflammatory stimuli.

Epidermal sheets were prepared from I-A β -EGFP knock-in mice skin samples, then labeled with PE-conjugated anti-CD11C mAb and examined by conventional fluorescence microscopy. (A) Skin samples were collected from knock-mice and cultured for 16 hours at 37° C before preparing epidermal sheets. (B) TNF α was injected s.c. into the ears of I-A β -EGFP knock-in mice. Ear skin samples were collected after 16 hr, and epidermal sheets were immediately prepared. After both treatments, the LCs in the epidermis show morphological changes associated with maturation, including increased cell size and elongation of the dendritic processes. Even after skin organ culture or TNF α injection, all EGFP⁺ cells in the epidermis expressed CD11c, and vice versa. Scale bars, 20 μ m.

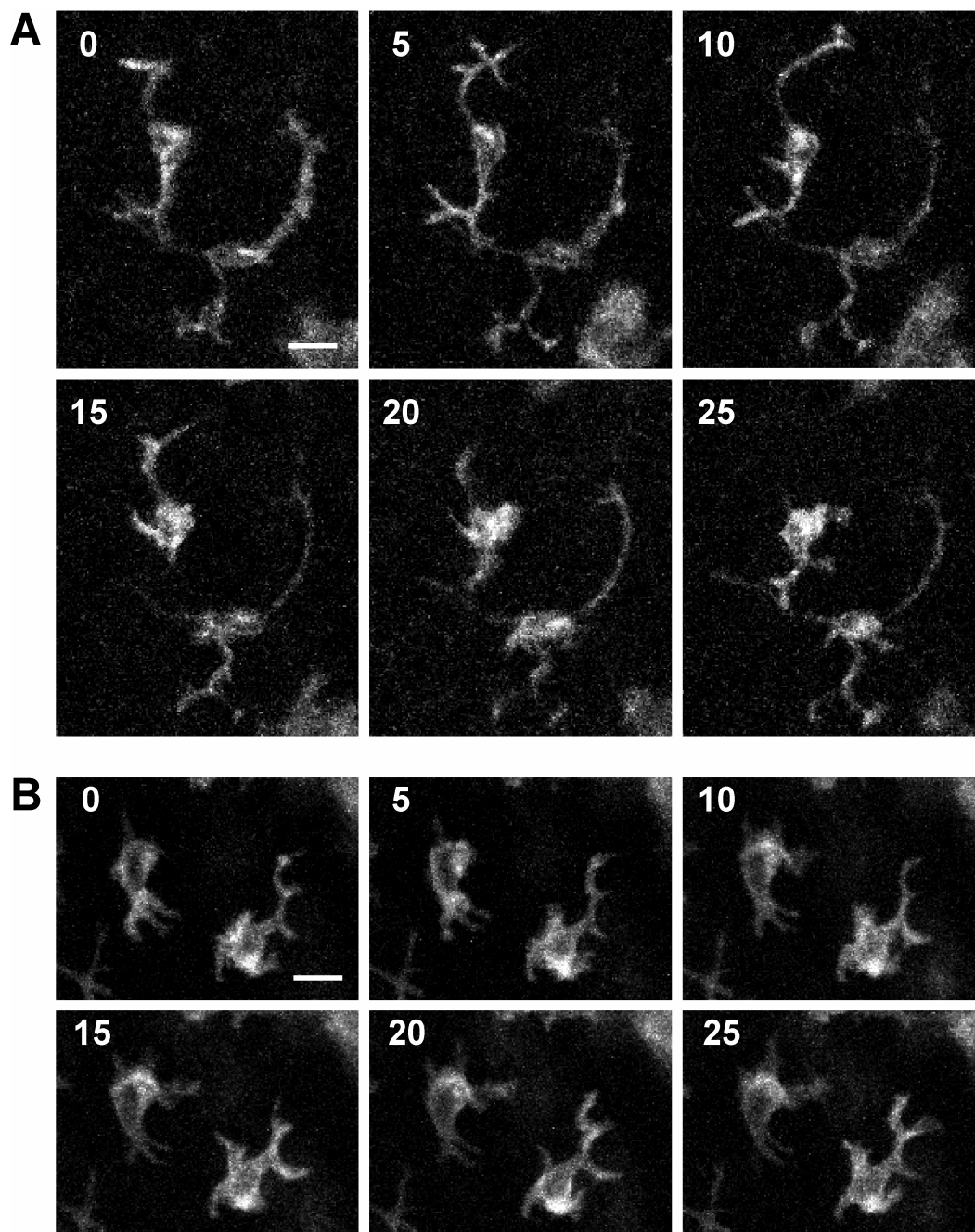


Figure 27. dSEARCH recorded *ex vivo* in EGFP⁺ epidermal LCs after diffuse inflammatory stimuli.

Representative dSEARCH is shown for I-A β -EGFP knock-in mice ear skin samples imaged by confocal microscopy after diffuse inflammatory stimuli. (A) Ear skin samples from knock-in mice were harvested and cultured for 16 hours at 37° C, and then imaged by confocal microscopy. (B) TNF α was injected s.c. into the ears of I-A β -EGFP knock-in mice, and 16 hours later the ear skin samples were collected and imaged by confocal microscopy. The panels display maximum intensity projections of three-dimensional data sets collected at 5 min intervals. Scale bars, 10 μ m.

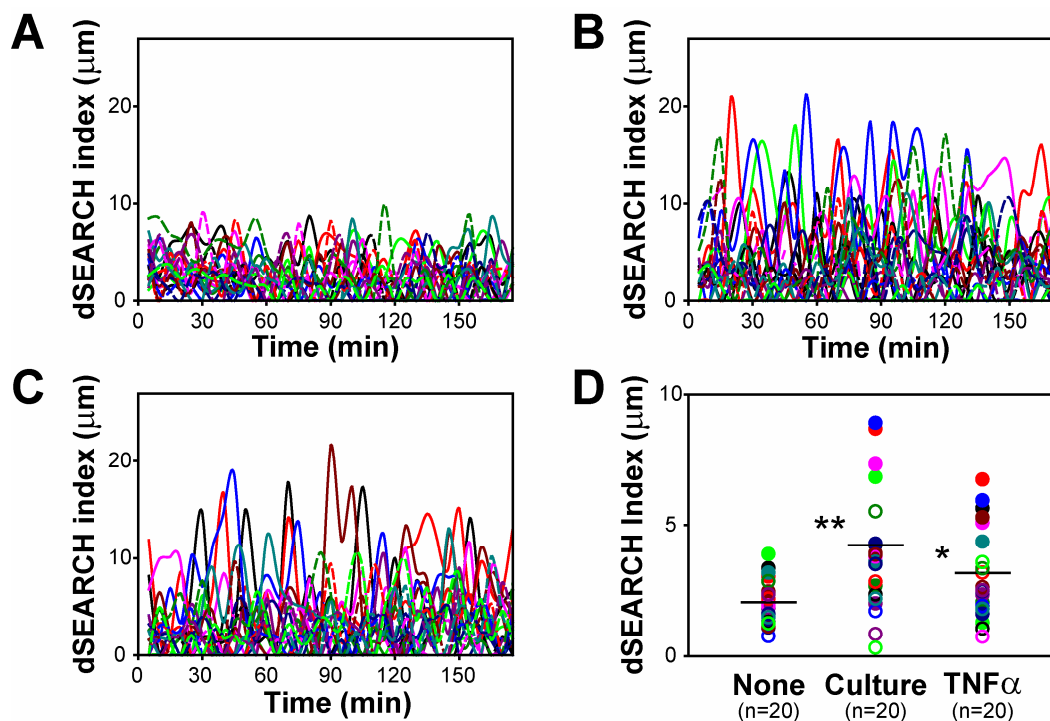


Figure 28. dSEARCH index of epidermal LCs is elevated by inflammatory stimuli *ex vivo*.

dSEARCH index values were calculated for individual EGFP⁺ epidermal LCs every 5 min for the entire 175 min observation period in ear skin samples freshly harvested from I-Aβ-EGFP knock in mice (A), after 16 hour skin organ culture (B), or 16 hours after s.c. injection of TNFα (C). Each line indicates the dSEARCH index values calculated for an individual LC. (D) Mean dSEARCH index values were calculated for all LCs over the entire imaging period. Mean values amongst all LCs are indicated with bars, and statistically significant differences compared to baseline (no treatment) are indicated with asterisks (* $P < 0.05$, ** $P < 0.01$). Filled and open circles of a given color correspond to the solid and dashed lines in (A) through (C).

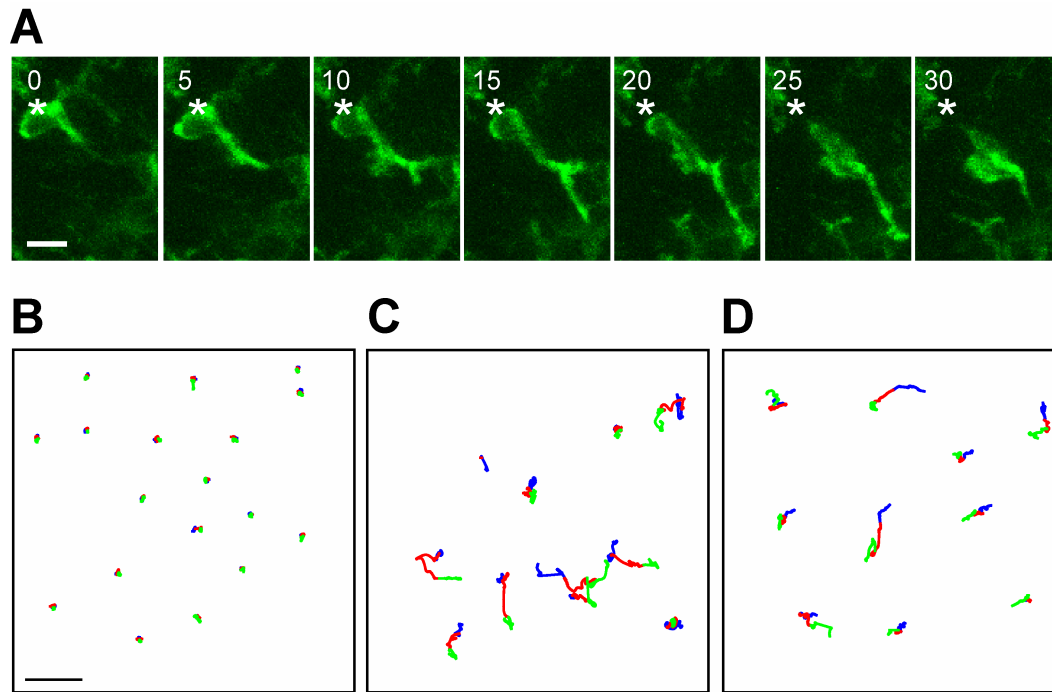


Figure 29. Inflammation-associated lateral migration of EGFP⁺ epidermal LCs *ex vivo*.

Skin samples from I-A β -EGFP knock-in mice were imaged by confocal microscopy, and lateral migration by LCs was monitored by recording the x-y positions of the cell bodies over time. (A) Lateral migration by a representative LC after 16 hour skin organ culture is shown. Panels show maximum intensity projections of three-dimensional data sets acquired every 5 min. Asterisks indicate the original location of the LC at time 0. Scale bar, 10 μ m. (B-D) The x-y locations of EGFP⁺ LCs were recorded in skin samples freshly harvested from I-A β -EGFP knock-in mice (B), after 16 hour skin organ culture (C), or 16 hours after s.c. injection of TNF α (D). The panels show the x-y positions of LCs from 0 to 60 min (blue), 60 to 120 min (red), and 120 to 180 min (green). Scale bar, 30 μ m.

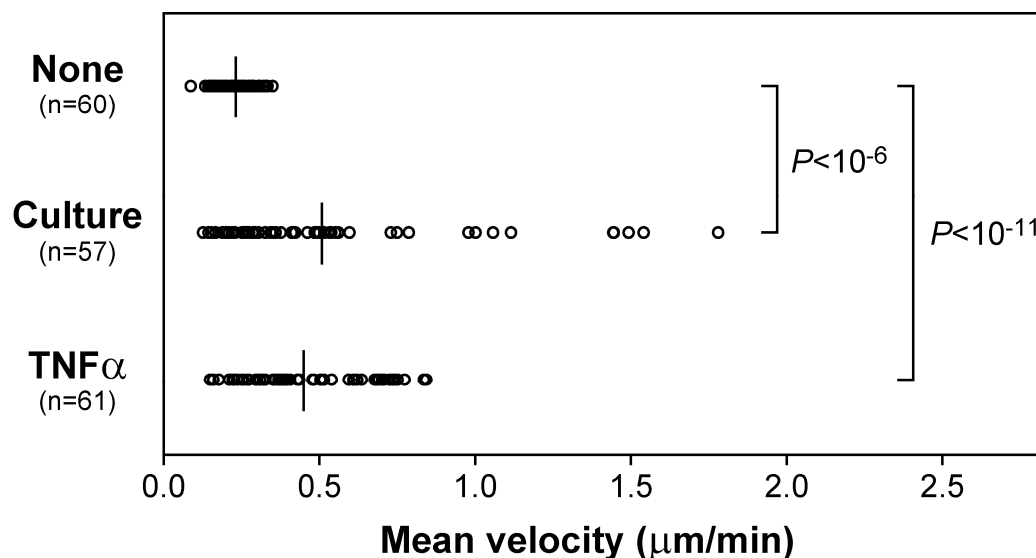


Figure 30. Inflammatory stimuli increase lateral migration of epidermal LCs *ex vivo*.

The x-y positions of EGFP⁺ epidermal LCs were recorded for every image frame (i.e., every 5 min) in skin samples freshly harvested from I-Aβ-EGFP knock-in mice (None), after 16 hour skin organ culture (Culture), and 16 hours after s.c. injection of TNFα (TNFα). These values were then used to calculate the mean velocity of each LC over the entire imaging period. The Mean values among all LCs for a given experimental condition are indicated with bars, and the statistical differences between groups are indicated.

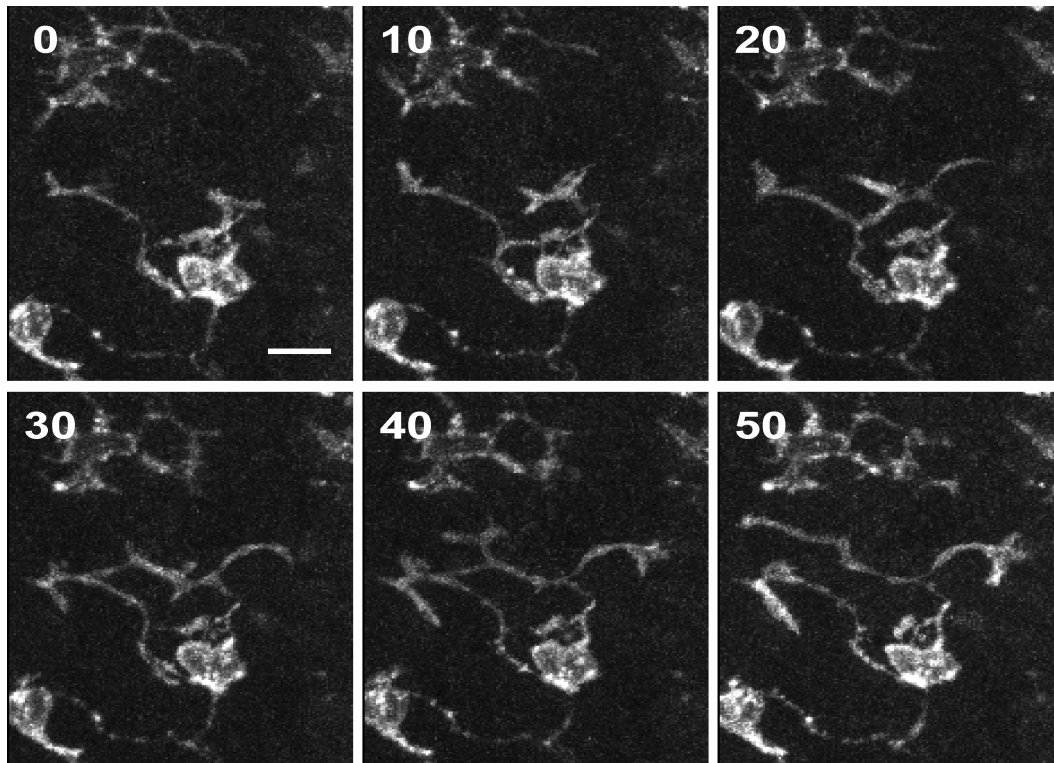


Figure 31. Topical hapten application induces augmented dSEARCH by EGFP⁺ epidermal LCs *in vivo*.

The ear skin of anesthetized I-A β -EGFP knock-in mice were examined by intravital confocal microscopy 30 hours after topical application of DNFB. The panels show representative maximum intensity projections of three-dimensional data sets collected at 10 min intervals. Scale bar, 20 μ m.

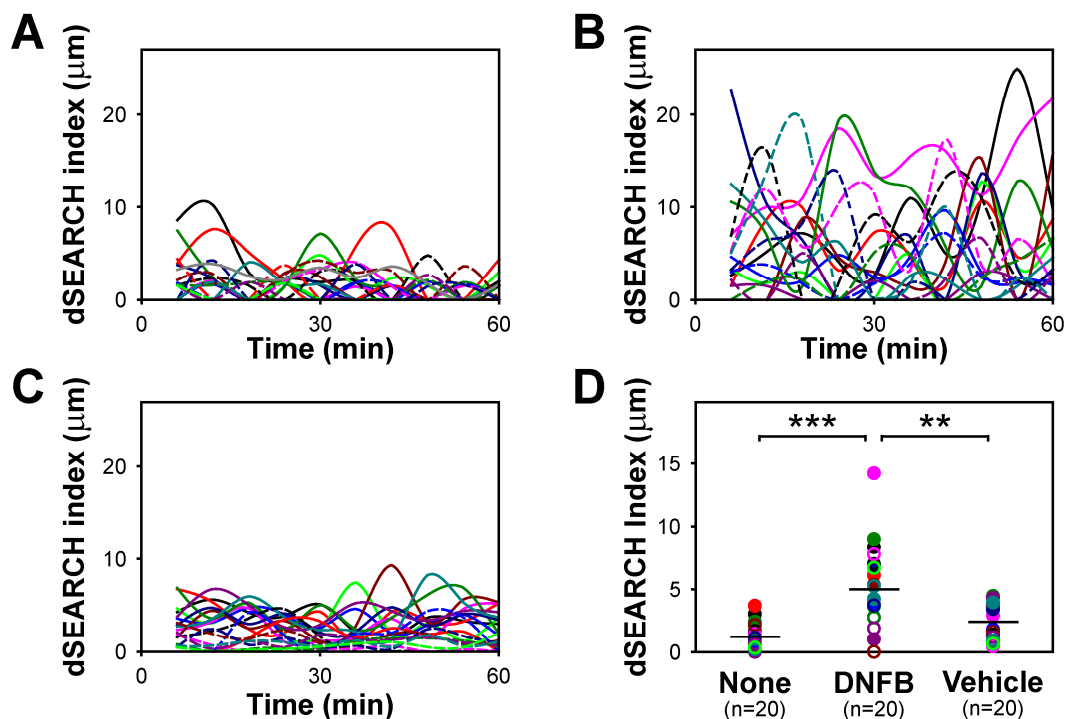


Figure 32. dSEARCH index values of epidermal LCs are elevated after hapten application *in vivo*.

EGFP⁺ LCs in the ear skin of anesthetized I-A β -EGFP knock-in mice were imaged by intravital microscopy. (A-C) dSEARCH index values were calculated for LCs in untreated skin (A) or 30 hours after application of DNFB (B) or vehicle alone (C). Each line represents the dSEARCH index values of a single LC. (D) Mean dSEARCH index values for the entire imaging period were calculated for each LC. Mean values among the LCs in each treatment group are indicated with bars, and statistically significant differences between groups are indicated with asterisks (** $P < 0.01$, *** $P < 0.001$). The filled and open circles of a given color correspond to the solid and dashed lines, respectively, in (A) through (C).

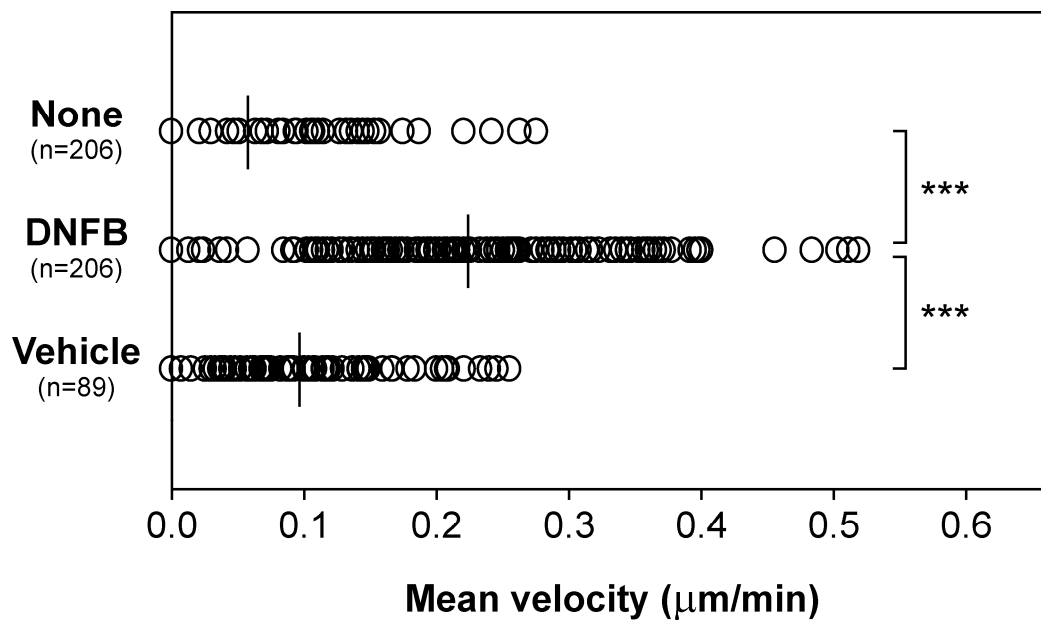


Figure 33. Application of reactive hapten induces lateral migration of epidermal LCs *in vivo*.

Anesthetized I-A β -EGFP knock-in mice were examined by intravital confocal microscopy for the migratory activities of EGFP⁺ epidermal LCs in the steady state (None) or 30 hours after the application of DNFB (DNFB) or vehicle alone (Vehicle). The x-y positions of the cell bodies were tracked over time, and the mean velocities over the imaging period were calculated. Mean values among all the LCs for different treatment protocols are indicated with bars, and statistically significant differences between groups are indicated with asterisks (***) $P < 0.001$).

Legends to Supplemental Movies

Movies 9-11. Time-lapse images of injury induced augmentation of dSEARCH and lateral movement in corneal LCs.

The three movies demonstrate injury-induced amplification of dSEARCH and lateral migration of EGFP⁺ corneal LCs observed consistently in 8 independent imaging experiments. After 60 min recording of baseline behaviors, pinpoint thermal injury was produced at time 0 in an EGFP⁺ LC indicated with an arrow. Note the increased activity of the dendrites and the propensity for lateral movement within the epithelium after injury.

Movie 12. Time-lapse images of injury-induced lateral migration by corneal LCs.

After 60 min recording of baseline behaviors, pinpoint thermal injury was produced at time 0 in and EGFP⁺ LC indicated with an arrow. Two LCs in the vicinity of the injury site show immediate and drastic migratory responses. While these cells are seen migrating toward the site of injury, in general LC migration after injury occurred in random paths with no apparent directional bias (e.g., toward the injury site). Additionally, a large EGFP⁺ stromal cell with an amorphous shape (indicated with an asterisk) exhibits an unusual response characterized by rapid migration toward the injury site followed by casting fine, mesh-like projections toward the neighboring LCs.

Movies 13-14. Time-lapse images of the impact of IL-1Ra on injury-triggered changes in corneal LC behaviors.

Data sets shown in Figure 16 (Movie 13) and from an independent experiment (Movie 14) were compiled to show the dynamic behavioral responses of corneal LCs to local injury in the presence of IL-1Ra, which was added to the circulating media at time -60 to achieve a concentration of 200 ng/ml. After 60 min recording of baseline behaviors, pinpoint thermal injury was produced at time 0 in an EGFP⁺ LC indicated with an arrow. Note how the activity of the dendrites does not change appreciably after injury and how EGFP⁺ LCs do not move significantly from their original positions. In Movie 13, a large, amorphously shaped EGFP⁺ cell in the stroma is indicated with an asterisk.

Movies 15-16. Time-lapse images of IL-1-induced amplification of dSEARCH in corneal LCs.

The data set shown in Figure 19 (Movie 15) and the data set from an independent experiment (Movie 16) were compiled to show the dynamic behavioral responses of corneal LCs to IL-1. After 60 min recording of baseline behaviors, IL-1 α was added to the circulating media at time 0 to achieve a final concentration of 5 pg/ml. Note the increase in the activity of the dendrites after addition of IL-1 and the relative absence of lateral movement by LCs.

Movie 17. Time-lapse images of dendrite hyper-elongation in corneal LCs triggered by IL-1 at a high concentration.

The data set shown in Figure 22 was compiled to show the dynamic behavioral responses of corneal LCs to IL-1. After 60 min recording of baseline behaviors, recombinant IL-1 α was added to the circulating medium at time 0 to achieve a final concentration of 100 pg/ml. Note the profound elongation of the dendrites in the absence of significant lateral movement.

Movies 18-19. Time-lapse images of TNF α -induced changes in corneal LC behaviors.

Data sets shown in Figure 23 (Movie 18) and from an independent experiment (Movie 19) were compiled to show the dynamic behavioral responses of corneal LCs to TNF α . After 60 min recording of baseline behaviors, recombinant TNF α was added to the circulating culture media at time 0 to achieve a final concentration of 50 pg/ml. Note an increase in dendrite activity and lateral movement similar to the changes seen after tissue injury.

Movies 20-21. Time-lapse images of *ex vivo* behaviors of epidermal LCs after skin organ culture.

The same data set shown in Figure 27A (Movie 20) and the data set from an independent experiment (Movie 21) were compiled to show the dynamic behaviors of EGFP⁺ epidermal LCs after prolonged skin organ culture. Ear skin samples were harvested and cultured for 16 hours before imaging by confocal

microscopy. Note the increased dendrite activity and lateral movement observed after prolonged culture.

Movie 22. Time-lapse images of *ex vivo* behaviors of epidermal LCs after local TNF α injection.

Imaging data were compiled to show the dynamic behaviors of EGFP⁺ epidermal LCs after injection of TNF α . Sixteen hours after s.c. injection of recombinant TNF α into the ear, skin samples were harvested and imaged by confocal microscopy. Note the provoked dSEARCH and motile activities of the EGFP⁺ epidermal LCs.

Movie 23. Time-lapse images of exacerbated *in vivo* behaviors of epidermal LCs in hapten-treated skin.

The same data set shown in Figure 31 was compiled to show the provoked motile activities of EGFP⁺ epidermal LCs recorded *in vivo* 30 hours after the application of DNFB. An overlap of dendrite-associated EGFP signals between neighboring LCs is indicated with an arrow.

LC BEHAVIORAL RESPONSES TO PATHOGENIC ORGANISMS

Generation of Fluorescent Bacteria for *In Situ* Imaging

Having discovered several unique behavioral responses of LCs to inflammatory stimuli, specifically augmentation of dSEARCH and lateral migration, we reasoned that the phenomena associated with bacterial infection would also lead to similar dynamic responses by LCs. However, in order to observe the infection of the epithelial tissue and the interactions between LCs and the pathogens, bacterial cells were needed that could be directly observed by fluorescence.

Transformation of Pseudomonas aeruginosa by the Mini-Tn7 Transposon

As an opportunistic Gram-negative bacterium that infects a variety of epithelial tissues, including both the cornea and the epidermis, *Pseudomonas aeruginosa* was chosen as a model pathogen for use in imaging experiments with corneal and epidermal LCs. Several different methods of fluorescent labeling were considered, but stable integration of a fluorescent protein gene into the chromosome using a transposon was seen as the optimal technique, since plasmid selection pressure would not have to be maintained and there would be fewer

complications than with chemical labeling. To achieve stable integration without fear of deleterious effects from random insertion into vital genes, the mini-Tn7 system was chosen, as the Tn7 transposon is known to stably integrate into the well characterized *attTn7* site downstream of the *glmS* gene in a location that does not interfere with bacterial growth or performance (167).

Plasmids containing the genes encoding ECFP, EYFP, and DsRed were obtained, and transformation of the *P. aeruginosa* strain PA01 was performed according the protocol developed by Lambertsen, et al (168). Immediately after transformation, individual colonies were chosen and examined for ECFP, EYFP, or DsRed expression by confocal microscopy. Intense fluorescence was seen in these samples (data not shown), and therefore the cultures were frozen to create stock cultures. Unfortunately, examination of cultures grown in LB broth from the stock sample failed to show fluorescence under confocal examination.

To exclude the possibility that expression of the fluorescent protein was causing harm to the bacterial cells, via inclusion bodies or aggregates, transformed PA01 cells were grown under selection pressure in parallel with untransformed cells. No differences were observed in the growth or viability of the bacterial cells between the transformed and non-transformed controls after overnight culture. Furthermore, as fluorescent proteins need time to mature after

translation to attain their fluorescent properties, transformed and non-transformed cells were grown in liquid cultures for extended times, and fluorescence intensity was measured with a photon counter. Again, no differences in fluorescence intensity were observed between the transformed and non-transformed controls at any time point up to 72 hours after the start of the culture (Figure 34). Moreover, insertion of the Tn7 transposon into the PA01 cells was confirmed by Dr. Kevin McIver using PCR, and the viability of the fluorescent protein genes within the transposon was determined by positive expression of the ECFP, EYFP, and DsRed in the *Escherichia coli* strains harboring the original transposon plasmids (Figure 35). Therefore, while the transformation had indeed taken place, DsRed expression by the transformed PA01 cells was not sufficient for detection by the confocal microscope. Thus, an alternative strategy for fluorescent labeling of the bacterial cells needed to be used.

Labelling of Pseudomonas aeruginosa Cells by CMTMR

Though the procedures for preparing the cells for imaging experiments are more complicated, chemical labeling of the bacterial cells was chosen over fluorescent protein expression from a plasmid because the absence of antibiotic selection pressure in the infected tissue would not interfere with the detection of fluorescence. The cell tracking dye CMTMR was chosen for its fluorescent properties, as it could be imaged along with EGFP using standard fluorescence

filter sets. Like CFSE and other cell tracking dyes, CMTMR is freely diffusible across biological membranes and enters the cytoplasm of the bacterial cells. Once inside the cell, intracellular esterases catalyze a reaction that links a functional group of the dye to intracellular components, most likely glutathione via glutathione-S-transferases. The process results in cells that can be detected by fluorescence, until such time as cell division by the labeled cells dilutes the amount of dye in each cell to undetectable levels.

Cells of the *P. aeruginosa* strain PA01 were grown in overnight broth cultures and then labeled with CMTMR. Indeed, after labeling in this manner, the bacterial cells exhibited marked fluorescence under confocal microscopy (Figure 36A). Regrettably, after as little as 8 hours of further growth in liquid culture or in infections *in vivo*, fluorescence by the CMTMR-labeled bacteria was completely absent. Upon further examination, it became evident that the dye was not only being diluted by division of the bacterial cells, but was being actively secreted as well, as fluorescence could be identified in strands of extracellular material within clumps of cells after observation by confocal microscopy (Figure 36B).

ECFP and EYFP Expression by Plasmid Vectors

As a final means of obtaining bacterial cells that could be detected by fluorescence *in situ*, plasmid vectors encoding ECFP and EYFP under the control of a robust promoter were obtained. With extremely strong fluorescent protein expression observed by the investigators that developed the plasmids, we hoped that the absence of selection pressure during infection would be countered high level of protein expression at the time of inoculation. Indeed, intense fluorescence was observed in transformed cells of both *P. aeruginosa* strain PA01 and *E. coli* strain DH5 α after overnight culture in liquid medium and even 18 hours after inoculation *in vivo* (Figure 37, see also Movie 27).

LC Responses to Bacterial Cells *In Vivo*

With possession of fluorescent bacteria that could be observed along with LCs under the confocal microscope, we decided to test the LCs behavioral responses to infection. It was decided that all further imaging experiments would be performed *in vivo*, since the dynamic behaviors observed in this setting would obviously be the most physiologically relevant to naturally acquired infections. Unfortunately, *in vivo* imaging of corneal tissues by laser scanning techniques, including multiphoton and confocal laser scanning microscopy, is impractical with current technology; random, involuntary movements of the eye, even under

anesthesia, result in disruption of the field of view while the tissue is being scanned. Therefore, the behavioral responses of LCs to invading organisms were studied exclusively in skin of living animals, and as such, fluorescent *E. coli* was used as a more relevant pathogen of the epidermis.

Epidermal LCs Show Augmented dSEARCH in Response to Bacterial Infection

In healthy animals, the stratum corneum of the skin provides a resilient exterior barrier that prevents potential pathogens from gaining access to the underlying tissues. With this barrier in place, experimental infections are difficult to initiate, and interactions between pathogens and LCs, which occupy positions just above the basal keratinocytes, are not possible. Thus, tape-stripping, a standard protocol for removing the stratum corneum in which adhesive tape was repeatedly applied and removed from the skin, was performed on the ear skin of I-A β -EGFP knock-in mice before infection (169-172). Mechanical removal of the stratum corneum in a manner such as this is known to induce slight irritation and inflammation in the skin, and so the LCs in the ears of anesthetized I-A β -EGFP knock-in mice were first examined by intravital confocal microscopy 18 hours after tape-stripping in the absence of infection (169,173-175).

As expected, LCs in the epidermis exhibited visibly augmented dSEARCH after tape-stripping (Figure 38 and Movies 24 & 25). Indeed, the

dSEARHC index values of LCs in tape-stripped skin, measured at 8 min intervals, were significantly elevated above the steady-state controls (Figure 39). It was surprising to note, however, that the morphology of the LCs after tape-stripping was more reminiscent of LCs in the steady than that seen after DNFB application (compare Figures 31 and 38 and Movies 23 and 24). This suggests that tape-stripping did not produce maximal levels of inflammation and/or LC activation.

Conversely, extreme activation was seen in LCs after infection of the ear skin. Immediately after tape-stripping the ear skin, fluorescent *E. coli* from a fresh overnight liquid culture were applied to the ears of I-A β -EGFP knock-in mice. After an 18 hour incubation period, the mice were anesthetized and the ear skin examined by intravital confocal microscopy. LCs in infected skin exhibited markedly increased dSEARCH, as well as the characteristic morphological changes associated with *in situ* activation (Figure 40 and Movies 26 & 27). This observation was substantiated by measuring the dSEARCH index values of the epidermal LCs, which were significantly elevated over both steady state and tape-stripping alone (Figure 39). Thus, infection of the skin elicits robust intensification of the dSEARCH activity of the dendrites in LCs and suggests that additional inflammatory factors are elicited during infection compared to mechanical injury alone.

Epidermal LC Migration After Infection of the Skin

In previous experiments, the migratory activities of epidermal LCs were augmented after diffuse inflammatory stimuli, a property that correlated with amplified dSEARCH. Likewise, the intermediate level of activation seen in LCs after tape-stripping alone, as identified by elevated dSEARCH, corresponded to a modest increase in lateral migration. Furthermore, LCs in skin infected with *E. coli* exhibited an exceptional increase in lateral migration (Figure 41). By measuring the average distance traveled by each LC between imaging frames, statistically significant increases in lateral migration were displayed by LCs in tape-stripped skin versus the steady state, and LCs in skin infected by *E. coli* showed significant elevation above both steady state and tape-stripped controls (Figure 42). Thus, the same step-wise increase in LC activation found in the dSEARCH index measurements was observed for lateral migration after tape-stripping and infection.

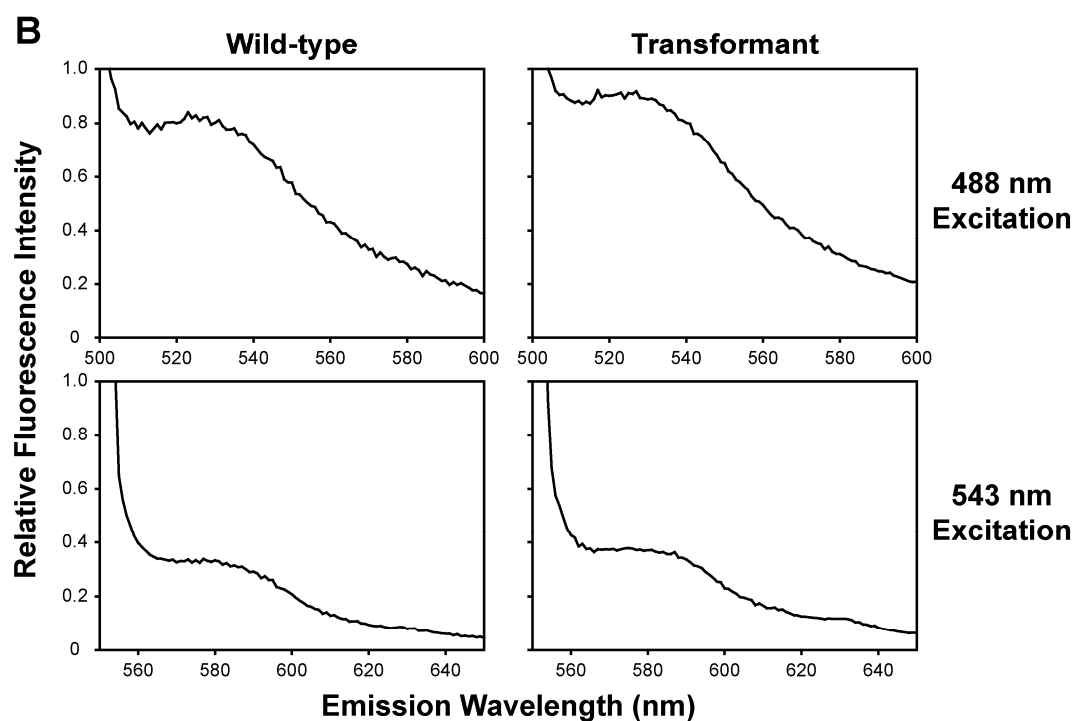
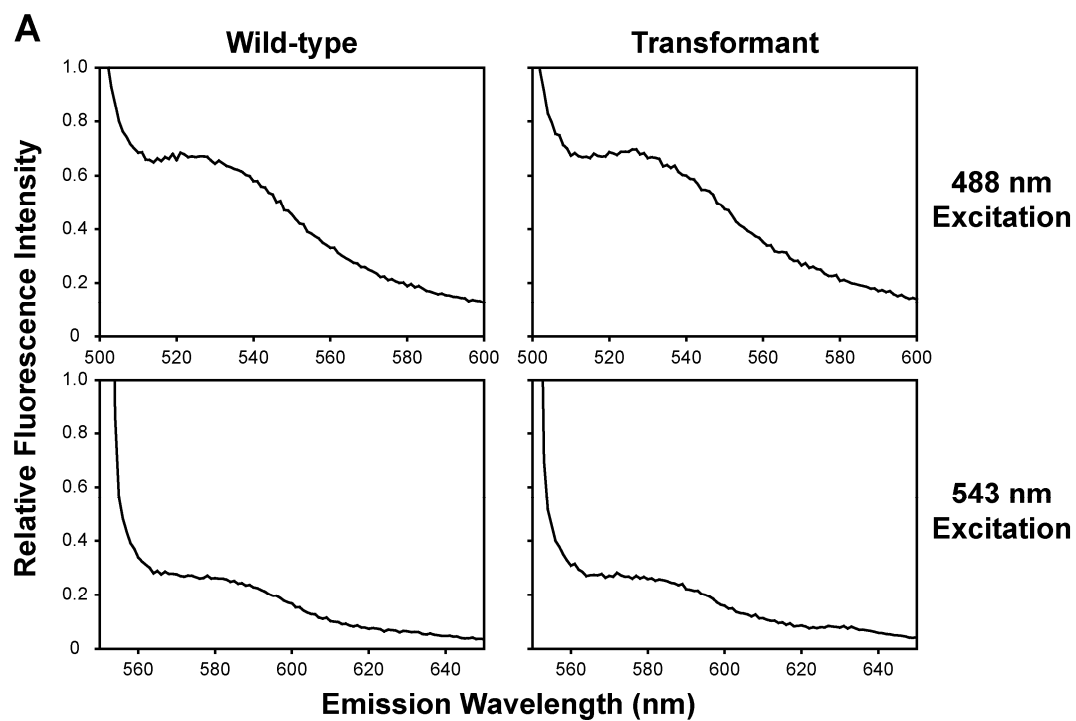


Figure 34. DsRed fluorescence emission by mini-Tn7-transformed *Pseudomonas aeruginosa*.

P. aeruginosa clone PA01 cells were transformed using a mini-Tn7 transposon containing the *dsred* gene. After one overnight passage post-transformation, transformed and control PA01 cells were grown at 37° C with constant shaking for varying lengths of time. Fluorescence was measured at several time points, including 48 hours (A) and 72 (B) after the start of the cultures, using a photon counter. Panels show the relative fluorescence intensity of control and transformed cultures at different emission wavelengths when excited with 488 nm and 543 nm light. The peaks on the left-most sides of the panels represent bleed-through from the excitation light.

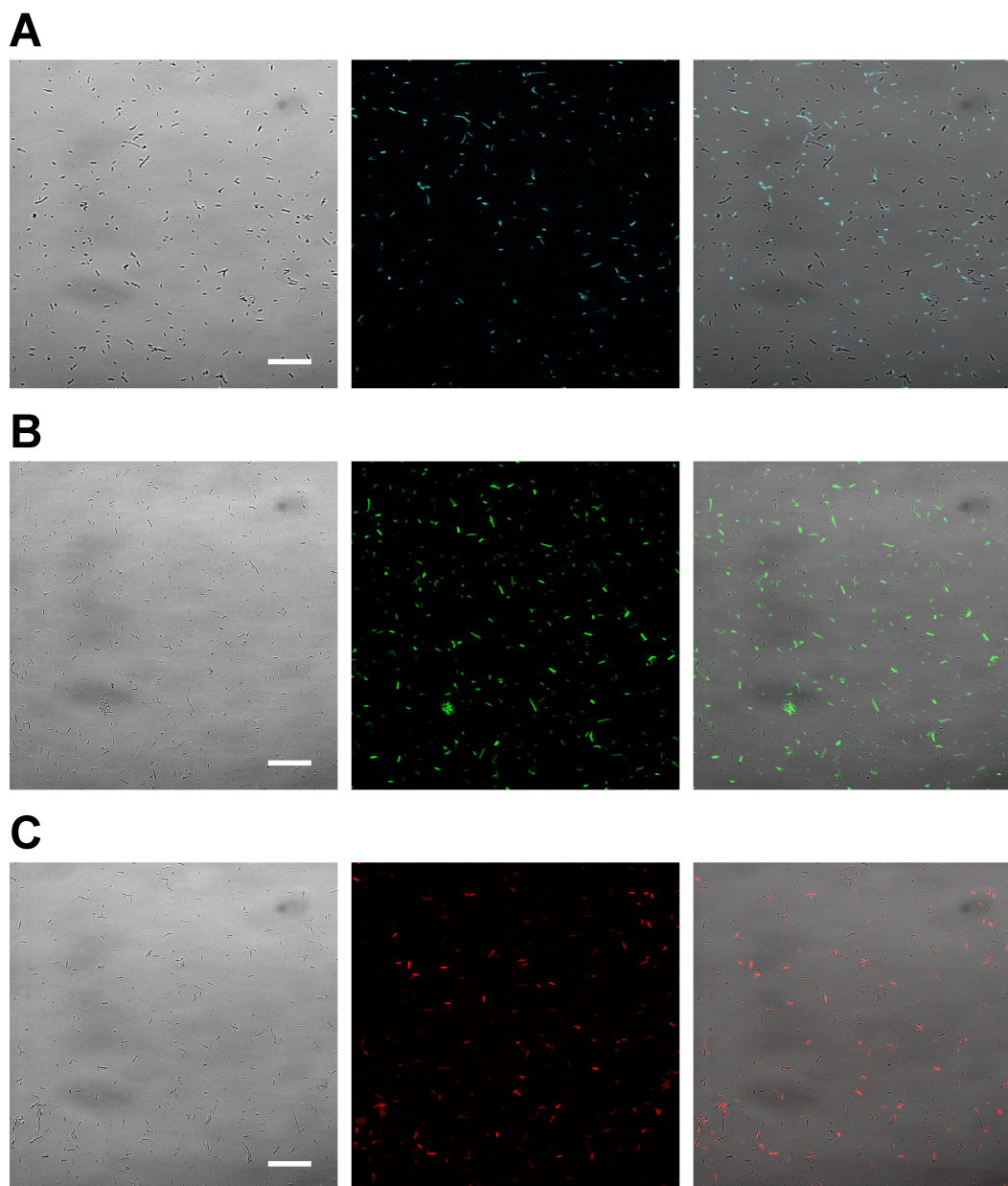


Figure 35. Fluorescent protein expression in *Escherichia coli* vectors.

Mini-Tn7 transposon plasmids containing the *ecfp*, *eyfp*, or *dsred* genes were obtained in *E. coli* carrier cells. After overnight broth culture of the cells at 37°C, ECFP (A), EYFP (B), and DsRed (C) protein expression was detected by

confocal microscopy. Panels show the transmitted light, fluorescence, and overlay images. Scale bar, 30 μm .

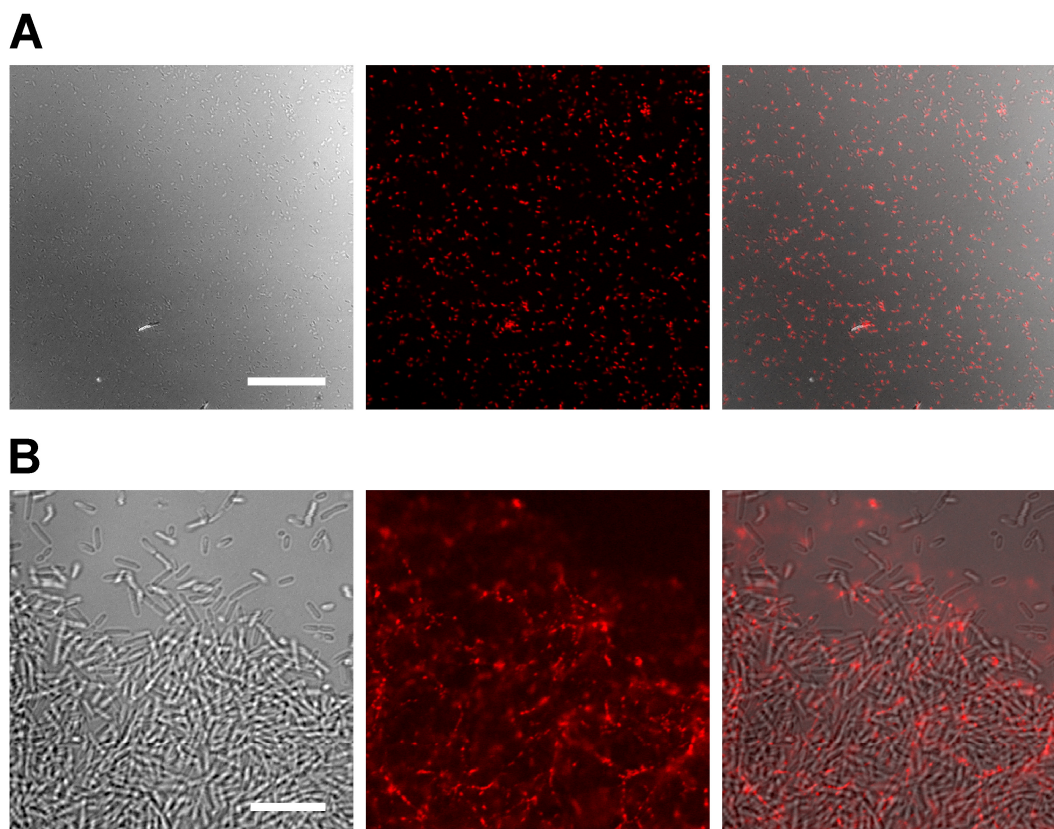


Figure 36. Fluorescence in *Pseudomonas aeruginosa* cells labeled with CMTMR.

Normal cells of the *P. aeruginosa* clone PA01 were grown in overnight liquid cultures. Cells were then labeled with the cell tracking dye, CMTMR, which freely diffuses into cells and is rendered membrane impermeant by intracellular enzymes. (A) Cells in log phase growth were labeled with CMTMR, washed, and immediately imaged by confocal microscopy. Panels show transmitted light, fluorescence, and overlay images. Scale bar, 30 μm . (B) PA01 cells in log phase growth were labeled with CMTMR and washed extensively. The cells were resuspended in fresh culture medium, incubated at 37° C for an additional 8 hours, and then imaged by confocal microscopy. Scale bar, 10 μm .

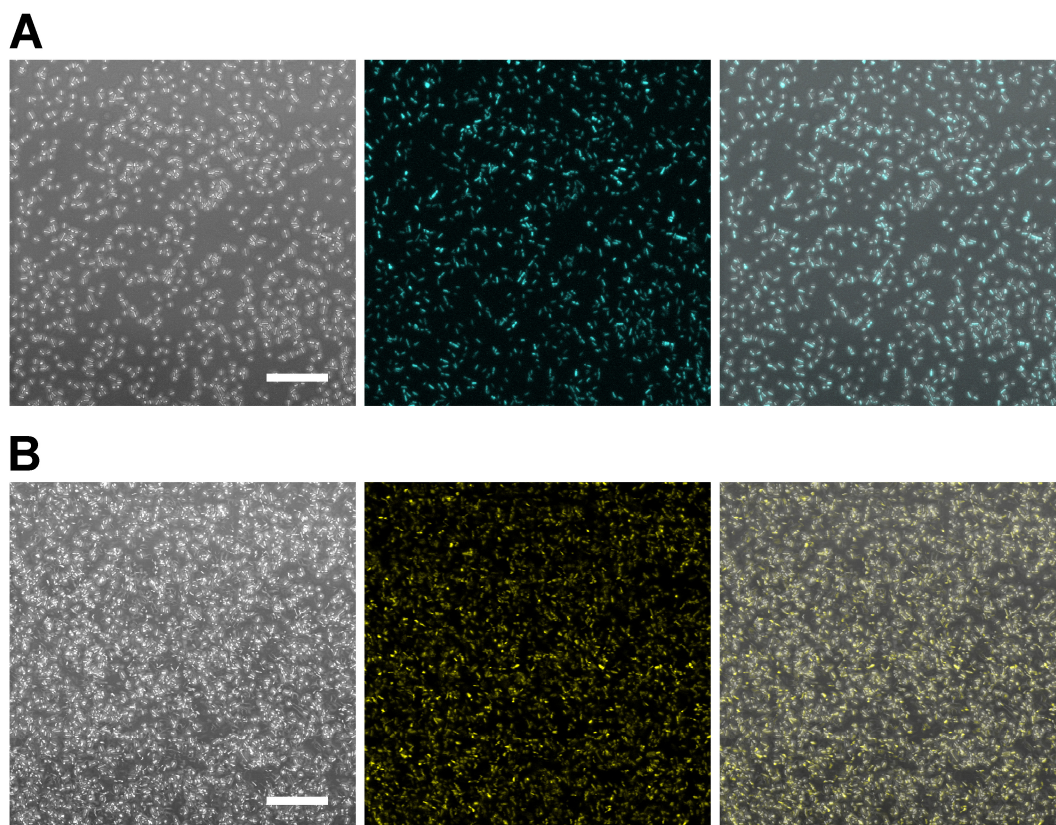


Figure 37. Fluorescence by *Pseudomonas aeruginosa* cells expressing ECFP or EYFP.

Cells from *P. aeruginosa* clone PA01 were transformed with plasmids containing the *ecfp* or *eyfp* genes. After overnight culture in liquid medium, cells were examined for ECFP (A) and EYFP (B) expression by confocal microscopy. Panels display the maximum intensity projections of transmitted light and fluorescence data sets, as well as an overlay image. Scale bars, 20 μm .

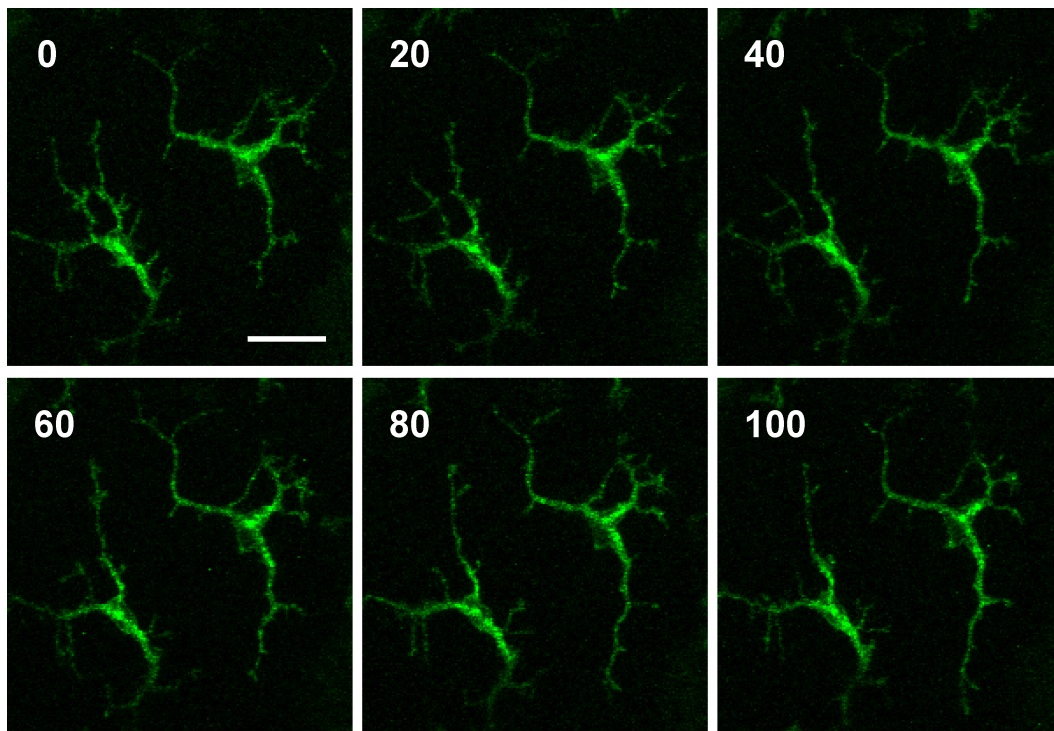


Figure 38. dSEARCH activity in epidermal LCs is increased after tape-stripping *in vivo*.

The stratum corneum was removed from the ear skin of I-A β -EGFP knock-in mice, and LC behaviors in the epidermis were observed by intravital confocal microscopy. The panels show maximum intensity projections of three-dimensional data sets collect every 20 min. Scale bar, 20 μ m.

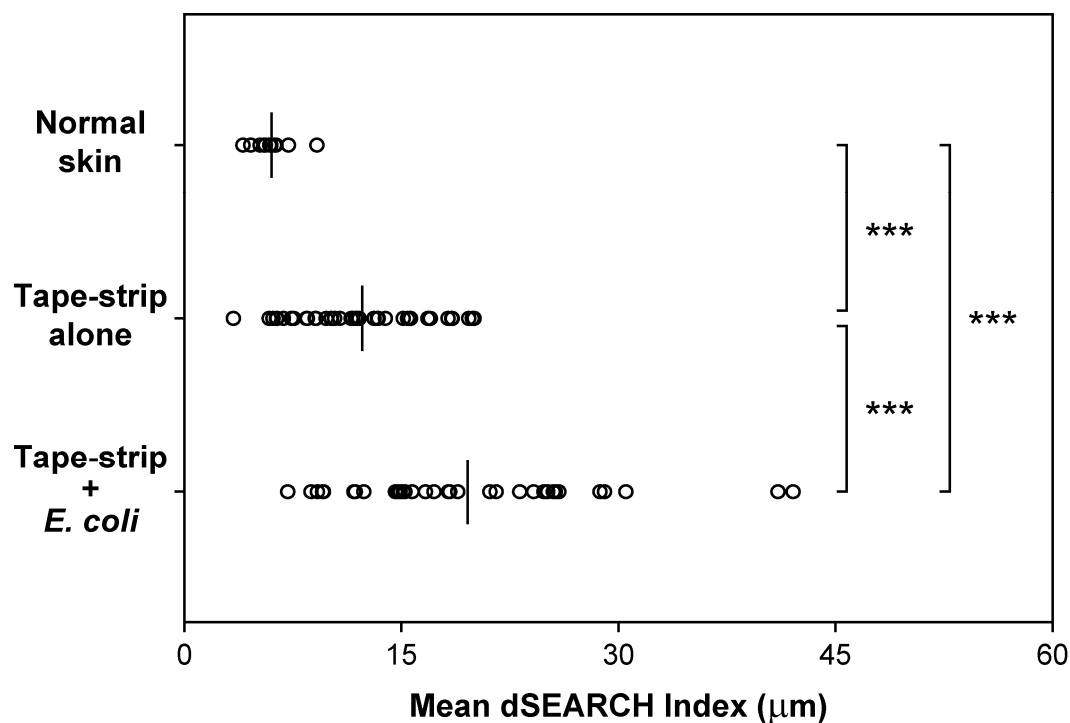


Figure 39. dSEARCH index values are increased after tape-stripping and infection with *Escherichia coli*.

Anesthetized I-A β -EGFP knock-in mice were examined by intravital confocal microscopy. The dSEARCH index was calculated for LCs in the steady state (Normal skin), 18 hours after removal of the stratum corneum by tape-stripping (Tape-strip alone), and 18 hours after tape-stripping plus infection with *E. coli*, and mean values were calculated for each cell over the imaging period. Mean values among all LCs in a treatment group are indicated with bars, and statistically significant differences between groups are indicated with asterisks (***) ($P < 0.001$).

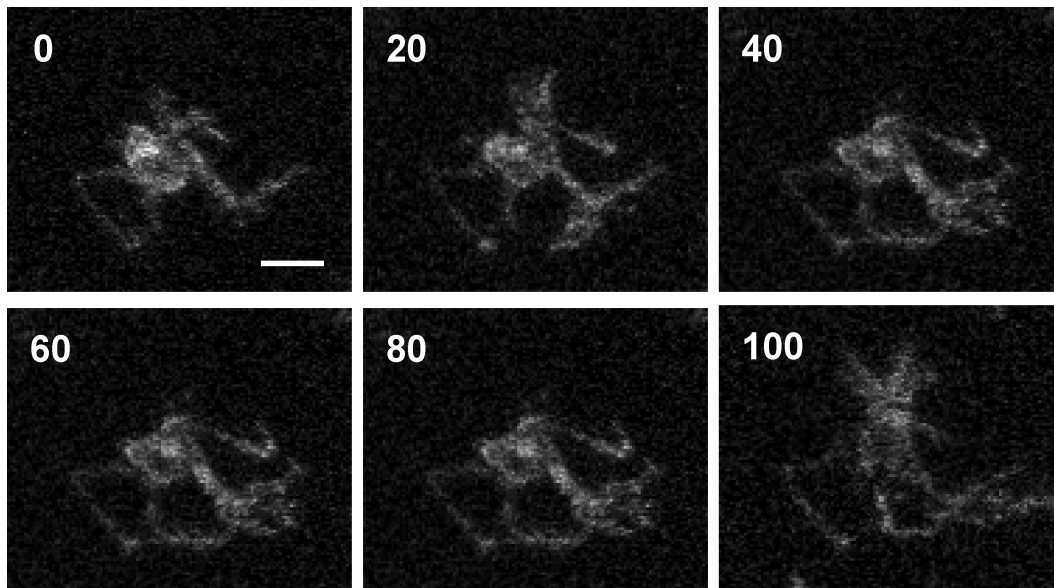


Figure 40. Epidermal LCs display hyper-augmented dSEARCH after bacterial infection of tape-stripped skin.

The stratum corneum was removed from the ear skin of I-A β -EGFP knock-in mice by tape stripping immediately before infection with *Escherichia coli* cells. LCs in the epidermis were imaged 18 hours later by intravital confocal microscopy. Panels show the maximum intensity projections of three-dimensional data sets collected every 20 min. Scale bar, 10 μ m.

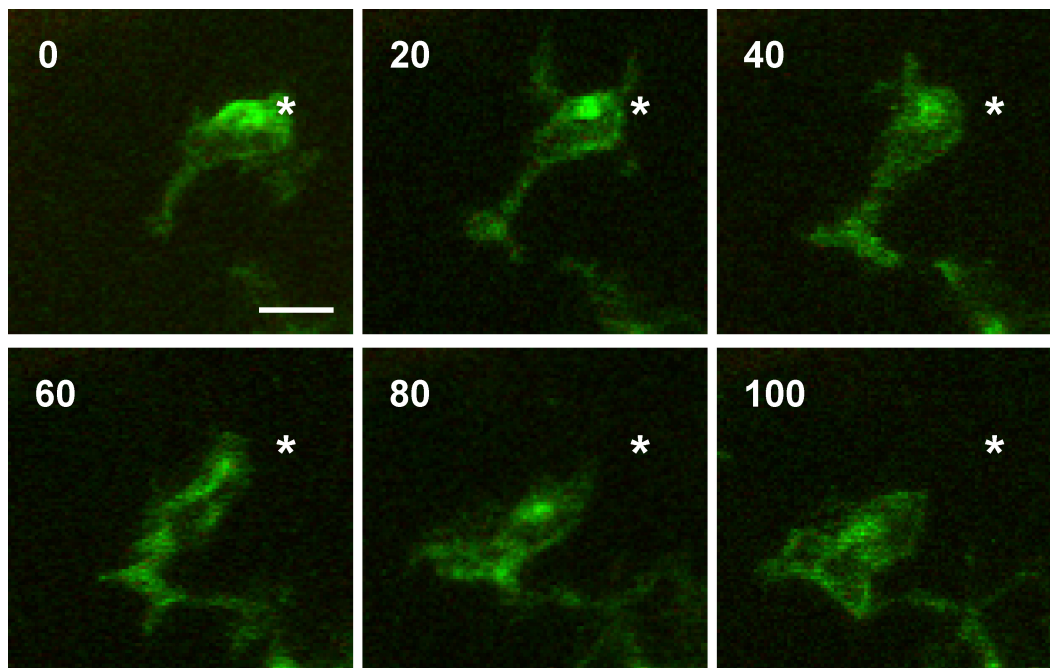


Figure 41. Lateral migration of epidermal LCs is seen after infection of tape-stripped skin *in vivo*.

The ears of I-A β -EGFP knock-in mice were infected with *Escherichia coli* after removal of the stratum corneum by tape-stripping. After 18 hours, the mice were anesthetized and the ears were imaged by intravital confocal microscopy. Panels display maximum intensity projections of three-dimensional data sets acquired every 20 min. Scale bar, 10 μ m.

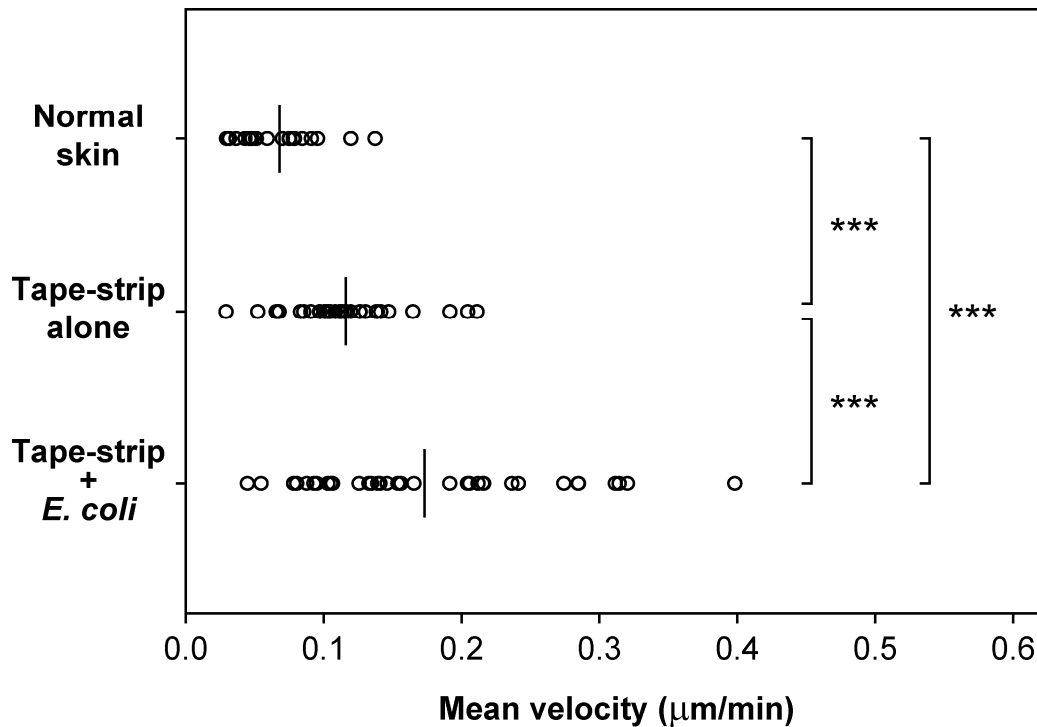


Figure 42. Tape-stripping and infection with *Escherichia coli* induces increased lateral migration by epidermal LCs *in vivo*.

The mean distance traveled between imaging frames was calculated for LCs in the ear skin of I-A β -EGFP knock-in mice over the entire imaging period. LCs were imaged in the epidermis in the steady state (Normal skin), 18 hours after removal of the stratum corneum by tape-stripping (Tape-strip alone), and 18 hours after tape-stripping plus infection of the skin with *E. coli* (Tape-strip + *E. coli*). Mean values among all the LCs of a given treatment group are shown with bars, and statistically significant differences between groups are indicated with asterisks (***) ($P < 0.001$).

Legends to Supplemental Movies

Movies 24-25. Time-lapse images of *in vivo* behaviors of epidermal LCs after tape stripping.

The stratum corneum of the ear skins in I-A β -EGFP knock in mice were removed by repeated tape-stripping. After 18 hours, EGFP⁺ epidermal LCs were imaged by intravital confocal microscopy. Note that while some dSEARCH activity is appreciable, the cells retain a more immature morphology and exhibit no little lateral movement.

Movies 26-27. Time-lapse images of *in vivo* behaviors of EGFP⁺ epidermal LCs after tape-stripping plus infection with *Escherichia coli*.

The stratum corneum was removed from the ear skin anesthetized I-A β -EGFP knock-in mice, and fluorescent *E. coli* cells were applied to the tape-stripped surface. LCs in the epidermis were then imaged by intravital confocal microscopy 18 hours later. Note the mature morphology and the active dSEARCH and lateral migration of the LCs. While the bacteria did, in fact, fluoresce in all experiments, they rested on the surface of the tape-stripped skin while the LCs were positioned in the suprabasal layers of the epidermis. Thus, the two cell populations occupied different positions in the z-axis. The imaging volume was chosen to monitor the LCs specifically, but in some cases bacteria can be seen as they transiently drift into the imaging volume.

CHAPTER FIVE

Conclusions and Discussion

SUMMARY OF EXPERIMENTAL FINDINGS

While the activation of T cells in the lymph nodes is indeed crucial to the development of the adaptive immune response, one could argue that the activation of the APCs in the tissues where Ags are first encountered is equally vital. Therefore, this study was performed to elucidate the behaviors accompanying the initial activation of LCs, as model APCs, within the epithelium.

LC Behaviors at Baseline

LC behaviors were examined within two different epithelial tissues, i.e., the cornea and the epidermis, so as to take advantage of the benefits that each tissue offered for *in situ* microscopic investigation. As an optically transparent tissue, the cornea is ideal for use with fluorescent observation, and the natural absence of blood vessels and lymph drainage lends the cornea to organ culture techniques. However, involuntary eye movements preclude *in vivo* examination of the cornea by laser scanning microscopy. The presence of hair, melanin, and keratin in the skin complicates microscopic examination, particularly with two-photon excitation. However, there is arguably more known about the biology of

LCs in the skin, and isolation of the skin for *in vivo* observation is relatively straightforward. Thus, both models were used to uncover the behaviors of LCs *in situ*, as the strengths of each tissue complemented those of the other.

Baseline LC Behaviors Observed Ex Vivo

In both model tissues, LCs exhibited distinctive behaviors under physiologic conditions. In the corneal samples, a few LCs displayed minimal lateral movement, while no movement was observed for LCs in the epidermis at baseline. The most obvious and striking behavior, however, was characterized by extension of the dendritic processes in random directions between the adjacent epithelial cells or keratinocytes, retraction of the processes through the same paths, and repetition of the extension-retraction cycle. Designated the dendrite surveillance extension and retraction cycling habitude, or dSEARCH, this behavior was detected in an overwhelming majority of LCs in corneal and epidermal samples *ex vivo*. Interestingly, by subjective observation, LCs in the cornea appeared to display greater dSEARCH activity at baseline than those in the epidermis, perhaps due to differences in the physical environments in which they reside. However, due to the disparity in the experimental conditions used to observe LCs in the skin and cornea, the difference in dSEARCH activity between these two populations is not directly testable.

In Vivo Behaviors of LCs in the Steady State

In contrast to the corneal and epidermal LCs examined *ex vivo*, in which dSEARCH was exhibited by nearly all the cells, only a small proportion of epidermal LCs observed *in vivo* displayed active dSEARCH. Fascinatingly, the proclivity of a given LC to perform active dSEARCH correlated with increases in cell size and MHC II expression. As these features are typically seen after maturation of LCs *in situ*, it suggests that spontaneous maturation of LCs occurs in the steady state (144,164,176-178). As was the case for epidermal LCs observed *ex vivo*, LCs examined *in vivo* were wholly sessile, and no apparent lateral migration was discovered in any sample.

LC Responses to Injury and Inflammatory Stimuli

Behavioral Responses After Pinpoint Thermal Injury

Using the corneal organ culture system, pinpoint thermal injury as inflicted to LCs while acquiring time-lapse images, and the behaviors of neighboring LCs were observe for several hours thenceforth. The inherent advantage of observing the same LCs before and after injury allowed for determination of the acute behavioral responses, and interesting insights into the time course of LC activation after injury were obtained. Almost immediately after injury, corneal LCs in the area showed a dramatic increase in dendrite

activity, quantified by measuring the dSEARCH index. Additionally, LCs began to migrate laterally through the corneal epithelium, a phenomenon enumerated by calculating the mean distance traveled per imaging frame.

As IL-1 is known to be released in the cornea in response to injury, the role of this cytokine in the injury-mediated behavioral responses was tested by blocking its function with the addition of IL-1Ra (153,179-182). While it had no effect on the baseline behaviors of LCs, this treatment completely abrogated the augmented dSEARCH and lateral migration seen after injury. To further explore this concept, exogenous IL-1 α was added to the corneal organ cultures.

Treatment with this cytokine induced an increase in dSEARCH index—though this effect was only temporary—but failed to cause increased lateral migration. However, the addition of TNF α , another inflammatory cytokine known to be released upon tissue injury, triggered an increase in both dSEARCH index and mean traveled distance throughout the entire imaging period (183-185). These results indicate that the behavioral responses of LCs to pinpoint injury are dependent on IL-1 release, and that other mediators such as TNF α are required as well, as IL-1 alone is not sufficient to fully induce LCs responses. These conclusions are supported by experimental evidence demonstrating IL-1 α and TNF α regulate the synthesis and functions of one another in a variety of cell types (186-191).

Responses to Diffuse Stimuli in the Epidermis

Because pinpoint injury could not be delivered to LCs in the epidermis either *ex vivo* or *in vivo*, diffuse inflammatory stimuli were given skin samples before imaging the tissues (144,145,192-196). In skin samples either cultured for 16 hours or harvested 16 hours after s.c. injection of $\text{TNF}\alpha$ and then imaged *ex vivo*, LCs exhibited behaviors very reminiscent of those seen after pinpoint injury to the cornea. After either treatment, LCs displayed vigorous movement of their dendritic processes and moved with fervor throughout the epidermis. Likewise, after application of DNFB, a reactive hapten, to the skin, epidermal LCs in living animals demonstrated significantly elevated dSEARCH index values and increased lateral migration. These results connote that LCs in differing epithelial tissues display common behavioral responses to inflammatory stimuli that are characterized by increased activity of the dendrites and lateral movement through the tissues.

LC Responses to Pathogenic Organisms

Bacterial Infection of Skin In Vivo

Should infectious pathogens find their way past the physical barriers protecting the body, sentinel cells like LCs sense the danger and alert the immune

system to the invaders. Based on the previous findings that LCs respond to injury or inflammatory stimuli with characteristic behavioral responses, it seemed reasonable that LCs would display the same responses, and possibly additional behaviors, after infection of the tissue by bacterial cells. To test this theory, the ear skins of mice were infected with Gram-negative bacteria, and the LCs in the epidermis were imaged by intravital confocal microscopy. In order to establish an infection of the skin, the outermost physical barrier of the epidermis, the stratum corneum, was removed by tape-stripping, a technique that itself is a form of diffuse mechanical injury (169,197-199). As demonstrated before, diffuse injury caused augmentation of dSEARCH and increased lateral migration in epidermal LCs. Infection of the skin after tape-stripping, however, caused hyperactivation of dendrite activity and lateral movement. Thus, the presence of pathogenic organisms on the skin results in increased LC activation expressed as distinctive behavioral responses.

QUESTIONS AND SIGNIFICANCE

Imaging the Immune System

Over the past several years, the development of technologies for imaging live cells and the resulting observations of dynamic leukocyte behaviors have

revolutionized the way we perceive the activation of immune cells and the initiation of immune responses (200). DCs, in particular, are critically important to the initiation of adaptive immune responses, for example having been shown to be the only cell type capable of activating CD8 T cells (201). Because of the significance of this interaction, much study has been performed to increase our understanding of the events surrounding the Ag-specific activation of T cells by DC. Despite this, relatively little is known of the behaviors of immature DCs within the tissues.

Dynamic Behaviors of DCs

As the initiators and regulators of the immune response, APCs have naturally been prime targets for dynamic imaging. Using time-lapse videomicroscopy, the migratory activities of freshly isolated LCs and DCs were observed in a three-dimensional collagen matrix and were shown to be dependent on the maturation state of the cells (202). DC networks have been visualized *in vivo* using two-photon microscopy and mice possessing a transgenic EYFP reporter under the control of the CD11c promoter (203). DCs in the subcapsular space of lymph nodes within living animals exhibited extensive movement of membrane ruffles and mean “crawling” speeds of approximately 2.5 $\mu\text{m}/\text{min}$. By contrast, DCs in T cell areas were relatively sessile, with observed speeds less than 1 $\mu\text{m}/\text{min}$.

In addition to exploring the cellular behaviors of DCs , investigators have used microscopy to elucidate the subcellular and molecular events associated with antigen presentation. Transduction of bone marrow DC cultures with a gene encoding an EGFP-tagged version of the I-E α protein facilitated the observation of MHC II movement within DCs (204). When maturation of the DC cultures was triggered by the addition of LPS, MHC II molecules rapidly translocated from lysosomes/late endosomes to the cell surface. In a complementary study, BM-derived DCs from I-A β -EGFP knock-in mice displayed tubular endosomal structures containing MHC II that extended and polarized toward the site of T cell contact (205). This reorganization of MHC II compartments only occurs, however, when the TCRs of the interacting T cells specifically recognize Ags presented by the DCs.

Dynamics of DC-T Cell Interactions

Videomicroscopy has been used to examine the interactions of bone marrow-derived DCs loaded with OVA peptide and T cells expressing an OVA-specific transgenic TCR within collagen matrices (206). In these experiments, T cells crawled across the surfaces of DCs they encountered, but rapidly detached after relatively brief interactions lasting only 5-10 min. In later experiments, antigen presentation in lymph node explants was observed after the adoptive

transfer of fluorescently-labeled, Ag-loaded DCs as well as Ag-specific T cells labeled with a different fluorescent dye (207). Interestingly, Ag-specific CD4 T cells were relatively sessile, and formed long-lasting (>15 hours) contacts with Ag loaded DCs. Using two-photon microscopy, DCs in lymph node explants were shown to interact with large numbers of CD8 T cells, establishing brief physical contacts with up to 500 T cells per hour (208). Further experimentation proved that the dynamics of the interactions between DCs and CD4 or CD8 T cells occur in sequential steps and are dictated not only by Ag specificity but by the maturation state of the DCs (209,210).

While the above studies were performed *ex vivo*, more recent experiments have utilized intravital imaging to explore the events of antigen presentation *in vivo*. The previously observed behaviors of adoptively transferred DCs and T cells were confirmed in intact lymph nodes of anesthetized mice (211). Moreover, after injection of a fluorescently labeled Ag/adjuvant complex, the behaviors of DCs that had carried the complex to the lymph node were monitored as they interacted with CD4 and CD8 T cells (212,213). Finally, using the CD11c-promoter-driven EYFP transgenic mouse described above, the differing dynamics of interactions between T cells and either mature or immature DCs were confirmed *in vivo* by intravital imaging (214). While the functional outcomes of these interactions have not yet been experimentally determined, the experiments

have greatly increased our understanding of the behavioral mechanisms that govern DC-T cell interactions and T cell activation.

Imaging of Langerhans Cells in Living Tissues

The discovery and characterization of langerin as a LC-specific marker has allowed for the discrimination of LCs from other DC subsets, therefore allowing investigators to fully explore the biology and function of LCs (83,215-219). With our continued understanding of the mouse genome has come insight on the promoter regions that control langerin expression, and several investigators have capitalized on this to drive the expression of genes specifically within LCs. In one recent report, the langerin promoter was utilized to express the diphtheria toxin receptor (DTR), as well EGFP as a reporter of DTR expression (220). While the purpose for constructing this knock-in animal was to explore the relative functions of LCs and other DCs subsets by specifically deleting the LCs via injection of diphtheria toxin, the investigators took advantage of the expression of EGFP to observe LC behaviors *in vivo*. Anesthetized mice were examined by confocal microscopy, and EGFP⁺ LCs in the epidermis exhibit little motility, either in terms of dendrite activity or lateral migration. However, 24 hours after tape-stripping, considerable dendrite and cell body motility was exhibited by EGFP⁺ LCs, confirming the results obtained *in vivo* in this study.

Technical Significance of This Study

While our understanding of the dynamics of the presentation of Ags to T cells has increased dramatically from the imaging studies mentioned above, up until now there was still relatively little known concerning the dynamic events associated with the capture of antigens and initial activation of DCs in the peripheral tissues *in situ*. To the best of our knowledge, this study represents the first systematic and thorough examination of LCs, a subset of immature DCs, *in situ*.

Multiphoton microscopy has been used to observe the behaviors of immune cells in previous studies, but had never been employed to examine leukocyte populations in the cornea. By utilizing a unique organ culture system and EGFP BM chimeric mice, in which the corneal LCs express EGFP, multiphoton laser microscopy has allowed, for the first time, the detection of the dynamic behaviors of corneal LCs. Also, SHG has permitted the study of EGFP⁺ leukocytes and their spatial relationships to the tissue environment. By using the infrared laser to produce tissue injury and by adding recombinant cytokines into the organ culture system, this work has demonstrated the extremely rapid kinetics by which cytokines mediate LC behavioral responses to tissue injury. Other investigators have used confocal microscopy to examine the behaviors of immune cells, even LCs in the epidermis. However, this study represents a significant

breakthrough in the imaging and analysis of LC populations *ex vivo* and *in vivo*. The combination of tissue explants and live animals has allowed for the investigation of LC behaviors under several different inflammatory conditions. Moreover, the use of spectral detection and linear unmixing has allowed the study of LC responses to bacteria *in vivo*. Finally, this is the first study in which the dynamic behaviors of immature corneal or epidermal LCs *in situ* have been rigorously characterized, using the dSEARCH index and mean velocity of migration.

Implications of LC Behaviors

Differences in dSEARCH Between Tissue Preparations

One of the most striking differences noted between LCs observed in the various tissues used in this study is the variation in overall dSEARCH activity. Based on subjective observation, EGFP⁺ LCs in the cornea displayed more dynamic dendrite motility at baseline than did LCs in the epidermis. However, direct statistical comparison of the dSEARCH index values calculated for cells in the cornea and skin is not appropriate considering the differences in the ways the data sets were acquired, e.g., image sets were collected every 2 min by multiphoton microscopy in the corneal samples, while images of epidermal LCs were acquired every 5 min by confocal microscopy. Nevertheless, the relative

dSEARCH index values serve as a rough guide to the differences between tissues, highlighting the increased activity of corneal LCs over epidermal LCs and implying the existence of intrinsic differences between the corneal and epidermal LCs themselves and/or the physical environment of the tissues in which they reside.

Perhaps of greater consequence is the difference in dSEARCH activity seen between epidermal LCs observed *ex vivo* and *in vivo*. LCs observed in the *ex vivo* organ culture system all displayed an appreciable level of dendrite motility, while LCs observed in living animals *in vivo* on average displayed almost no discernable dendrite activity. Those cells that did exhibit dSEARCH concurrently demonstrated signs of maturation, namely increased cell size and MHC II expression (221). The apparent conclusion from these observations is that the dSEARCH observed in the *ex vivo* tissue samples is a consequence of inflammation associated tissue preparation and handling. Indeed, it was shown some time ago that the culturing of skin explants induces phenotypic alterations in LCs and their migration out of the epidermis, changes associated with inflammation-induced maturation (222), as early as 4 hours after harvesting (223). While the mechanisms of immune activation *ex vivo* are not known, the possible causes include oxidative stress triggered by the loss of blood and/or lymph circulation in vascular tissues like the skin, or even the loss of tonic

neuronal signaling in the tissues after explantation in both the skin and cornea (224-228).

While the cause of dSEARCH in the baseline state *ex vivo* is an important issue that remains to be clarified, the physiologic relevance of the LC behavioral responses seen *ex vivo* after pathogenic stimuli is supported by the following observations. First, experimentally produced thermal injury, exogenous cytokines, and extended organ culture provoked the behavior of LCs substantially above the baseline level, suggesting that handling of the tissue did not produce inflammation causing the maximal activation of LCs. Secondly, migration of LCs through the tissues, considered a hallmark of activation in both the cornea and skin, was regularly seen only after administration of the inflammatory stimuli listed above. Finally, the continuous presence of IL-1Ra, which completely abrogated injury-induced augmentation of dSEARCH in the cornea, failed to affect the baseline level of dendrite activity, thus excluding the possibility that the baseline dSEARCH was attributable to IL-1 release consequent to *ex vivo* manipulation, at least in the cornea.

Functions of Dynamic LC Behaviors

Although the functions of dSEARCH and lateral migration within the epithelial tissues remain to be determined, it seems reasonable to discuss their

potential relationship to the local immunosurveillance roles of LCs. The dynamic movement of dendrites has recently been demonstrated with lymph node-resident DCs (229,230). By projecting and waving their pseudopods, those DCs established dynamic physical contacts with T cells in the lymph nodes. While the immunological function of that motion remains to be determined, it has been postulated that the DCs maximize the chances of developing physical contacts with antigen-specific T cells by moving the pseudopods. As dSEARCH resembled the waving motion, except that dendrites were confined to the same paths between neighboring cells in the epithelial tissues, it is tempting to speculate that the behaviors of LCs may help facilitate Ag sampling by maximizing the amount of tissue with which the LCs may interact.

While the surface densities of epidermal LCs vary significantly between skin sites and individuals, the x-y plane area covered by LCs in the skin remains remarkably consistent, i.e., about 25% of the total skin area (231). This phenomenon is accomplished by 3- to 4-fold increases in cell volume by LCs in areas with reduced densities of LCs, highlighting a compensatory mechanism for maintaining LCs at the environmental interfaces. Based on static confocal images, it has been estimated that each epidermal LC in the steady state is responsible for monitoring 53 keratinocytes (232). Thus, dSEARCH and lateral migration may represent dynamic mechanisms by which LCs monitor an

increased area and survey the intercellular spaces more efficiently through the extension of dendritic processes in multiple different directions.

In support of this hypothesis, LCs are known to internalize a variety of Ag, including pathogenic microbes (62,233). The murine LC-like immature DC line XS52 has been shown to internalize *Treponema pallidum* by extending and coiling the dendrites *in vitro* (234). Evidence also suggest that melanosomes are internalized by LCs and transported to skin-draining lymph nodes in the steady state (235). If dSEARCH and lateral migration help facilitate Ag uptake, then it is conceivable that LCs would show increased melanosome uptake in the mature state. This was indeed proven when melanosomes were identified by electron microscopy in the phagocytic vacuoles of LCs in tape-stripped skin, but not untreated normal skin (236). While this evidence supports a role for dSEARCH and lateral migration in Ag uptake, further studies are clearly required to determine whether the dynamic LC behaviors are indeed coupled to the internalization of Ags.

LCs in Corneal Pathology

Though normally associated with the initiation of protective immune responses in other tissues, the presence of LCs in the cornea is correlated with the initiation of immunopathologic responses that can severely damage the sensitive

ocular tissue. For example, while damage to the tissue as a direct result of viral replication is possible, permanent blindness as a result of HSV-1 infection of the cornea occurs as a consequence of inflammatory responses in the corneal stroma, a condition known as herpes simplex keratitis (HSK) (237,238). Interestingly, the induction of centripetal LC migration into the central cornea before HSV infection increases the incidence and severity of HSK, while inhibition of LC migration or depletion of LCs from the cornea before infection interferes with the development of HSK (239-241). Consequently, corneal LCs are thought to play an important role in mediating the damage inflicted to the cornea during HSV-1 infection.

Similar to HSV, *Pseudomonas aeruginosa* is capable of causing a rapid and severe infection of the cornea, often leading to blindness. A Gram-negative bacterium, *P. aeruginosa* infects injured epithelia and invades into the stromal compartment, leading to bacterial keratitis (242). Destruction of the corneal tissue occurs not only due to protease secretion from the bacterial cells, but as a result of reactive oxygen species generated from host cells as well in a process apparently regulated by CD4 T cells (243,244). Fascinatingly, mouse strains favoring Th1 responses displayed greater LC migration and CD80 expression than Th2-inclined strains upon infection with *P. aeruginosa*, a trait that correlated with increased susceptibility to corneal perforation as a result of the infection

(245,246). On the other hand, severe corneal perforation was seen in the Th2-favoring mouse strains, which are normally more resistant to perforation, when LC migration was induced in the cornea before infection (247). These observations are consistent with the idea that LC-mediated presentation of bacterial Ags to T cells is one mechanism that regulates the susceptibility to bacterial keratitis (248,249). Thus, the instigation of motile LC behaviors may actually contribute to the development of pathological outcomes during corneal infections.

Epidermal LCs in Cutaneous Disease

Given the extent of motility seen in LCs after inflammatory stimuli, it is not surprising to note that alterations in epidermal LC migratory activity is associated with or can result in pathological changes in the skin. For example, upon skin transplantation, donor-derived LCs in the skin graft are activated and migrate out of the epidermis (250). Presumably, these cells migrate to the draining lymph nodes and activate allo-reactive T cells, which in turn mediate rejection of the skin graft. Type 1 interferons are produced during viral infections and have numerous effects to limit the extent of viral replication (251). While the type 1 interferons normally act to enhance the immune response by activating leukocytes such as DCs, the exposure of epidermal LCs to type 1 interferons results in the inhibition of maturation and a reduction in the ability of LCs to

stimulate T cell proliferation (252). Finally, after percutaneous infection of the skin by *Schistosoma mansoni* parasites, epidermal LCs near the site of infection demonstrate the phenotypic changes associated with maturation, such as increased size, elongation of the dendrites, and expression of CD86, but failed to migrate out of the epidermis (253). Even after treatment with TNF α , LCs in *Schistosoma*-infected skin showed marked retention within the epidermis, implying that factors produced by the parasite prevent LC migration and contribute to parasite escape from the immune system. Thus, disruption of the link between LC maturation and the induction of LC dynamic behavioral responses may contribute the development of pathology in various cutaneous diseases.

Prospects for the Future

Challenges to the Role of LCs as APCs

Based on the finding that LCs that had emigrated from skin explant possessed the ability to activate T cells *in vitro*, LCs have classically been considered the principal APC population in the skin (65). A wave of recent studies, however, has challenged the view of LCs as the major APC in the skin. For instance, in two different models of HSV infection, LCs were shown to be incapable of directly presenting HSV-associated Ags to T cells in the draining lymph nodes, with T cells activation instead instigated by resident DCs within the

lymph nodes (254,255). Similarly, in a model of cutaneous *Leishmania major* infection, only cells of non-LC origin were found to display *L. major*-associated Ags in the skin draining lymph nodes 3 days after infection (256). One possibility suggested by the data from these studies is that LCs may transfer Ags they have acquired in the epithelial tissues to a second DC population in the lymph node that then presents the Ags resulting in T cell activation. A second possibility evoked by these data is that the kinetics of LC and tissue DC differ, with DCs reaching the lymph node and presenting the Ags before the arrival of LCs. This is supported by recent work using *Lang*-EGFP knock-in mice, in which EGFP expression is controlled by the endogenous langerin promoter; LCs migrated to the lymph nodes with much slower kinetics than dermal DCs after painting the skin with a fluorescent dye (257). Finally, it is possible that other DC populations in the skin contribute a greater proportion of functional antigen presentation than do LCs. This was predicted several years ago after the original characterization of dermal DC subsets in the skin (258,259). Further evidence for this was reported in knock-in mice in which the expression of the diphtheria toxin receptor is under the control of the endogenous langerin promoter. After complete ablation of LCs by injection of diphtheria toxin, contact hypersensitivity (CHS) responses are still inducible, implying a role for dermal DCs (260,261). Finally, CHS responses in mice lacking LCs due to expression of the diphtheria toxin under the control of

the langerin promoter were amplified, rather than diminished, suggesting roles for dermal DCs in the initiation, and LCs in the suppression, of CHS responses (262).

The HSV and *Leishmania* models of infection described above represent cutaneous pathological processes, but neither may portray the role of the epidermal LCs with complete accuracy, as the method HSV infection results in destruction of the epidermis and the delivery of *Leishmania* parasites is by s.c. injection. Therefore, two questions still remain concerning the role of epidermal LCs as APCs in the skin: are the behavioral responses of activated LCs coupled with the ability of LCs to internalize Ags, and do LCs present Ags that are truly restricted to the epidermis to T cells?

The imaging systems developed for this study provide the perfect means to explore the first question. However, the internalization of Ags by LCs is difficult to observe due to the fact that Ags are difficult to deliver to within the epidermis. One possible solution to this problem would be the development of a knock-in mouse in which a fluorescent Ag would generated specifically within the epidermis. Because of the limits of resolution in live cell imaging, observation of a soluble Ag is not practical, as the endocytic vesicles in which the Ag would accumulate would be difficult to detect. Therefore, a particulate Ag would be required, such as the melanosomes, which LCs are known to internalize

under a variety of conditions (263,264). Since melanin granules cannot be easily seen by laser scanning microscopy, a fluorescent marker would have to be incorporated into the melanosome. The melanosomal matrix protein, Pmel17 (or gp100), is incorporated into melanosomes during their formation and initiates their maturation into fibrillar structures (265). As truncation of the C-terminal domain of Pmel17 did not affect the trafficking or processing of the protein, it is reasonable to theorize that expression of a fusion protein containing EYFP linked to the C-terminus of Pmel17 would not adversely affect the function of the protein and that the fusion protein would be incorporated into melanosome that could then be monitored by confocal or multiphoton microscopy. Thus, by crossing the Pmel17-EYFP knock-in mice to mice expressing EGFP in the LCs, the internalization of antigenic particles could be observed and studied *in vivo*.

To answer the second question, only a small change in the knock-in strategy is needed. It was shown in transgenic mice expressing OVA under the control of the K14 promoter that continuous expression of a model Ag in the epidermis in the steady state results in immunologic tolerance (266). Therefore, an inducible system would be required to test the ability of LCs to present the model Ag to T cells. By the addition of the Tet-On inducible transcription factor system, production of the EYFP-labeled melanosomes could be regulated by the administration of tetracycline to the animal (267). Therefore, induction of

labeled-melanosome production concurrent with the administration of a LC maturation signal such as tape-stripping, reactive hapten, or $\text{TNF}\alpha$ injection would enable the investigation of the ability of LCs to activate T cells through conventional immunologic experimental procedures.

LIST OF WORKS CITED

1. Janeway, C. A., P. Travers, M. Walport, and M. J. Shlomchik. *Immunobiology: The Immune System in Health and Disease*. Taylor and Francis Group, New York.
2. Figdor, C. G., Y. van Kooyk, and G. J. Adema. 2002. C-type lectin receptors on dendritic cells and Langerhans cells. *Nat.Rev.Immunol.* 2:77-84.
3. Austyn, J. M. 1996. New insights into the mobilization and phagocytic activity of dendritic cells. *J.Exp.Med.* 183:1287-1292.
4. Takeda, K., T. Kaisho, and S. Akira. 2003. Toll-like receptors. *Annu.Rev.Immunol.* 21:335-376.
5. La Sala, A., D. Ferrari, F. Di Virgilio, M. Idzko, J. Norgauer, and G. Girolomoni. 2003. Alerting and tuning the immune response by extracellular nucleotides. *J.Leukoc.Biol.* 73:339-343.
6. Fredholm, B. B. 1997. Purines and neutrophil leukocytes. *Gen.Pharmacol.* 28:345-350.
7. Shi, Y., J. E. Evans, and K. L. Rock. 2003. Molecular identification of a danger signal that alerts the immune system to dying cells. *Nature* 425:516-521.
8. Pulendran, B. 2004. Immune activation: death, danger and dendritic cells. *Curr.Biol.* 14:R30-R32.
9. Ferrari, D., A. La Sala, P. Chiozzi, A. Morelli, S. Falzoni, G. Girolomoni, M. Idzko, S. Dichmann, J. Norgauer, and F. Di Virgilio. 2000. The P2 purinergic receptors of human dendritic cells: identification and coupling to cytokine release. *FASEB J.* 14:2466-2476.
10. La Sala, A., D. Ferrari, S. Corinti, A. Cavani, F. Di Virgilio, and G. Girolomoni. 2001. Extracellular ATP induces a distorted maturation of dendritic cells and inhibits their capacity to initiate Th1 responses. *J.Immunol.* 166:1611-1617.

11. Idzko, M., S. Dichmann, D. Ferrari, F. Di Virgilio, A. La Sala, G. Girolomoni, E. Panther, and J. Norgauer. 2002. Nucleotides induce chemotaxis and actin polymerization in immature but not mature human dendritic cells via activation of pertussis toxin-sensitive P2y receptors. *Blood* 100:925-932.
12. La Sala, A., S. Sebastiani, D. Ferrari, F. Di Virgilio, M. Idzko, J. Norgauer, and G. Girolomoni. 2002. Dendritic cells exposed to extracellular adenosine triphosphate acquire the migratory properties of mature cells and show a reduced capacity to attract type 1 T lymphocytes. *Blood* 99:1715-1722.
13. Kupper, T. S. and R. C. Fuhlbrigge. 2004. Immune surveillance in the skin: Mechanisms and clinical consequences. *Nat Rev Immunol* 4:211-222.
14. Wilson, S. E., J. J. Liu, and R. R. Mohan. 1999. Stromal-epithelial interactions in the cornea. *Prog.Retin.Eye Res.* 18:293-309.
15. Ansel, J. C., T. A. Luger, D. Lowy, P. Perry, D. R. Roop, and J. D. Mountz. 1988. The expression and modulation of IL-1a in murine keratinocytes. *J.Immunol.* 140:2274-2278.
16. Hogquist, K. A., M. A. Nett, E. R. Unanue, and D. D. Chaplin. 1991. Interleukin 1 is processed and released during apoptosis. *Proc.Natl.Acad.Sci.USA* 88:8485-8489.
17. Kumar, A., J. Zhang, and F. S. X. Yu. 2004. Innate immune response of corneal epithelial cells to Staphylococcus aureus infection: Role of peptidoglycan in stimulating proinflammatory cytokine secretion. *Invest.Ophthalmol.Vis.Sci.* 45:3513-3522.
18. Wilson, S. E., G. S. Schultz, N. Chegini, J. A. Weng, and Y. G. He. 1994. Epidermal Growth-Factor, Transforming Growth-Factor-Alpha, Transforming Growth-Factor-Beta, Acidic Fibroblast Growth-Factor, Basic Fibroblast Growth-Factor, and Interleukin-1 Proteins in the Cornea. *Exp.Eye Res.* 59:63-71.
19. Xue, M. L., A. Thakur, L. Lutze-Mann, and M. D. P. Willcox. 2000. Pro-inflammatory cytokine/chemokine gene expression in human corneal epithelial cells colonized by Pseudomonas aeruginosa. *Clinical and Experimental Ophthalmology* 28:197-200.

20. Cole, N., S. Bao, M. Willcox, and A. J. Husband. 1999. TNF-alpha production in the cornea in response to *Pseudomonas aeruginosa* challenge. *Immunol. Cell Biol. imm* 77:164-166.
21. Niederkorn, J. Y., J. S. Peeler, and J. Mellon. 1989. Phagocytosis of particulate antigens by corneal epithelial cells stimulates interleukin-1 secretion and migration of Langerhans cells into the central cornea. *Reg. Immunol.* 2:83-90.
22. Hart, D. N. J. 1997. Dendritic cells: unique leukocyte populations which control the primary immune response. *Blood* 90:3245-3287.
23. Banchereau, J. and R. M. Steinman. 1998. Dendritic cells and the control of immunity. *Nature* 392:245-252.
24. Banchereau, J., F. Briere, C. Caux, J. Davoust, S. Lebecque, Y.-J. Liu, B. Pulendran, and K. Palucka. 2000. Immunobiology of dendritic cells. *Annu. Rev. Immunol.* 18:767-811.
25. Fogg, D. K., C. Sibon, C. Miled, S. Jung, P. Aucouturier, D. R. Littman, A. Cumano, and F. Geissmann. 2006. A clonogenic bone marrow progenitor specific for macrophages and dendritic cells. *Science* 311:83-87.
26. Kamath, A. T., S. Henri, F. Battye, D. F. Tough, and K. Shortman. 2002. Developmental kinetics and lifespan of dendritic cells in mouse lymphoid organs. *Blood* 100:1734-1741.
27. Merad, M., M. G. Manz, H. Karsunky, A. Wagers, W. Peters, I. Charo, I. L. Weissman, J. G. Cyster, and E. G. Engleman. 2002. Langerhans cells renew in the skin throughout life under steady-state conditions. *Nat. Immunol.* 3:1135-1141.
28. Fogg, D. K., C. Sibon, C. Miled, S. Jung, P. Aucouturier, D. R. Littman, A. Cumano, and F. Geissmann. 2006. A clonogenic bone marrow progenitor specific for macrophages and dendritic cells. *Science* 311:83-87.
29. Liu, Y. J., H. Kanzler, V. Soumelis, and M. Gilliet. 2001. Dendritic cell lineage, plasticity and cross-regulation. *Nat. Immunol.* 2:585-589.
30. Liu, Y. J. 2001. Dendritic cell subsets and lineages, and their functions in innate and adaptive immunity. *Cell* 106:259-262.

31. Figdor, C. G., Y. van Kooyk, and G. J. Adema. 2002. C-type lectin receptors on dendritic cells and Langerhans cells. *Nat.Rev.Immunol.* 2:77-84.
32. Maldonado-Lopez, R. and M. Moser. 2001. Dendritic cell subsets and the regulation of Th1/Th2 responses. *Semin.Immunol.* 13:275-282.
33. Moser, M. and K. M. Murphy. 2000. Dendritic cell regulation of T_H1-T_H2 development. *Nat.Immunol.* 1:199-205.
34. Asselin-Paturel, C., A. Boonstra, M. Dalod, I. Durand, N. Yessaad, C. Dezutter-Dambuyant, A. Vicari, A. O'Garra, C. Biron, F. Briere, and G. Trinchieri. 2001. Mouse type I IFN-producing cells are immature APCs with plasmacytoid morphology. *Nat.Immunol.* 2:1144-1150.
35. Nakano, H., M. Yanagita, and M. D. Gunn. 2001. CD11c⁺B220⁺Gr-1⁺ cells in mouse lymph nodes and spleen display characteristics of plasmacytoid dendritic cells. *J.Exp.Med.* 194:1171-1178.
36. Kadowaki, N., S. Antonenko, J. Y. Lau, and Y. J. Liu. 2000. Natural interferon α/β -producing cells link innate and adaptive immunity. *J.Exp.Med.* 192:219-226.
37. Lund, J., A. Sato, S. Akira, R. Medzhitov, and A. Iwasaki. 2003. Toll-like receptor 9-mediated recognition of Herpes simplex virus-2 by plasmacytoid dendritic cells. *J.Exp.Med.* 198:513-520.
38. Gibson, S. J., J. M. Lindh, T. R. Riter, R. M. Gleason, L. M. Rogers, A. E. Fuller, J. L. Oesterich, K. B. Gorden, X. Qiu, S. W. McKane, R. J. Noelle, R. L. Miller, R. M. Kedl, P. Fitzgerald-Bocarsly, M. A. Tomai, and J. P. Vasilakos. 2002. Plasmacytoid dendritic cells produce cytokines and mature in response to the TLR7 agonists, imiquimod and resiquimod. *Cell.Immunol.* 218:74-86.
39. Diebold, S. S., T. Kaisho, H. Hemmi, S. Akira, and Reis e Sousa. 2004. Innate antiviral responses by means of TLR7-mediated recognition of single-stranded RNA. *Science* 303:1529-1531.
40. Chan, C. W. 2006. Interferon-producing killer dendritic cells provide a link between innate and adaptive immunity. *Nat.Med.* 12:207-213.

41. Re, F. and J. L. Strominger. 2001. Toll-like receptor 2 (TLR2) and TLR4 differentially activate human dendritic cells. *J.Biol.Chem.* 276:37692-37699.
42. Michelsen, K. S., A. Aicher, M. Mohaupt, T. Hartung, S. Dimmeler, C. J. Kirschning, and R. R. Schumann. 2001. The role of toll-like receptors (TLRs) in bacteria-induced maturation of murine dendritic cells (DCs). Peptidoglycan and lipoteichoic acid are inducers of DC maturation and require TLR2. *J.Biol.Chem.* 276:25680-25686.
43. Kadowaki, N., S. Ho, S. Antonenko, R. W. Malefyt, R. A. Kastelein, F. Bazan, and Y. J. Liu. 2001. Subsets of human dendritic cell precursors express different toll-like receptors and respond to different microbial antigens. *J.Exp.Med.* 194:863-869.
44. Di Virgilio, F., P. Chiozzi, D. Ferrari, S. Falzoni, J. M. Sanz, A. Morelli, M. Torboli, G. Bolognesi, and O. R. Baricordi. 2001. Nucleotide receptors: an emerging family of regulatory molecules in blood cells. *Blood* 97:587-600.
45. Shi, Y., J. E. Evans, and K. L. Rock. 2003. Molecular identification of a danger signal that alerts the immune system to dying cells. *Nature* 425:516-521.
46. Pulendran, B. 2004. Immune activation: death, danger and dendritic cells. *Curr.Biol.* 14:R30-R32.
47. Granucci, F., C. Vizzardelli, E. Virzi, M. Rescigno, and P. Ricciardi-Castagnoli. 2001. Transcriptional reprogramming of dendritic cells by differentiation stimuli. *Eur.J.Immunol.* 31:2539-2546.
48. Chan, C. W. 2006. Interferon-producing killer dendritic cells provide a link between innate and adaptive immunity. *Nat.Med.* 12:207-213.
49. Yanagihara, S., E. Komura, J. Nagafune, H. Watari, and Y. Yamaguchi. 1998. EB11/CCR7 is a new member of Dendritic cell chemokine receptor that is up-regulated upon maturation. *J.Immunol.* 161:3096-3102.

50. Rescigno, M., F. Granucci, S. Citterio, M. Foti, and P. Ricciardi-Castagnoli. 1999. Coordinated events during bacteria-induced DC maturation. *Immunol.Today* 20:200-203.
51. Bachmann, M. F., M. B. Lutz, G. T. Layton, S. J. Harris, T. Fehr, M. Rescigno, and P. Ricciardi-Castagnoli. 1996. Dendritic cells process exogenous viral proteins and virus-like particles for class I presentation to CD8⁺ cytotoxic T lymphocytes. *Eur.J.Immunol.* 26:2595-2600.
52. Guermónprez, P., J. Valladeau, L. Zitvogel, C. Thery, and S. Amigorena. 2002. Antigen presentation and T cell stimulation by dendritic cells. *Annu.Rev.Immunol.* 20:621-667.
53. Steinman, R. M. and J. Swanson. 1995. The endocytic activity of dendritic cells. *J.Exp.Med.* 182:283-288.
54. Mellman, I. and R. M. Steinman. 2001. Dendritic cells: Specialized and regulated antigen processing machines. *Cell* 106:255-258.
55. Hawiger, D., K. Inaba, Y. Dorsett, M. Guo, K. Mahnke, M. Rivera, J. V. Ravetch, R. M. Steinman, and M. C. Nussenzweig. 2001. Dendritic cells induce peripheral T cell unresponsiveness under steady state conditions in vivo. *J.Exp.Med.* 194:769-779.
56. Steinman, R. M. and M. C. Nussenzweig. 2002. Avoiding horror autotoxicus: the importance of dendritic cells in peripheral T cell tolerance. *Proc.Natl.Acad.Sci.USA* 99:351-358.
57. Banchereau, J., F. Bazan, D. Blanchard, F. Briere, J. P. Galizzi, C. Kooten, Y. J. Liu, F. Rousset, and S. Saeland. 1994. The CD40 antigen and its ligand. *Ann.Rev.Immunol.* 12:881-922.
58. Rissoan, M. C., V. Soumelis, N. Kadowaki, G. Grouard, F. Briere, R. W. Waal-Malefyt, and Y. J. Liu. 1999. Reciprocal control of T helper cell and dendritic cell differentiation. *Science* 283:1183-1186.
59. Larrengina, A. T. and L. D. Falo. 2005. Changing paradigms in cutaneous immunology: adapting with dendritic cells. *J.Invest.Dermatol.* 124:1-12.

60. Romani, N., S. Holzmann, C. H. Tripp, F. Koch, and P. Stoitzner. 2003. Langerhans cells - dendritic cells of the epidermis. *Apmis* 111:725-740.
61. Dana, M. R., Y. Qian, and P. Hamrah. 2000. Twenty-five-year panorama of corneal immunology: emerging concepts in the immunopathogenesis of microbial keratitis, peripheral ulcerative keratitis, and corneal transplant rejection. *Cornea* 19:625-643.
62. Moll, H., S. Flohé, and M. Rölinghoff. 1995. Dendritic cells in *Leishmania major*-immune mice harbor persistent parasites and mediate an antigen-specific T cell immune response. *Eur.J.Immunol.* 25:693-699.
63. Romani, N., S. Holzmann, C. H. Tripp, F. Koch, and P. Stoitzner. 2003. Langerhans cells - dendritic cells of the epidermis. *Apmis* 111:725-740.
64. Hemmi, H., M. Yoshino, H. Yamazaki, M. Naito, T. Iyoda, Y. Omatsu, S. Shimoyama, J. J. Letterio, T. Nakabayashi, H. Tagaya, T. Yamane, M. Ogawa, S. Nishikawa, K. Ryo, K. Inaba, S. Hayashi, and T. Kunisada. 2001. Skin antigens in the steady state are trafficked to regional lymph nodes by transforming growth factor- β 1-dependent cells. *Int.Immunol.* 13:695-704.
65. Schuler, G. and R. M. Steinman. 1985. Murine epidermal Langerhans cells mature into potent immunostimulatory dendritic cells in vitro. *J.Exp.Med.* 161:526-546.
66. Larsen, C. P., R. M. Steinman, M. Witmer-Pack, D. F. Hankins, P. J. Morris, and J. M. Austyn. 1990. Migration and maturation of Langerhans cells in skin transplants and explants. *J.Exp.Med.* 172:1483-1493.
67. Cumberbatch, M. and I. Kimber. 1992. Dermal tumour necrosis factor- α induces dendritic cell migration to draining lymph nodes, and possibly provides one stimulus for Langerhans' cell migration. *Immunology* 75:257-263.
68. Cumberbatch, M., I. Fielding, and I. Kimber. 1994. Modulation of epidermal Langerhans' cell frequency by tumour necrosis factor- α . *Immunology* 81:395-401.

69. Hamrah, P., S. O. Huq, Y. Liu, Q. Zhang, and M. R. Dana. 2003. Corneal immunity is mediated by heterogeneous population of antigen-presenting cells. *J.Leukoc.Biol.* 74:172-178.
70. Liu, Y., P. Hamrah, Q. Zhang, A. W. Taylor, and M. R. Dana. 2002. Draining lymph nodes of corneal transplant hosts exhibit evidence for donor major histocompatibility complex (MHC) class II-positive dendritic cells derived from MHC class II-negative grafts. *J.Exp.Med.* 195:259-268.
71. Shibaki, A., A. Sato, J. C. Vogel, F. Miyagawa, and S. I. Katz. 2004. Induction of GVHD-like skin disease by passively transferred CD8⁺ T-cell receptor transgenic T cells into keratin 14-ovalbumin transgenic mice. *J.Invest.Dermatol.* 123:109-115.
72. Hemmi, H., M. Yoshino, H. Yamazaki, M. Naito, T. Iyoda, Y. Omatsu, S. Shimoyama, J. J. Letterio, T. Nakabayashi, H. Tagaya, T. Yamane, M. Ogawa, S. Nishikawa, K. Ryoike, K. Inaba, S. Hayashi, and T. Kunisada. 2001. Skin antigens in the steady state are trafficked to regional lymph nodes by transforming growth factor- β 1-dependent cells. *Int.Immunol.* 13:695-704.
73. Stoitzner, P., S. Holzmann, A. D. McLellan, L. Ivarsson, H. Stossel, M. Kapp, U. Kammerer, P. Douillard, E. Kampgen, F. Koch, S. Saeland, and N. Romani. 2003. Visualization and characterization of migratory Langerhans cells in murine skin and lymph nodes by antibodies against Langerin/CD207. *J.Invest.Dermatol.* 120:266-274.
74. Ginhoux, F., F. Tacke, V. Angeli, M. Bogunovic, M. Loubeau, X. M. Dai, E. R. Stanley, G. J. Randolph, and M. Merad. 2006. Langerhans cells arise from monocytes in vivo. *Nat Immunol* 7:265-273.
75. Tang, A., M. Amagai, L. G. Granger, J. R. Stanley, and M. C. Udey. 1993. Adhesion of epidermal Langerhans cells to keratinocytes mediated by E-cadherin. *Nature* 361:82-85.
76. Blauvelt, A., S. I. Katz, and M. C. Udey. 1995. Human langerhans cells express E-cadherin. *J.Invest.Dermatol.* 104:293-296.

77. Birbeck, M. S., A. S. Breathnach, and J. D. Everall. 1961. An electron microscope study of basal melanocytes and high-level clear cells (Langerhans cells) in vitiligo. *J.Invest.Dermatol.* 37:51-64.
78. Valladeau, J., C. zutter-Dambuyant, and S. Saeland. 2003. Langerin/CD207 sheds light on formation of birbeck granules and their possible function in Langerhans cells. *Immunol.Res.* 28:93-107.
79. Valladeau, J., O. Ravel, C. Dezutter-Dambuyant, K. Moore, M. Kleijmeer, Y. Liu, V. Duvert-Frances, C. Vincent, D. Schmitt, J. Davoust, C. Caux, S. Lebecque, and S. Saeland. 2000. Langerin, a novel C-type lectin specific to Langerhans cells, is an endocytic receptor that induces the formation of Birbeck granules. *Immunity* 12:71-81.
80. McDermott, R., U. Ziylan, D. Spehner, H. Bausinger, D. Lipsker, M. Mommaas, J. P. Cazenave, G. Raposo, B. Goud, S. H. de la, J. Salamero, and D. Hanau. 2002. Birbeck granules are subdomains of endosomal recycling compartment in human epidermal Langerhans cells, which form where Langerin accumulates. *Mol.Biol.Cell* 13:317-335.
81. Plzak, J., Z. Holikova, B. Dvorankova, K. Smetana, Jr., J. Betka, J. Hercogova, S. Saeland, N. V. Bovin, and H. J. Gabius. 2002. Analysis of binding of mannosides in relation to Langerin (CD207) in Langerhans cells of normal and transformed epithelia. *Histochem.J.* 34:247-253.
82. Stambach, N. S. and M. E. Taylor. 2003. Characterization of carbohydrate recognition by langerin, a C-type lectin of Langerhans cells. *Glycobiology* 13:401-410.
83. Hunger, R. E., P. A. Sieling, M. T. Ochoa, M. Sugaya, A. E. Burdick, T. H. Rea, P. J. Brennan, J. T. Belisle, A. Blauvelt, S. A. Porcelli, and R. L. Modlin. 2004. Langerhans cells utilize CD1a and langerin to efficiently present non-peptide antigens to T cells. *J.Clin.Invest.* (in press).
84. Apte, R. S. and J. Y. Niederkorn. 1996. Isolation and characterization of a unique natural killer cell inhibitory factor present in the anterior chamber of the eye. *J.Immunol.* 156:2667-2673.

85. Niederkorn, J. Y. 2002. Immune privilege in the anterior chamber of the eye. *Crit Rev.Immunol.* 22:13-46.
86. Streilein, J. W., S. Masli, M. Takeuchi, and T. Kezuka. 2002. The eye's view of antigen presentation. *Hum.Immunol.* 63:435-443.
87. Dana, M. R., Y. Qian, and P. Hamrah. 2000. Twenty-five-year panorama of corneal immunology: emerging concepts in the immunopathogenesis of microbial keratitis, peripheral ulcerative keratitis, and corneal transplant rejection. *Cornea* 19:625-643.
88. Williams, K. A. and D. J. Coster. 1997. Rethinking immunological privilege: implications for corneal and limbal stem cell transplantation. *Mol.Med.Today* 3:495-501.
89. He, Y. G. and J. Y. Niederkorn. 1996. Depletion of donor-derived Langerhans cells promotes corneal allograft survival. *Cornea* 15:82-89.
90. Ross, J., D. Callanan, H. Kunz, and J. Niederkorn. 1991. Evidence that the fate of class II-disparate corneal grafts is determined by the timing of class II expression. *Transplantation* 51:532-536.
91. Peeler, J. S. and J. Y. Niederkorn. 1986. Antigen presentation by Langerhans cells in vivo: donor-derived Ia⁺ Langerhans cells are required for induction of delayed-type hypersensitivity but not for cytotoxic T lymphocyte responses to alloantigens. *J.Immunol.* 136:4362-4371.
92. Hegde, S. and J. Y. Niederkorn. 2000. The role of cytotoxic T lymphocytes in corneal allograft rejection. *Invest.Ophthalmol.Vis.Sci.* 41:3341-3347.
93. Williamson, J. S., S. DiMarco, and J. W. Streilein. 1987. Immunobiology of Langerhans cells on the ocular surface. I. Langerhans cells within the central cornea interfere with induction of anterior chamber associated immune deviation. *Invest.Ophthalmol.Vis.Sci.* 28:1527-1532.
94. Dana, M. R., R. Dai, S. Zhu, J. Yamada, and J. W. Streilein. 1998. Interleukin-1 receptor antagonist suppresses Langerhans cell

- activity and promotes ocular immune privilege.
Invest.Ophthalmol.Vis.Sci. 39:70-77.
95. Asbell, P. A. and T. Kamenar. 1987. The response of Langerhans cells in the cornea to herpetic keratitis. *Curr.Eye Res.* 6:179-182.
 96. Miller, J. K., K. A. Laycock, M. M. Nash, and J. S. Pepose. 1993. Corneal Langerhans cell dynamics after herpes simplex virus reactivation. *Invest.Ophthalmol.Vis.Sci.* 34:2282-2290.
 97. Thomas, J. and B. T. Rouse. 1998. Immunopathology of herpetic stromal keratitis: discordance in CD4+ T cell function between euthymic host and reconstituted SCID recipients. *J.Immunol.* 160:3965-3970.
 98. Suzuki, T., Y. Sano, and S. Kinoshita. 2000. Conjunctival inflammation induces Langerhans cell migration into the cornea. *Curr.Eye Res.* 21:550-553.
 99. Hazlett, L. D., S. M. McClellan, E. B. Hume, J. J. Dajcs, R. J. O'Callaghan, and M. D. Willcox. 1999. Extended wear contact lens usage induces Langerhans cell migration into cornea. *Exp.Eye Res.* 69:575-577.
 100. Dana, M. R., R. Dai, S. Zhu, J. Yamada, and J. W. Streilein. 1998. Interleukin-1 receptor antagonist suppresses Langerhans cell activity and promotes ocular immune privilege. *Invest.Ophthalmol.Vis.Sci.* 39:70-77.
 101. Dana, M. R., J. Yamada, and J. W. Streilein. 1997. Topical interleukin 1 receptor antagonist promotes corneal transplant survival. *Transplantation* 63:1501-1507.
 102. Dekaris, I., S. N. Zhu, and M. R. Dana. 1999. TNF- α regulates corneal Langerhans cell migration. *J.Immunol.* 162:4235-4239.
 103. Liu, Y., P. Hamrah, Q. Zhang, A. W. Taylor, and M. R. Dana. 2002. Draining lymph nodes of corneal transplant hosts exhibit evidence for donor major histocompatibility complex (MHC) class II-positive dendritic cells derived from MHC class II-negative grafts. *J.Exp.Med.* 195:259-268.

104. Hamrah, P., Q. Zhang, Y. Liu, and M. R. Dana. 2002. Novel characterization of MHC class II-negative population of resident corneal Langerhans cell-type dendritic cells. *Invest.Ophthalmol.Vis.Sci.* 43:639-646.
105. Yu, R. C., D. C. Abrams, M. Alaibac, and A. C. Chu. 1994. Morphological and quantitative analyses of normal epidermal Langerhans cells using confocal scanning laser microscopy. *Br.J.Dermatol.* 131:843-848.
106. Ito, H., T. Takekoshi, M. Miyauchi, I. Ogawa, T. Takata, H. Nikai, and K. Takemoto. 1998. Three-dimensional appearance of Langerhans cells in human gingival epithelium as revealed by confocal laser scanning microscopy. *Arch.Oral Biol.* 43:741-744.
107. Rizova, H., P. Carayon, A. Barbier, F. Lacheretz, L. Dubertret, and L. Michel. 1999. Contact allergens, but not irritants, alter receptor-mediated endocytosis by human epidermal Langerhans cells. *Br.J.Dermatol.* 140:200-209.
108. Larsson, M., M. Majeed, J. D. Ernst, K. E. Magnusson, O. Stendahl, and U. Forsum. 1997. Role of annexins in endocytosis of antigens in immature human dendritic cells. *Immunology* 92:501-511.
109. von Andrian, U. H. 2002. Immunology. T cell activation in six dimensions. *Science* 296:1815-1817.
110. Stoll, S., J. Delon, T. M. Brotz, and R. N. Germain. 2002. Dynamic imaging of T cell-dendritic cell interactions in lymph nodes. *Science* 296:1873-1876.
111. Rajadhyaksha, M., M. Grossman, D. Esterowitz, R. H. Webb, and R. R. Anderson. 1995. In vivo confocal scanning laser microscopy of human skin: melanin provides strong contrast. *J.Invest.Dermatol.* 104:946-952.
112. Rajadhyaksha, M., S. Gonzalez, J. M. Zavislan, R. R. Anderson, and R. H. Webb. 1999. In vivo confocal scanning laser microscopy of human skin II: advances in instrumentation and comparison with histology. *J.Invest.Dermatol.* 113:293-303.

113. Langley, R. G., M. Rajadhyaksha, P. J. Dwyer, A. J. Sober, T. J. Flotte, and R. R. Anderson. 2001. Confocal scanning laser microscopy of benign and malignant melanocytic skin lesions in vivo. *J.Am.Acad.Dermatol.* 45:365-376.
114. Busam, K. J., C. Charles, C. M. Lohmann, A. Marghoob, M. Goldgeier, and A. C. Halpern. 2002. Detection of intraepidermal malignant melanoma *in vivo* by confocal scanning laser microscopy. *Melanoma Res.* 12:349-355.
115. Denk, W., J. H. Strickler, and W. W. Webb. 1990. 2-Photon Laser Scanning Fluorescence Microscopy. *Science* 248:73-76.
116. Cahalan, M. D., I. Parker, S. H. Wei, and M. J. Miller. 2002. Two-photon tissue imaging: seeing the immune system in a fresh light. *Nat.Rev.Immunol.* 2:872-880.
117. Masters, B. R., P. T. So, and E. Gratton. 1997. Multiphoton excitation fluorescence microscopy and spectroscopy of in vivo human skin. *Biophys.J.* 72:2405-2412.
118. Masters, B. R., P. T. C. So, and E. Gratton. 1999. Multiphoton excitation microscopy and confocal microscopy of human skin in vivo. *Comments Mol.Cel.Biophys.* 9:379-405.
119. Malone, J. C., A. F. Hood, T. Conley, J. Nurnberger, L. A. Baldrige, J. L. Clendenon, K. W. Dunn, and C. L. Phillips. 2002. Three-dimensional imaging of human skin and mucosa by two-photon laser scanning microscopy. *J.Cutan.Pathol.* 29:453-458.
120. Bousso, P., N. R. Bhakta, R. S. Lewis, and E. Robey. 2002. Dynamics of thymocyte-stromal cell interactions visualized by two-photon microscopy. *Science* 296:1876-1880.
121. Miller, M. J., S. H. Wei, I. Parker, and M. D. Cahalan. 2002. Two-photon imaging of lymphocyte motility and antigen response in intact lymph node. *Science* 296:1869-1873.
122. Ruan, Q., Y. Chen, E. Gratton, M. Glaser, and W. W. Mantulin. 2002. Cellular characterization of adenylate kinase and its isoform: two-photon excitation fluorescence imaging and fluorescence correlation spectroscopy. *Biophys.J.* 83:3177-3187.

123. Gratton, E., S. Breusegem, J. Sutin, Q. Ruan, and N. Barry. 2003. Fluorescence lifetime imaging for the two-photon microscope: time-domain and frequency-domain methods. *J.Biomed.Opt.* 8:381-390.
124. Denk, W. and K. Svoboda. 1997. Photon upmanship: Why multiphoton imaging is more than a gimmick. *Neuron* 18:351-357.
125. Kim, B. M., J. Eichler, K. M. Reiser, A. M. Rubenchik, and L. B. Da Silva. 2000. Collagen structure and nonlinear susceptibility: effects of heat, glycation, and enzymatic cleavage on second harmonic signal intensity. *Lasers Surg.Med.* 27:329-335.
126. Cox, G., E. Kable, A. Jones, I. Fraser, F. Manconi, and M. D. Gorrell. 2003. 3-dimensional imaging of collagen using second harmonic generation. *J.Struct.Biol.* 141:53-62.
127. Campagnola, P. J. and L. M. Loew. 2003. Second-harmonic imaging microscopy for visualizing biomolecular arrays in cells, tissues and organisms. *Nat.Biotechnol.* 21:1356-1360.
128. Mohler, W., A. C. Millard, and P. J. Campagnola. 2003. Second harmonic generation imaging of endogenous structural proteins. *Methods* 29:97-109.
129. Zoumi, A., A. Yeh, and B. J. Tromberg. 2002. Imaging cells and extracellular matrix *in vivo* by using second-harmonic generation and two-photon excited fluorescence. *Proc.Natl.Acad.Sci.U.S.A* 99:11014-11019.
130. Brown, E., T. McKee, E. diTomaso, A. Pluen, B. Seed, Y. Boucher, and R. K. Jain. 2003. Dynamic imaging of collagen and its modulation in tumors *in vivo* using second-harmonic generation. *Nat.Med.* 9:796-800.
131. SHIMOMURA, O., F. H. JOHNSON, and Y. SAIGA. 1962. Extraction, purification and properties of aequorin, a bioluminescent protein from the luminous hydromedusan, *Aequorea*. *J Cell Comp Physiol* 59:223-239.

132. Farkas, D. L. and D. Becker. 2001. Applications of spectral imaging: detection and analysis of human melanoma and its precursors. *Pigment Cell Res.* 14:2-8.
133. Zimmermann, T., J. Rietdorf, and R. Pepperkok. 2003. Spectral imaging and its applications in live cell microscopy. *FEBS Lett.* 546:87-92.
134. Schieker, M., C. Pautke, K. Reitz, I. Hemraj, P. Neth, W. Mutschler, and S. Milz. 2004. The use of four-colour immunofluorescence techniques to identify mesenchymal stem cells. *J.Anat.* 204:133-139.
135. Dickinson, M. E., E. Simbuerger, B. Zimmermann, C. W. Waters, and S. E. Fraser. 2003. Multiphoton excitation spectra in biological samples. *Journal of Biomedical Optics* 8:329-338.
136. Nadrigny, F., I. Rivals, P. Hirrlinger, A. Koulakoff, L. +. Personnaz, M. Vernet, M. Allieux, M. Chaumeil, N. Ropert, C. Giaume, F. Kirchhoff, and M. Oheim. 2006. Detecting fluorescent protein expression and co-localisation on single secretory vesicles with linear spectral unmixing. *Eur.Biophys.J.* 1-15.
137. Okabe, M., M. Ikawa, K. Kominami, T. Nakanishi, and Y. Nishimune. 1997. 'Green mice' as a source of ubiquitous green cells. *FEBS Lett.* 407:313-319.
138. Boes, M., J. Cerny, R. Massol, d. B. Op, T. Kirchhausen, J. Chen, and H. L. Ploegh. 2002. T-cell engagement of dendritic cells rapidly rearranges MHC class II transport. *Nature* 418:983-988.
139. Larsen, C. P., R. M. Steinman, M. Witmer-Pack, D. F. Hankins, P. J. Morris, and J. M. Austyn. 1990. Migration and maturation of Langerhans cells in skin transplants and explants. *J.Exp.Med.* 172:1483-1493.
140. Rambukkana, A., J. D. Bos, D. Irik, W. J. Menko, M. L. Kapsenberg, and P. K. Das. 1995. *In situ* behavior of human Langerhans cells in skin organ culture. *Lab Invest* 73:521-531.
141. Stoitzner, P., M. Zanella, U. Ortner, M. Lukas, A. Tagwerker, K. Janke, M. B. Lutz, G. Schuler, B. Echtenacher, B. Ryffel, F. Koch, and N. Romani. 1999. Migration of Langerhans cells and dermal dendritic

- cells in skin organ cultures: augmentation by TNF- α and IL-1 β . *J.Leukoc.Biol.* 66:462-470.
142. Kimber, I. and M. Cumberbatch. 1992. Stimulation of Langerhans cell migration by tumor necrosis factor alpha (TNF-alpha). *J.Invest.Dermatol.* 99:48S-50S.
 143. Streilein, J. W., G. T. Toews, J. N. Gilliam, and P. R. Bergstresser. 1980. Tolerance or hypersensitivity to 2,4-dinitro-1-fluorobenzene: the role of Langerhans cell density within epidermis. *J.Invest.Dermatol.* 74:319-322.
 144. Aiba, S. and S. I. Katz. 1990. Phenotypic and functional characteristics of in vivo-activated Langerhans cells. *J.Immunol.* 145:2791-2796.
 145. Grabbe, S., M. Steinert, K. Mahnke, A. Schwarz, T. A. Luger, and T. Schwarz. 1996. Dissection of antigenic and irritative effects of epicutaneously applied haptens in mice. Evidence that not the antigenic component but nonspecific proinflammatory effects of haptens determine the concentration-dependent elicitation of allergic contact dermatitis. *J.Clin.Invest.* 98:1158-1164.
 146. Lambertsen, L., C. Sternberg, and S. Molin. 2004. Mini-Tn7 transposons for site-specific tagging of bacteria with fluorescent proteins. *Environ.Microbiol.* 6:726-732.
 147. Lambertsen, L., C. Sternberg, and S. Molin. 2004. Mini-Tn7 transposons for site-specific tagging of bacteria with fluorescent proteins. *Environ.Microbiol.* 6:726-732.
 148. Merad, M., M. G. Manz, H. Karsunky, A. Wagers, W. Peters, I. Charo, I. L. Weissman, J. G. Cyster, and E. G. Engleman. 2002. Langerhans cells renew in the skin throughout life under steady-state conditions. *Nat.Immunol.* 3:1135-1141.
 149. Merad, M., P. Hoffmann, E. Ranheim, S. Slaymaker, M. G. Manz, S. A. Lira, I. Charo, D. N. Cook, I. L. Weissman, S. Strober, and E. G. Engleman. 2004. Depletion of host Langerhans cells before transplantation of donor alloreactive T cells prevents skin graft-versus-host disease. *Nat.Med.* 10:510-517.

150. Niederkorn, J. Y., J. S. Peeler, and J. Mellon. 1989. Phagocytosis of particulate antigens by corneal epithelial cells stimulates interleukin-1 secretion and migration of Langerhans cells into the central cornea. *Reg Immunol* 2:83-90.
151. Lausch, R. N., S. H. Chen, T. M. Tumpey, Y. H. Su, and J. E. Oakes. 1996. Early cytokine synthesis in the excised mouse cornea. *J.Interferon Cytokine Res.* 16:35-40.
152. Sotozono, C., J. He, Y. Matsumoto, M. Kita, J. Imanishi, and S. Kinoshita. 1997. Cytokine expression in the alkali-burned cornea. *Curr.Eye Res.* 16:670-676.
153. Enk, A. H. and S. I. Katz. 1992. Early molecular events in the induction phase of contact sensitivity. *Proc.Natl.Acad.Sci.USA* 89:1398-1402.
154. Mester, M., E. A. Carter, R. G. Tompkins, J. A. Gelfand, C. A. Dinarello, J. F. Burke, and B. D. Clark. 1994. Thermal injury induces very early production of interleukin-1 alpha in the rat by mechanisms other than endotoxemia. *Surgery* 115:588-596.
155. Niederkorn, J. Y., J. S. Peeler, and J. Mellon. 1989. Phagocytosis of particulate antigens by corneal epithelial cells stimulates interleukin-1 secretion and migration of Langerhans cells into the central cornea. *Reg Immunol* 2:83-90.
156. Lausch, R. N., S. H. Chen, T. M. Tumpey, Y. H. Su, and J. E. Oakes. 1996. Early cytokine synthesis in the excised mouse cornea. *J.Interferon Cytokine Res.* 16:35-40.
157. Sotozono, C., J. He, Y. Matsumoto, M. Kita, J. Imanishi, and S. Kinoshita. 1997. Cytokine expression in the alkali-burned cornea. *Curr.Eye Res.* 16:670-676.
158. Dekaris, I., S. N. Zhu, and M. R. Dana. 1999. TNF- α regulates corneal Langerhans cell migration. *J.Immunol.* 162:4235-4239.
159. Mohri, M., P. S. Reinach, A. Kanayama, M. Shimizu, J. Moskovitz, T. Hisatsune, and Y. Miyamoto. 2002. Suppression of the TNF α -induced increase in IL-1 α expression by hypochlorite in human corneal epithelial cells. *Invest.Ophthalmol.Vis.Sci.* 43:3190-3195.

160. Larsen, C. P., R. M. Steinman, M. Witmer-Pack, D. F. Hankins, P. J. Morris, and J. M. Austyn. 1990. Migration and maturation of Langerhans cells in skin transplants and explants. *J.Exp.Med.* 172:1483-1493.
161. Rambukkana, A., J. D. Bos, D. Irik, W. J. Menko, M. L. Kapsenberg, and P. K. Das. 1995. *In situ* behavior of human Langerhans cells in skin organ culture. *Lab Invest* 73:521-531.
162. Stoitzner, P., M. Zanella, U. Ortner, M. Lukas, A. Tagwerker, K. Janke, M. B. Lutz, G. Schuler, B. Echtenacher, B. Ryffel, F. Koch, and N. Romani. 1999. Migration of Langerhans cells and dermal dendritic cells in skin organ cultures: augmentation by TNF- α and IL-1 β . *J.Leukoc.Biol.* 66:462-470.
163. Kimber, I. and M. Cumberbatch. 1992. Stimulation of Langerhans cell migration by tumor necrosis factor alpha (TNF-alpha). *J.Invest.Dermatol.* 99:48S-50S.
164. Teunissen, M. B. M., J. Wormmeester, S. R. Krieg, P. J. Peters, I. M. C. Vogels, M. L. Kapsenberg, and J. D. Bos. 1990. Human epidermal Langerhans cells undergo profound morphologic and phenotypical changes during in vitro culture. *J.Invest.Dermatol.* 94:166-173.
165. Larsen, C. P., R. M. Steinman, M. Witmer-Pack, D. F. Hankins, P. J. Morris, and J. M. Austyn. 1990. Migration and maturation of Langerhans cells in skin transplants and explants. *J.Exp.Med.* 172:1483-1493.
166. Streilein, J. W., G. T. Toews, J. N. Gilliam, and P. R. Bergstresser. 1980. Tolerance or hypersensitivity to 2,4-dinitro-1-fluorobenzene: the role of Langerhans cell density within epidermis. *J.Invest.Dermatol.* 74:319-322.
167. Lambertsen, L., C. Sternberg, and S. Molin. 2004. Mini-Tn7 transposons for site-specific tagging of bacteria with fluorescent proteins. *Environ.Microbiol.* 6:726-732.
168. Lambertsen, L., C. Sternberg, and S. Molin. 2004. Mini-Tn7 transposons for site-specific tagging of bacteria with fluorescent proteins. *Environ.Microbiol.* 6:726-732.

169. Streilein, J. W., L. W. Lonsberry, and P. R. Bergstresser. 1982. Depletion of epidermal Langerhans cells and Ia immunogenicity from tape-stripped mouse skin. *J.Exp.Med.* 155:863-871.
170. Holzmann, S., C. H. Tripp, M. Schmuth, K. Janke, F. Koch, S. Saeland, P. Stoitzner, and N. Romani. 2004. A model system using tape stripping for characterization of langerhans cell-precursors in vivo. *J.Invest.Dermatol.* 122:1165-1174.
171. Kissenpfennig, A., S. Henri, B. Dubois, C. Laplace-Builhe, P. Perrin, N. Romani, C. H. Tripp, P. Douillard, L. Leserman, D. Kaiserlian, S. Saeland, J. Davoust, and B. Malissen. 2005. Dynamics and function of Langerhans cells in vivo dermal dendritic cells colonize lymph node areas distinct from slower migrating Langerhans cells. *Immunity* 22:643-654.
172. Mishima, Y. 1966. Melanosomes in phagocytic vacuoles in Langerhans cells. Electron microscopy of keratin-stripped human epidermis. *J.Cell Biol.* 30:417-423.
173. Kissenpfennig, A., S. Henri, B. Dubois, C. Laplace-Builhe, P. Perrin, N. Romani, C. H. Tripp, P. Douillard, L. Leserman, D. Kaiserlian, S. Saeland, J. Davoust, and B. Malissen. 2005. Dynamics and function of Langerhans cells in vivo dermal dendritic cells colonize lymph node areas distinct from slower migrating Langerhans cells. *Immunity* 22:643-654.
174. Mishima, Y. 1966. Melanosomes in phagocytic vacuoles in Langerhans cells. Electron microscopy of keratin-stripped human epidermis. *J.Cell Biol.* 30:417-423.
175. Holzmann, S., C. H. Tripp, M. Schmuth, K. Janke, F. Koch, S. Saeland, P. Stoitzner, and N. Romani. 2004. A model system using tape stripping for characterization of langerhans cell-precursors in vivo. *J.Invest.Dermatol.* 122:1165-1174.
176. Shimada, S., S. W. Caughman, S. O. Sharrow, D. Stephany, and S. I. Katz. 1987. Enhanced antigen-presenting capacity of cultured Langerhans' cells is associated with markedly increased expression of Ia antigen. *J.Immunol.* 139:2551-2555.

177. Larsen, C. P., R. M. Steinman, M. Witmer-Pack, D. F. Hankins, P. J. Morris, and J. M. Austyn. 1990. Migration and maturation of Langerhans cells in skin transplants and explants. *J.Exp.Med.* 172:1483-1493.
178. Rambukkana, A., J. D. Bos, D. Irik, W. J. Menko, M. L. Kapsenberg, and P. K. Das. 1995. *In situ* behavior of human Langerhans cells in skin organ culture. *Lab Invest* 73:521-531.
179. Mester, M., E. A. Carter, R. G. Tompkins, J. A. Gelfand, C. A. Dinarello, J. F. Burke, and B. D. Clark. 1994. Thermal injury induces very early production of interleukin-1 alpha in the rat by mechanisms other than endotoxemia. *Surgery* 115:588-596.
180. Sotozono, C., J. He, Y. Matsumoto, M. Kita, J. Imanishi, and S. Kinoshita. 1997. Cytokine expression in the alkali-burned cornea. *Curr.Eye Res.* 16:670-676.
181. Lausch, R. N., S. H. Chen, T. M. Tumpey, Y. H. Su, and J. E. Oakes. 1996. Early cytokine synthesis in the excised mouse cornea. *J.Interferon Cytokine Res.* 16:35-40.
182. Niederkorn, J. Y., J. S. Peeler, and J. Mellon. 1989. Phagocytosis of particulate antigens by corneal epithelial cells stimulates interleukin-1 secretion and migration of Langerhans cells into the central cornea. *Reg Immunol* 2:83-90.
183. Sotozono, C., J. He, Y. Matsumoto, M. Kita, J. Imanishi, and S. Kinoshita. 1997. Cytokine expression in the alkali-burned cornea. *Curr.Eye Res.* 16:670-676.
184. Lausch, R. N., S. H. Chen, T. M. Tumpey, Y. H. Su, and J. E. Oakes. 1996. Early cytokine synthesis in the excised mouse cornea. *J.Interferon Cytokine Res.* 16:35-40.
185. Niederkorn, J. Y., J. S. Peeler, and J. Mellon. 1989. Phagocytosis of particulate antigens by corneal epithelial cells stimulates interleukin-1 secretion and migration of Langerhans cells into the central cornea. *Reg Immunol* 2:83-90.
186. Yard, B. A., M. R. Daha, M. Kooymans-Couthino, J. A. Bruijn, M. E. Paape, E. Schrama, L. A. van Es, and F. J. van der Woude. 1992.

IL-1 α stimulated TNF alpha production by cultured human proximal tubular epithelial cells. *Kidney Int.* 42:383-389.

187. Ikejima, T., S. Okusawa, P. Ghezzi, J. W. van der Meer, and C. A. Dinarello. 1990. Interleukin-1 induces tumor necrosis factor (TNF) in human peripheral blood mononuclear cells in vitro and a circulating TNF-like activity in rabbits. *J.Infect.Dis.* 162:215-223.
188. Dekaris, I., S. N. Zhu, and M. R. Dana. 1999. TNF- α regulates corneal Langerhans cell migration. *J.Immunol.* 162:4235-4239.
189. Mohri, M., P. S. Reinach, A. Kanayama, M. Shimizu, J. Moskovitz, T. Hisatsune, and Y. Miyamoto. 2002. Suppression of the TNF α -induced increase in IL-1 α expression by hypochlorite in human corneal epithelial cells. *Invest.Ophthalmol.Vis.Sci.* 43:3190-3195.
190. Lisby, S. and C. Hauser. 2002. Transcriptional regulation of tumor necrosis factor-alpha in keratinocytes mediated by interleukin-1beta and tumor necrosis factor-alpha. *Exp.Dermatol.* 11:592-598.
191. Werth, V. P. and W. Zhang. 1999. Wavelength-specific synergy between ultraviolet radiation and interleukin-1 α in the regulation of matrix-related genes: mechanistic role for tumor necrosis factor- α . *J.Invest.Dermatol.* 113:196-201.
192. Larsen, C. P., R. M. Steinman, M. Witmer-Pack, D. F. Hankins, P. J. Morris, and J. M. Austyn. 1990. Migration and maturation of Langerhans cells in skin transplants and explants. *J.Exp.Med.* 172:1483-1493.
193. Rambukkana, A., J. D. Bos, D. Irik, W. J. Menko, M. L. Kapsenberg, and P. K. Das. 1995. *In situ* behavior of human Langerhans cells in skin organ culture. *Lab Invest* 73:521-531.
194. Stoitzner, P., M. Zanella, U. Ortner, M. Lukas, A. Tagwerker, K. Janke, M. B. Lutz, G. Schuler, B. Echtenacher, B. Ryffel, F. Koch, and N. Romani. 1999. Migration of Langerhans cells and dermal dendritic cells in skin organ cultures: augmentation by TNF- α and IL-1 β . *J.Leukoc.Biol.* 66:462-470.

195. Kimber, I. and M. Cumberbatch. 1992. Stimulation of Langerhans cell migration by tumor necrosis factor alpha (TNF-alpha). *J.Invest.Dermatol.* 99:48S-50S.
196. Streilein, J. W., G. T. Toews, J. N. Gilliam, and P. R. Bergstresser. 1980. Tolerance or hypersensitivity to 2,4-dinitro-1-fluorobenzene: the role of Langerhans cell density within epidermis. *J.Invest.Dermatol.* 74:319-322.
197. Kissenpfennig, A., S. Henri, B. Dubois, C. Laplace-Builhe, P. Perrin, N. Romani, C. H. Tripp, P. Douillard, L. Leserman, D. Kaiserlian, S. Saeland, J. Davoust, and B. Malissen. 2005. Dynamics and function of Langerhans cells in vivo dermal dendritic cells colonize lymph node areas distinct from slower migrating Langerhans cells. *Immunity* 22:643-654.
198. Mishima, Y. 1966. Melanosomes in phagocytic vacuoles in Langerhans cells. Electron microscopy of keratin-stripped human epidermis. *J.Cell Biol.* 30:417-423.
199. Holzmann, S., C. H. Tripp, M. Schmuth, K. Janke, F. Koch, S. Saeland, P. Stoitzner, and N. Romani. 2004. A model system using tape stripping for characterization of langerhans cell-precursors in vivo. *J.Invest.Dermatol.* 122:1165-1174.
200. Cahalan, M. D., I. Parker, S. H. Wei, and M. J. Miller. 2002. Two-photon tissue imaging: seeing the immune system in a fresh light. *Nat.Rev.Immunol.* 2:872-880.
201. Inaba, K., J. W. Young, and R. M. Steinman. 1987. Direct activation of CD8⁺ cytotoxic T lymphocytes by dendritic cells. *J.Exp.Med.* 166:182-194.
202. Gunzer, M., P. Friedl, B. Niggemann, E. B. Bröcker, E. Kampgen, and K. S. Zanker. 2000. Migration of dendritic cells within 3-D collagen lattices is dependent on tissue origin, state of maturation, and matrix structure and is maintained by proinflammatory cytokines. *J.Leukoc.Biol.* 67:622-629.
203. Lindquist, R. L., G. Shakhar, D. Dudziak, H. Wardemann, T. Eisenreich, M. L. Dustin, and M. C. Nussenzweig. 2004. Visualizing dendritic cell networks *in vivo*. *Nat.Immunol.* 5:1243-1250.

204. Chow, A., D. Toomre, W. Garrett, and I. Mellman. 2002. Dendritic cell maturation triggers retrograde MHC class II transport from lysosomes to the plasma membrane. *Nature* 418:988-994.
205. Boes, M., J. Cerny, R. Massol, d. B. Op, T. Kirchhausen, J. Chen, and H. L. Ploegh. 2002. T-cell engagement of dendritic cells rapidly rearranges MHC class II transport. *Nature* 418:983-988.
206. Gunzer, M., A. Schafer, S. Borgmann, S. Grabbe, K. S. Zanker, E. B. Bröcker, E. Kampgen, and P. Friedl. 2000. Antigen presentation in extracellular matrix: interactions of T cells with dendritic cells are dynamic, short lived, and sequential. *Immunity* 13:323-332.
207. Stoll, S., J. Delon, T. M. Brotz, and R. N. Germain. 2002. Dynamic imaging of T cell-dendritic cell interactions in lymph nodes. *Science* 296:1873-1876.
208. Bousso, P. and E. Robey. 2003. Dynamics of CD8⁺ T cell priming by dendritic cells in intact lymph nodes. *Nat.Immunol.* 4:579-585.
209. Hugues, S., L. Fetler, L. Bonifaz, J. Helft, F. Amblard, and S. Amigorena. 2004. Distinct T cell dynamics in lymph nodes during the induction of tolerance and immunity. *Nat.Immunol.* 5:1235-1242.
210. Benvenuti, F., S. Hugues, M. Walmsley, S. Ruf, L. Fetler, M. Popoff, V. L. Tybulewicz, and S. Amigorena. 2004. Requirement of Rac1 and Rac2 expression by mature dendritic cells for T cell priming. *Science* 305:1150-1153.
211. Mempel, T. R., S. E. Henrickson, and U. H. von Andrian. 2004. T-cell priming by dendritic cells in lymph nodes occurs in three distinct phases. *Nature* 427:154-159.
212. Miller, M. J., A. S. Hejazi, S. H. Wei, M. D. Cahalan, and I. Parker. 2004. T cell repertoire scanning is promoted by dynamic dendritic cell behavior and random T cell motility in the lymph node. *Proc.Natl.Acad.Sci.U.S.A* 101:998-1003.
213. Miller, M. J., O. Safrina, I. Parker, and M. D. Cahalan. 2004. Imaging the single cell dynamics of CD4⁺ T cell activation by dendritic cells in lymph nodes. *J.Exp.Med.* 200:847-856.

214. Lindquist, R. L., G. Shakhar, D. Dudziak, H. Wardemann, T. Eisenreich, M. L. Dustin, and M. C. Nussenzweig. 2004. Visualizing dendritic cell networks *in vivo*. *Nat.Immunol.* 5:1243-1250.
215. Valladeau, J., V. Duvert-Frances, J. J. Pin, C. Dezutter-Dambuyant, C. Vincent, C. Massacrier, J. Vincent, K. Yoneda, J. Banchereau, C. Caux, J. Davoust, and S. Saeland. 1999. The monoclonal antibody DCGM4 recognizes Langerin, a protein specific of Langerhans cells, and is rapidly internalized from the cell surface. *Eur.J.Immunol.* 29:2695-2704.
216. Valladeau, J., O. Ravel, C. Dezutter-Dambuyant, K. Moore, M. Kleijmeer, Y. Liu, V. Duvert-Frances, C. Vincent, D. Schmitt, J. Davoust, C. Caux, S. Lebecque, and S. Saeland. 2000. Langerin, a novel C-type lectin specific to Langerhans cells, is an endocytic receptor that induces the formation of Birbeck granules. *Immunity* 12:71-81.
217. McDermott, R., U. Ziylan, D. Spehner, H. Bausinger, D. Lipsker, M. Mommaas, J. P. Cazenave, G. Raposo, B. Goud, S. H. de la, J. Salamero, and D. Hanau. 2002. Birbeck granules are subdomains of endosomal recycling compartment in human epidermal Langerhans cells, which form where Langerin accumulates. *Mol.Biol.Cell* 13:317-335.
218. Stoitzner, P., S. Holzmann, A. D. McLellan, L. Ivarsson, H. Stossel, M. Kapp, U. Kammerer, P. Douillard, E. Kampgen, F. Koch, S. Saeland, and N. Romani. 2003. Visualization and characterization of migratory Langerhans cells in murine skin and lymph nodes by antibodies against Langerin/CD207. *J.Invest.Dermatol.* 120:266-274.
219. Tripp, C. H., S. Chang-Rodriguez, P. Stoitzner, S. Holzmann, H. Stossel, P. Douillard, S. Saeland, F. Koch, A. Elbe-Burger, and N. Romani. 2004. Ontogeny of Langerin/CD207 expression in the epidermis of mice. *J.Invest.Dermatol.* 122:670-672.
220. Kissenpfennig, A., S. Henri, B. Dubois, C. Laplace-Builhe, P. Perrin, N. Romani, C. H. Tripp, P. Douillard, L. Leserman, D. Kaiserlian, S. Saeland, J. Davoust, and B. Malissen. 2005. Dynamics and function of Langerhans cells in vivo dermal dendritic cells colonize lymph node areas distinct from slower migrating Langerhans cells. *Immunity* 22:643-654.

221. Aiba, S. and S. I. Katz. 1990. Phenotypic and functional characteristics of in vivo-activated Langerhans cells. *J.Immunol.* 145:2791-2796.
222. Aiba, S. and S. I. Katz. 1990. Phenotypic and functional characteristics of in vivo-activated Langerhans cells. *J.Immunol.* 145:2791-2796.
223. Larsen, C. P., R. M. Steinman, M. Witmer-Pack, D. F. Hankins, P. J. Morris, and J. M. Austyn. 1990. Migration and maturation of Langerhans cells in skin transplants and explants. *J.Exp.Med.* 172:1483-1493.
224. Buttkke, T. and P. A. Sadstrom. 1994. Oxidative stress as a mediator of apoptosis. *Immunol.Today* 15:7-10.
225. Verhasselt, V., M. Goldman, and F. Willems. 1998. Oxidative stress up-regulates IL-8 and TNF- α synthesis by human dendritic cells. *Eur.J.Immunol.* 28:3886-3890.
226. Torii, H., Z. Yan, J. Hosoi, and R. D. Granstein. 1997. Expression of neurotrophic factors and neuropeptide receptors by Langerhans cells and the Langerhans cell-like cell line XS52: further support for a functional relationship between Langerhans cells and epidermal nerves. *J.Invest.Dermatol.* 109:586-591.
227. Torii, H., J. Hosoi, A. Asahina, and R. D. Granstein. 1997. Calcitonin gene-related peptide and Langerhans cell function. *J.Investig.Dermatol.Symp.Proc.* 2:82-86.
228. Hosoi, J., H. Ozawa, and R. D. Granstein. 1999. beta-Endorphin binding and regulation of cytokine expression in Langerhans cells. *Ann.N.Y.Acad.Sci.* 885:405-413.
229. Lindquist, R. L., G. Shakhar, D. Dudziak, H. Wardemann, T. Eisenreich, M. L. Dustin, and M. C. Nussenzweig. 2004. Visualizing dendritic cell networks *in vivo*. *Nat.Immunol.* 5:1243-1250.
230. Hugues, S., L. Fetler, L. Bonifaz, J. Helft, F. Amblard, and S. Amigorena. 2004. Distinct T cell dynamics in lymph nodes during the induction of tolerance and immunity. *Nat.Immunol.* 5:1235-1242.
231. Yu, R. C., D. C. Abrams, M. Alaibac, and A. C. Chu. 1994. Morphological and quantitative analyses of normal epidermal

- Langerhans cells using confocal scanning laser microscopy. *Br.J.Dermatol.* 131:843-848.
232. Bauer, J., F. A. Bahmer, J. Worl, W. Neuhuber, G. Schuler, and M. Fartasch. 2001. A strikingly constant ratio exists between Langerhans cells and other epidermal cells in human skin. A stereologic study using the optical disector method and the confocal laser scanning microscope. *J.Invest.Dermatol.* 116:313-318.
 233. Romani, N., S. Holzmann, C. H. Tripp, F. Koch, and P. Stoitzner. 2003. Langerhans cells - dendritic cells of the epidermis. *Apmis* 111:725-740.
 234. Bouis, D. A., T. G. Popova, A. Takashima, and M. V. Norgard. 2001. Dendritic cells phagocytose and are activated by treponema pallidum. *Infect.Immun.* 69:518-528.
 235. Hemmi, H., M. Yoshino, H. Yamazaki, M. Naito, T. Iyoda, Y. Omatsu, S. Shimoyama, J. J. Letterio, T. Nakabayashi, H. Tagaya, T. Yamane, M. Ogawa, S. Nishikawa, K. Ryo, K. Inaba, S. Hayashi, and T. Kunisada. 2001. Skin antigens in the steady state are trafficked to regional lymph nodes by transforming growth factor- β 1-dependent cells. *Int.Immunol.* 13:695-704.
 236. Mishima, Y. 1966. Melanosomes in phagocytic vacuoles in Langerhans cells. Electron microscopy of keratin-stripped human epidermis. *J.Cell Biol.* 30:417-423.
 237. Hendricks, R. L. 1997. An immunologist's view of herpes simplex keratitis. *Cornea* 16:503-506.
 238. Dana, M. R., Y. Qian, and P. Hamrah. 2000. Twenty-five-year panorama of corneal immunology: emerging concepts in the immunopathogenesis of microbial keratitis, peripheral ulcerative keratitis, and corneal transplant rejection. *Cornea* 19:625-643.
 239. Hendricks, R. L., M. Janowicz, and T. M. Tumpey. 1992. Critical role of corneal Langerhans cells in the CD4- but not CD8-mediated immunopathology in herpes simplex virus-1-infected mouse corneas. *J.Immunol.* 148:2522-2529.

240. Dana, M. R., Y. Qian, and P. Hamrah. 2000. Twenty-five-year panorama of corneal immunology: emerging concepts in the immunopathogenesis of microbial keratitis, peripheral ulcerative keratitis, and corneal transplant rejection. *Cornea* 19:625-643.
241. Streilein, J. W., M. R. Dana, and B. R. Ksander. 1997. Immunity causing blindness: five different paths to herpes stromal keratitis. *Immunol.Today* 18:443-449.
242. Hazlett, L. D. 2004. Corneal response to *Pseudomonas aeruginosa* infection. *Progress in Retinal and Eye Research* 23:1-30.
243. Hazlett, L. D. 2002. Pathogenic mechanisms of *P. aeruginosa* keratitis: a review of the role of T cells, Langerhans cells, PMN, and cytokines. *DNA Cell Biol.* 21:383-390.
244. Dana, M. R., Y. Qian, and P. Hamrah. 2000. Twenty-five-year panorama of corneal immunology: emerging concepts in the immunopathogenesis of microbial keratitis, peripheral ulcerative keratitis, and corneal transplant rejection. *Cornea* 19:625-643.
245. Hazlett, L. D., S. McClellan, B. Kwon, and R. Barrett. 2000. Increased severity of *Pseudomonas aeruginosa* corneal infection in strains of mice designated as Th1 versus Th2 responsive. *Invest.Ophthalmol.Vis.Sci.* 41:805-810.
246. Hazlett, L. D., S. McClellan, R. Barrett, and X. Rudner. 2001. B7/CD28 costimulation is critical in susceptibility to *Pseudomonas aeruginosa* corneal infection: a comparative study using monoclonal antibody blockade and CD28-deficient mice. *J.Immunol.* 166:1292-1299.
247. Hazlett, L. D., S. A. McClellan, X. L. Rudner, and R. P. Barrett. 2002. The role of Langerhans cells in *Pseudomonas aeruginosa* infection. *Invest.Ophthalmol.Vis.Sci.* 43:189-197.
248. Hazlett, L. D. 2002. Pathogenic mechanisms of *P. aeruginosa* keratitis: a review of the role of T cells, Langerhans cells, PMN, and cytokines. *DNA Cell Biol.* 21:383-390.
249. Hazlett, L. D., S. McClellan, R. Barrett, and X. Rudner. 2001. B7/CD28 costimulation is critical in susceptibility to *Pseudomonas*

aeruginosa corneal infection: a comparative study using monoclonal antibody blockade and CD28-deficient mice. *J.Immunol.* 166:1292-1299.

250. Larsen, C. P., R. M. Steinman, M. Witmer-Pack, D. F. Hankins, P. J. Morris, and J. M. Austyn. 1990. Migration and maturation of Langerhans cells in skin transplants and explants. *J.Exp.Med.* 172:1483-1493.
251. Asselin-Paturel, C., A. Boonstra, M. Dalod, I. Durand, N. Yessaad, C. Dezutter-Dambuyant, A. Vicari, A. O'Garra, C. Biron, F. Briere, and G. Trinchieri. 2001. Mouse type I IFN-producing cells are immature APCs with plasmacytoid morphology. *Nat.Immunol.* 2:1144-1150.
252. Fujita, H., A. Asahina, Y. Tada, H. Fujiwara, and K. Tamaki. 2005. Type I interferons inhibit maturation and activation of mouse langerhans cells. *J.Invest.Dermatol.* 125:126-133.
253. Angeli, V., C. Faveeuw, O. Roye, J. Fontaine, E. Teissier, A. Capron, I. Wolowczuk, M. Capron, and F. Trottein. 2001. Role of the parasite-derived prostaglandin D₂ in the inhibition of epidermal Langerhans cell migration during schistosomiasis infection. *J.Exp.Med.* 193:1135-1147.
254. Allan, R. S., C. M. Smith, G. T. Belz, A. L. van Lint, L. M. Wakim, W. R. Heath, and F. R. Carbone. 2003. Epidermal viral immunity induced by CD8 α^+ dendritic cells but not by Langerhans cells. *Science* 301:1925-1928.
255. Zhao, X., E. Deak, K. Soderberg, M. Linehan, D. Spezzano, J. Zhu, D. M. Knipe, and A. Iwasaki. 2003. Vaginal submucosal dendritic cells, but not Langerhans cells, induce protective Th1 responses to herpes simplex virus-2. *J.Exp.Med.* 197:153-162.
256. Ritter, U., A. Meissner, C. Scheidig, and H. Korner. 2004. CD8 α - and Langerin-negative dendritic cells, but not Langerhans cells, act as principal antigen-presenting cells in leishmaniasis. *Eur.J.Immunol.* 34:1542-1550.
257. Kissenpfennig, A., S. Henri, B. Dubois, C. Laplace-Builhe, P. Perrin, N. Romani, C. H. Tripp, P. Douillard, L. Leserman, D. Kaiserlian, S. Saeland, J. Davoust, and B. Malissen. 2005. Dynamics and

function of Langerhans cells in vivo dermal dendritic cells colonize lymph node areas distinct from slower migrating Langerhans cells. *Immunity* 22:643-654.

258. Nestle, F. O., X. G. Zheng, C. B. Thompson, L. A. Turka, and B. J. Nickoloff. 1993. Characterization of dermal dendritic cells obtained from normal human skin reveals phenotypic and functionally distinctive subsets. *J.Immunol.* 151:6535-6545.
259. Nestle, F. O., L. Filgueira, B. J. Nickoloff, and G. Burg. 1998. Human dermal dendritic cells process and present soluble protein antigens. *J.Invest.Dermatol.* 110:762-766.
260. Bennett, C. L., E. van Rijn, S. Jung, K. Inaba, R. M. Steinman, M. L. Kapsenberg, and B. E. Clausen. 2005. Inducible ablation of mouse Langerhans cells diminishes but fails to abrogate contact hypersensitivity. *J.Cell.Biol.* 169:569-576.
261. Kissenpfennig, A., S. Henri, B. Dubois, C. Laplace-Builhe, P. Perrin, N. Romani, C. H. Tripp, P. Douillard, L. Leserman, D. Kaiserlian, S. Saeland, J. Davoust, and B. Malissen. 2005. Dynamics and function of Langerhans cells in vivo dermal dendritic cells colonize lymph node areas distinct from slower migrating Langerhans cells. *Immunity* 22:643-654.
262. Kaplan, D. H., M. C. Jenison, S. Saeland, W. D. Shlomchik, and M. J. Shlomchik. 2005. Epidermal langerhans cell-deficient mice develop enhanced contact hypersensitivity. *Immunity.* 23:611-620.
263. Mishima, Y. 1966. Melanosomes in phagocytic vacuoles in Langerhans cells. Electron microscopy of keratin-stripped human epidermis. *J.Cell Biol.* 30:417-423.
264. Hemmi, H., M. Yoshino, H. Yamazaki, M. Naito, T. Iyoda, Y. Omatsu, S. Shimoyama, J. J. Letterio, T. Nakabayashi, H. Tagaya, T. Yamane, M. Ogawa, S. Nishikawa, K. Ryoike, K. Inaba, S. Hayashi, and T. Kunisada. 2001. Skin antigens in the steady state are trafficked to regional lymph nodes by transforming growth factor- β 1-dependent cells. *Int.Immunol.* 13:695-704.
265. Hoashi, T., J. Muller, W. D. Vieira, F. Rouzaud, K. Kikuchi, K. Tamaki, and V. J. Hearing. 2006. The repeat domain of the melanosomal

matrix protein Pmel17/gp100 is required for the formation of organellar fibers. *J.Biol.Chem.*M601643200.

266. Shibaki, A., A. Sato, J. C. Vogel, F. Miyagawa, and S. I. Katz. 2004. Induction of GVHD-like skin disease by passively transferred CD8⁺ T-cell receptor transgenic T cells into keratin 14-ovalbumin transgenic mice. *J.Invest.Dermatol.* 123:109-115.
267. Gossen, M. and H. Bujard. 1992. Tight control of gene expression in mammalian cells by tetracycline- responsive promoters. *Proc.Natl.Acad.Sci.USA* 89:5547-5551.

VITAE

Brant Russell Ward was born in Austin, Texas, on December 31, 1977, the son of Joan Ann Ward and Samuel Lynn Ward and the brother of Kara Allison Ward. After graduating from William Mitchell High School in Colorado Springs, Colorado, in 1996, he matriculated at the University of Arkansas at Fayetteville, Arkansas. During the summers of 1998 and 1999, he worked at the Oklahoma Medical Research Foundation in Oklahoma City, Oklahoma. He graduated Summa Cum Laude with a Bachelor of Science degree in Microbiology from the University of Arkansas in June, 2000. In August, 2000 he entered the Medical Scientist Training Program at the University of Texas Southwestern Medical Center at Dallas, Texas. After two years of medical school curricula, he joined the Immunology Graduate Program of the Graduate School of Biomedical Sciences in August, 2002.

Permanent Address: 3211 Kinkaid Drive
Dallas, TX 75220-1622